THE IMPACT OF A FLUCTUATING FREEZING FRONT

ON ICE FORMATION IN FREEZING SOIL

By

Matthew Ryan Dillon

RECOMMENDED:

Advisory Committee Chair

Chair, Department of Civil and Environmental Engineering

APPROVED:

Dean, College of Engineering and Mines

Dean of the Graduate School

12/17/12

Date

THE IMPACT OF A FLUCTUATING FREEZING FRONT ON ICE FORMATION IN FREEZING SOIL

A

THESIS

Presented to the Faculty

of the University of Alaska Fairbanks

in Partial Fulfillment of the Requirements

for the Degree of

MASTER OF SCIENCE

By

Matthew Ryan Dillon, B.S.

Fairbanks, Alaska

December 2012

Abstract

Frost heave is typically associated with the formation of segregation ice in fine-grained soil. Coarse-grained soil is generally considered to be non-frost susceptible. Field observations and laboratory experiments show that coarse-grained soil can be extremely ice-rich in specific conditions. Previous studies have shown that oscillation of the frozen-unfrozen boundary can lead to the formation of ice by a mechanism different from the segregation ice mechanism. Conditions related to the formation of ice in coarse-grained soil were investigated using modern laboratory techniques. Fourteen tests were conducted on five soil types. The thickness of soil subjected to freeze-thaw cycles was varied and controlled by the magnitude and duration of applied soil temperatures. The thickness of the ice formed increased when the sample drainage was limited or prevented during cooling. Under specific conditions, the formation of a discrete ice layer was observed in coarse-grained soils. Seven samples were scanned with the μCT scanner at the completion of the warming and cooling tests. The sub-samples scanned were analyzed in 2D cross-sections, and characterized as 3D reconstructions. Frost heave induced by the formation of ice was observed in both fine- and coarse-grained soils, including soils that were found to be traditionally non-frost susceptible.

Table of Contents **Page**

Page

Page

List of Figures **Page**

Page

Page

Page

List of Tables **Page**

List of Other Materials **Page**

List of Appendices **Page**

Acknowledgements

This study has been funded in part by a generous 2-year fellowship provided by the Alaska Experimental Program to Stimulate Competitive Research (AK EPSCoR).

I am forever thankful for the support, encouragement, and coaching from the following individuals: Dave Barnes, Adam Berkey, Tristan Berkey, Matthew Bray, Billie Connor, Jeremiah Drage, Walter Fourie, Leroy Hulsey, Torre Jorgenson, Duane Miller, Rick Mitchells, Mark Musial, Walter Phillips, Amara Savikko, Brenton Savikko, Mikayla Savikko, Amelia Spencer, Emma Spencer, Pat Spencer, Suzette Stachow, Susan Start, Eva Stephani, Horacio Toniolo, Gary Tyndall, Dan White, and Xiong Zhang. For some, the level of involvement is clear. For others, I imagine they have no idea how much they have influenced me. Thank you all.

My committee members – Margaret Darrow, Daniel Fortier, and Mikhail Kanevskiy – have helped guide me through this long, and sometimes arduous journey. They have provided clear insight into their own experiences with graduate-level research, and have pushed me to focus on my studies while teaching me about the scientific process. My advisor Yuri Shur has been my mentor and friend for many years now. He has pushed me to learn new things, to challenge my understanding of our discipline, and to be the best scientist and engineer I can be.

I have a wonderful family that has supported me through my academic career. Dustin Mondloch, Danielle (Patton) Mondloch, Keith Mondloch, and Laurie Mondloch – thank you for all of the encouragement. I am extremely fortunate to be a part of their family. Zachary Dillon, Aaron Dillon, and Jonathan Dillon – a man could not ask for better brothers. Special thanks go to my parents Joan Dillon and Timothy Dillon, who taught me to ask questions about the world, and to do my best at helping make it a better place.

I would not have been able to make it through this program without my wonderful wife, Danielle Dillon. As a recent graduate student, she knows all too well the challenges – and rewards – associated with conducting this level of research. She has spent countless nights and weekends editing and reading this manuscript, and guiding me through the process of making this work a cogent study. She is my best friend and my soulmate. I can't begin to express my gratitude for her support.

Chapter 1
Introduction

1.1 General introduction

This thesis describes the formation of thick layers of ice in soils, created by a frost heaving mechanism that has generally not been discussed in the mainstream scientific literature. These ice bodies do not form under the conditions that are usually associated with segregated ice, instead, they are created due to cyclic temperature variations (freeze-thaw cycles) applied to soil.

1.2 Historical background

Frost action is defined as the processes related to soil freezing and thawing, including frost heave and thaw subsidence (Andersland and Ladanyi, 2004). Frost heave may generally be viewed as the process of soil expansion, typically in the upward direction, when certain soils experience freezing temperatures, and the formation of segregated ice lenses in the soil. Thaw subsidence, on the other hand, is the loss of volume and bearing capacity upon thawing of frozen soils. For as long as humans have built structures in cold regions, freezing and thawing have inflicted varying degrees of damage to these creations.

The first modern study of segregated ice formation and frost heave was done by Taber (1929, 1930) as a follow-up to his observations of changes in soils left overnight outside during the winter of 1914-1915. He noted that frost heave in the soils he froze often exceeded the 9% volume expansion of pore water during freezing. This larger-than-expected volumetric expansion requires accumulation of ice upon freezing in the actively freezing portion of a soil sample. He called this process, "ice segregation." Segregated ice forms as ice lenses perpendicular to the direction of heat removal. It is "segregated" because the water is drawn out of the soil matrix and aggraded in discrete bodies of ice. Taber explained water movement as a result of a gradient in the soil moisture tension (pore water pressure). This phenomenon is commonly referred to as cryosuction. Taber demonstrated that the formation of segregated ice leads to uplifting the soil above it due to the pressure created by the formation of the ice crystals.

Taber conducted parametric studies to characterize soil properties influential to producing excessive frost heave. He found that the size of the soil particles are critical for segregated ice to form. Tested clean sands produced no segregated ice, while clay resulted in excessive frost heave. Taber attempted to discern a maximum grain size for a soil to

produce excessive frost heave. By utilizing barium sulphate crystals (precipitated to create crystals of a near uniform size) with an average grain size of 2 microns, Taber noted that the crystals "gave well-defined segregation under favorable conditions of cooling, [...] but no segregation under unfavorable conditions." There is little elaboration as to what qualifies as "favorable conditions." He also noted that in other soils with an average particle size of 1 micron "segregation took place without difficulty." (Taber, 1929, pgs. 12, 14)

Beskow (1935) studied the mechanics of frost heave in a manner similar to Taber. Using field observations and laboratory experiments, Beskow came to similar conclusions as Taber. Beskow found that a freezing soil can be compared to a drying one:

> In both cases water changes phase and the amount of liquid water in the soil decreases. Thus, water flow from above the water table to the zone where water is changing into ice is analogous to [the] flow of water to a zone where it is evaporating.
> (Henry, 2000)

In the last 70 years there have been numerous attempts to formulate a unified, all-encompassing theory of ice segregation. The history of these attempts prior to the 1990s are presented by Black and Hardenberg (1991). They report, "As the 1990s arrive, we find that we have no satisfactory explanation for the mechanics of frost heaving. There are many models that purport to explain it, but they all suffer from the common fault of little or no experimental verification."

In general, the first frost heave studies were focused on coarse-grained soils. Beskow postulated that regarding coarse soils, a discontinuity due to inclusions of fine-grained soil in an otherwise homogeneous, non-frost susceptible soil, can lead to appreciable ice formation. He gives an example of a non-heaving sand, with a very thin strata of silt:

> In sands, if an ever so thin layer of fine material, a silt, fine silt or clay seam exists, an appreciable ice layer can form under favorable circumstances. This gives the impression that the coarse sand has become ice-stratified. This occurrence may be of considerable practical importance, for while the sand may appear at the surface to be non-frost-heaving, the existence of thin layers of fine silt underneath may make the ground strongly frost-heaving.
> (Beskow, 1935, p. 11)

In 1931, Casagrande proposed the following rule-of-thumb identification for potentially frost susceptible soils:

> Under natural freezing conditions and with sufficient water supply one should expect considerable ice segregation in non-uniform soils containing more than 3% of grains smaller than 0.02 mm, and in very uniform soils containing more than 10% smaller than 0.02 mm. No ice segregation was observed in soils containing less than 1% of grains smaller than 0.02 mm, even if the groundwater level is as high as the frost line.
> (Casagrande, 1931, p. 169)

Application of the Casagrande criteria requires a hydrometer test of the soil to determine the distribution of particles passing the 0.075 mm sieve, and to compute the percentage of particles finer than 0.02 mm (Casagrande, 1931). Frost susceptibility classification (Table 1.1) was inspired by Casagrande and based on tests which reflect some, but not all applicable soil conditions.

In practice, the simple explanation of conditions leading to frost heave susceptibility is the three "W"s approach. These are: winter, water, and wicking (Rice, 1975). "Winter" refers to the typically prolonged occurrence of subfreezing air temperatures, inducing soil freezing. "Water" refers to the presence of soil moisture. Frost heave is a non-issue if there is no moisture present to undergo a phase change. "Wicking" is a reference to a soil that promotes moisture migration, typically through capillary action and/or cryosuction.

In general, gravel and sand without fines are considered as non-frost susceptible, and existing segregated ice hypotheses do not explain ice formation in these types of materials. Taber's style of frost heave tests only consider continuous freezing scenarios. It has been found, however, that extensive frost heave can occur during repetitive freezing and thawing.

1.2.1 "A new theory of frost heaving"

Shortly after the publication of Taber's experiments, an alternative mechanism of formation of segregated ice inclusions in soils was developed. Benkelman, Burton, and Olmstead worked for the Michigan State Highway Department as a research engineer, a Deputy Commissioner, and a research assistant, respectively. Their research of frost heave and ice formation in soils was primarily based on field analysis of frost heave occurring in and

Table 1.1. Frost-Susceptible Soils (After U.S. Army Corps. of Engineers, 1984)

Group	Soil Description
F1	Gravelly soils with between 3 and 20 percent finer than 0.02 mm by weight
F2	Sand with between 3 and 15 percent finer than 0.02 mm by weight
F3	a) Gravelly soils with more than 20 percent finer than 0.02 mm by weight
	b) Sands, except very fine silty sands, with more than 15 percent finer than 0.002 mm by weight
	c) Clays with plasticity indexes of more than 12
	d) Varied clay existing with uniform subgrade conditions
F4	a) All silts including sandy silts
	b) Very fine silty sands with more than 15 percent finer than 0.02 mm
	c) Clays with plasticity indexes less than 12
	d) Varied clays existing with non-uniform subgrade conditions

along Michigan roads (Burton and Benkelman, 1931a,b). Expanding upon the field results, the Michigan team embarked upon a series of lab tests and formulated a new theory of ice formation in soil (Benkelman and Olmstead, 1931).

The Michigan team summarized the work of Taber in the following: "[soil] heaving is due to the movement of water to the point of freezing resulting in the formation of ice layers and, furthermore, that the old theory of which attributed excessive heaving to the change in volume of water present in a soil on freezing was incorrect." Benkelman and Olmstead openly disagreed with Taber's findings and observed that freezing soil samples at a constant rate is not a realistic simulation of natural phenomena. The Michigan team concluded that to accurately simulate natural thermal conditions, temperatures reflecting diurnal (longer) fluctuations should be applied to the samples. It is important to note that the field of frost heave research was pioneered by Taber (and Beskow), and that the studies produced by these researchers are viewed as seminal works on frost heave and the formation of segregated ice in soil. The statements made by the Michigan team appear to have directly challenged Taber's views.

1.2.1.1 Field sampling

Field samples were collected at locations of known frost heave along several Michigan roadways. The cores were collected by split cylinder sampling (3 ft. length, 1 ft. diameter), and depending on the tests performed, were either placed in a split cylinder wooden tube, or a glass tube.

1.2.1.2 Laboratory studies

Tested samples were placed in a metal pan above a layer of gravel that was resting in a circulating water bath. The water supply could be shut off by isolating the gravel pan from the water source. The published record of the Michigan team's tests, especially regarding freezing conditions, is quite limited. They note that for "standard freezing tests" (where they are aiming to recreate the conditions presented by Taber), they applied -2°C to the top of the sample, and 2°C to the bottom. The only other reference to freezing/thawing conditions were that freezing was "gradual" and that it was initiated from the top, with the freezing front moving downwards.

Large samples were prepared in pairs, one sample of fine soil left undisturbed and one sample had a horizontal layer of gravel inserted approximately in the center of the core.

No information is given regarding the type of gravel, nor the thickness of this layer which was inserted to study moisture migration as vapor through the coarse soil.

Results were presented for one pair of samples, consisting of a uniform silt with 16% initial moisture content. The samples were initially frozen without access to the water supply. No heaving of soil was observed. The cores were then thawed, and allowed to re-freeze with access to the water supply. After the second freezing, the undisturbed core and the sample with the gravel layer had displacement of 0.74 and 0.46 inches (approximately 2.1% and 1.3% of initial length), respectively. Post-test examination of the cores revealed little visible ice had formed. The total moisture contents of the samples after the second freezing were 32%, with the exception of above the gravel layer, where the silt had 25% moisture.

Samples were prepared for tests in glass tubes (for visual inspection) via two methods. The first method involved filling the glass cylinder with water and then dispersing silt into it. The gradual settling of the silt produced graded samples. The second method involved trimming and tamping the large split cylinder cores to fit inside the glass cylinders, and then setting the sample upright in water to allow for the sample to become saturated.

The glass-tube samples were frozen in what is assumed to be a "slow" manner from the top down. In the samples created by dispersed silt, the formation of ice lenses was noted in the portion of the sample consisting of soil with an average grain size less than 0.005 mm diameter. It was also noted that the samples collected from the field produced no visible segregated ice.

For an unstated reason, the samples collected from the field were thawed from the bottom up (assumedly due to an accidental increase in the circulating water temperature). The authors noticed that a void in the soil began to form adjacent to the "thawing line." As the frozen-thawed interface moved upward, the void in the soil became larger. Benkelman and Olmstead stated that the void was filled with water, and when the freezing front moved downwards, this water was "converted into a pure ice layer." This is illustrated in the first five panels of Figure 1.1. The last three panels represent a subsequent upward movement of the freezing front to some location below the first ice layer, and then movement of the freezing front back down, to create a second ice layer.

The authors did not mention the number of freeze-thaw cycles they put the samples through, and they do not provide the thickness of the ice layers produced in their tests. They did note that they created ice layers through temperature cycling in silt, fine sand,

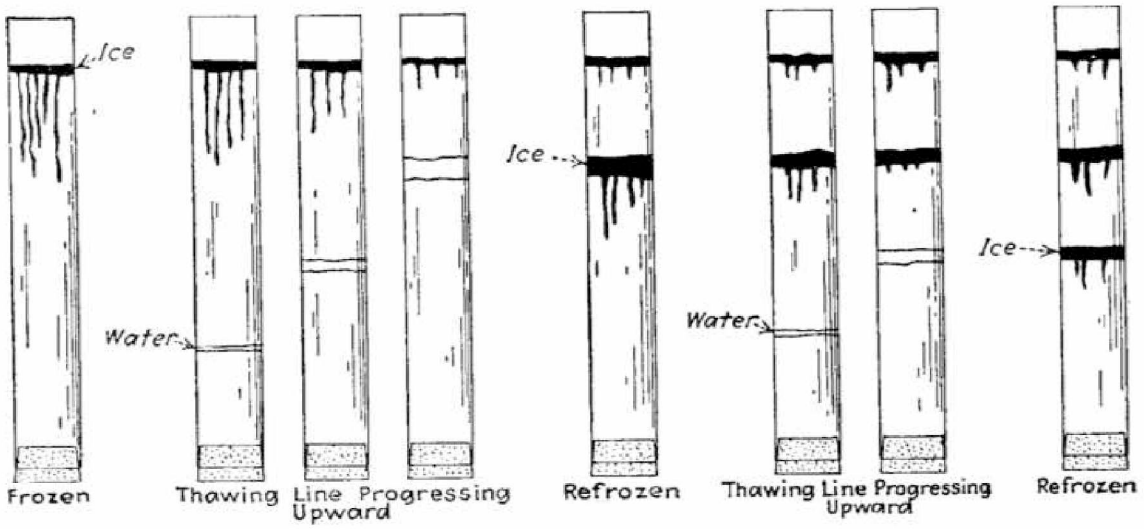

Figure 1.1. Development of ice layers in silt by alternate thawing and freezing (Burton and Benkelman, 1931a).

and clay soils. These observations are the basis of their theory of an alternative mechanism of ice formation in soil. When a soil experiences subfreezing temperatures at the ground surface for enough time, the soil will begin to freeze from the top down. The rate of freezing will depend on many factors, including soil type, water content, temperature gradient, hydraulic conductivity, and surcharge. While freezing, the interstitial water is converted to ice. After a period of time, if the surface temperature (or base temperature) is increased, the boundary of frozen and thawed soil will move upward, leaving a thawed zone below it. A water-filled void forms at the top of thawed zone, due to the volumetric reduction and thaw settlement of the soil water changing phase from ice to liquid. If the soil below the freezing front has a water supply, this water is either pulled into the thawed zone through vacuum forces, or due to a positive head. Upon subsequent cooling of the surface (or base) the freezing front moves downward, and freezes the water-filled void.

Their theory was based on tests of approximately 200 soil samples collected from roadway subgrade soil. The samples were collected in the summer at locations known to have heaved the prior winter. They discovered that approximately 70% of the sampled locations had subgrade soils that were comprised of sandy soils with excess moisture. The theory proposed by the Michigan team explained the formation of excess ice in coarse soils. The temperature cycle is present in the form of diurnal temperature variations associated with the rising and setting of the sun.

1.2.1.3 Critical Response to Benkleman, and Olmstead

The works of Burton, Benkelman, and Olmstead (Benkelman and Olmstead, 1931) was presented to the Highway Research Board, and had both positive and negative responses.

1.2.1.3.1 Willis E.A. Willis (Willis, 1931) provided direct support for the Michigan team. He found that results of Burton and Benkelman's experiments and their explanation are in agreement with his personal field experience. Willis used this response platform as an opportunity to applaud their efforts in regard to frost heave, and made a presentation of his own research and theories. This section of the discussion is only tangentially related to the work conducted by the Michigan team.

1.2.1.3.2 Watkins The discussion response submitted by W.I. Watkins of the U.S. Bureau of Chemistry and Soils is similar to that of E.A. Willis (Watkins, 1931). Watkins concurred with the findings of Benkelman and Olmstead, stating that his personal experience with subgrade cores sampled by the Minnesota Highway Department often included ice layers that have formed in sands. Watkins, however, believed that the mechanism of ice formation in sand is not entirely explained by the Michigan team's theory. Watkins noted that, in addition to observing thick ice plates in sands, he also observed very thin, evenly spaced ice layers, which he attempted to explain in his response. Watkins' response is presented in Section 4.1.2 in detail.

Responses by Casagrande and Taber read as a direct attack against Benkleman, Burton, and Olmstead. Only a few vocal researchers supported their work.

1.2.1.3.3 Casagrande Arthur Casagrande (1931) disagreed with the Michigan team:

1. "According to the new theory, alternate freezing and thawing of the bottom of the frozen layer is necessary in order to produce excessive ice accumulation; according to the older theory this is accomplished by steady freezing action." (Casagrande, 1931, p. 168)

2. "According to the new theory, ice layers can form in clean sand and gravel just as well as in fine grained soils; according to the older theory the presence of a certain amount of very fine grains is required in order to make the growth of ice layers possible under natural freezing conditions." (Casagrande, 1931, p. 168)

3. "In a test cylinder a sample is frozen and then partially thawed from beneath, the frozen portion will adhere to the wall of the cylinder and cannot follow the subsidence of the thawing portion, whereas in nature the frozen layer must follow every subsidence due to melting at the bottom." (Casagrande, 1931, p. 168)

Casagrande presented findings from one of his field studies where several soils were loaded with asphalt and concrete slabs exposed to the natural air temperatures and moisture present in the area, and their vertical movement was recorded. Casagrande concluded that the sand in the test did not produce any discernible ice plates, while the silt heaved up and had a large amount of visible ice. In his experiments, prominent ice layers were not formed.

Casagrande's first point is not completely fair. First, the Michigan team did not claim that cyclic temperatures were the only cause of excessive frost heaving — but it was the only factor that could explain the formation of ice layers in their experiments. As well, they never explicitly stated the "bottom half" of the sample should be thawed and frozen, just that the frost line should be moved vertically up and down in the soil.

Casagrande's second point assumes that these theories are mutually exclusive. In reality, these two theories of frost heave can easily coexist and supplement each other.

Lastly, the work presented in this thesis demonstrates with experimental data that the final point made by Casagrande is not necessarily true.

1.2.1.3.4 Taber Taber's response to the Michigan team was primarily defensive (Taber, 1931). Benkelman and Olmstead criticized Taber for not testing soils known to heave in nature (those from states in the "frost area"), to which Taber points out that his lab had tested such soils, but that the results were yet to be published.

Taber reminds the Michigan team that he studied repeated freeze-thaw, to which he found that, "prompt refreezing after thawing resulted in greater ice segregation and heaving than occurred on the first freezing." He attributes the increase in moisture content near the top of the sample on the first freeze cycle (thus allowing for more free moisture on the following cycles) to an increase in heave, and, the breaking up of consolidated soil on the first freeze increases the hydraulic conductivity on following cycles and decreases the tensile strength limiting heave resistance. The argument of the sample adhering to the sides of the test apparatus was repeated by Taber, of which he states that, in his experience, this friction phenomena is not "an appreciable factor when large areas of ground are frozen

under natural conditions."

According to Taber, the Michigan team's theory is not required to explain frost heaving. Taber highlights several of his published experiments as the supporting evidence (Taber, 1929, 1930). It appears that Taber possibly misunderstood the Michigan crew's experiment protocol, and was under the impression that the soil samples were allowed to fully freeze, as opposed to moving the freezing front up and down. It should be noted that there is a difference between these two criteria. At no point in the (published) Michigan glass tube tests were the samples fully thawed, they were only partially thawed by altering one side of the samples' temperature (however, the large sample tests were frozen, thawed, then frozen again). This confusion could partially explain Taber's response.

The negative reactions of Taber and Casagrande, who were (and still are) leading frost heave authorities, blocked further research in the direction opened by the Michigan team.

1.2.2 G.M. Fel'dman

Fifty years passed before G.M. Fel'dman explored mechanics of ice formation in soil in a manner similar to that of the Michigan team. Fel'dman was interested in the possibility of alternative methods of ice formation, specifically in regard to permafrost regions. Fel'dman:

> We are interested, first of all, in potential capabilities of different mechanisms of segregation ice formation in a sense of providing unlimited growth of ice streaks leading towards formation of not only ice saturated horizons but also of sheet ice deposits.
> (Fel'dman, 1988a, p. 339)

Fel'dman discussed the widely accepted theory of segregated ice formation, compared laboratory and field conditions of ice formation in soil, and came to the conclusion traditional frost heave theory is insufficient for describing this particular type of ice formation.

Fel'dman models two types of permafrost formation scenarios: epigenetic and syngenetic. Epigenetic permafrost is the formation of permafrost due to the lowering of the freezing front in a previously deposited soil. This type of permafrost formation is primarily due to changes in environmental conditions, such that the mean annual surface temperature is suitable for the formation of permafrost. Syngenetic permafrost is formed when sediment is deposited on the ground surface, and the base of the permafrost layer

moves upward in accordance, due to the new thermal conditions. Fel'dman modeled epigenetic permafrost by placing his free water reservoir below the zone of freezing, while for syngenetic modeling the reservoir was located above the zone of freezing.

Oscillations of the freezing front were performed in several experiments detailed by Fel'dman (1988b). Gradual downward freezing was initiated, with small fluctuations of approximately 0.5°C with a period of 15-20 minutes. Fel'dman noted significant accumulation of ice in samples comprised of silt that were frozen under open system conditions (water allowed to freely flow into and out of the sample). Fel'dman also alternated closed to open system conditions in several experiments on coarse-grained soils by manually opening and closing the water supply valve during temperature oscillations. Ice up to 6 cm thick in a gravel soil was formed by allowing the water valve to be open during thawing, and closed during freezing. Fel'dman summarized his hypothesis regarding the mechanism of this ice formation in the schematic reproduced in Figure 1.2. Fel'dman named the formation process of this ice the "vacuum-filtration mechanism," because during the upward movement of the frozen-unfrozen boundary, a vacuum forms in the pore space due to the volume reduction of the pore ice into water. The presence of a vacuum has the tendecy to suck, or filter, water towards the location of the vacuum, which is at the interface of the upwardly moving frozen-unfrozen boundary.

Fel'dman's experiments produced results similar to those presented by Benkleman, Burton, and Olmstead (Figure 1.3). Fel'dman found that by limiting the expulsion of water from the test apparatus, appreciable ice would form at the location of the water-filled void.

1.3 The impact of temperature cycles on the formation of ice in soil

Although the discussion of an alternate mechanism of ice formation has historically been viewed as controversial, the existence of ice in coarse material indicates that this type of soil can still be viewed as "frost susceptible" under certain conditions. The Michigan researchers, followed by Fel'dman have provided a compelling start to this line of research, however it has remained dormant for the last 25 years. The need for a modern, systematic, and detailed study of this topic is evident due to the continuing effects of frost heave on roads and other structures. Advances in sensor accuracy and digital acquisition allow for closely monitored and controlled experimentation. Through the use of current technology, the impact of freeze-thaw cycles on soils can be characterized and quantified to allow for consideration from new perspectives.

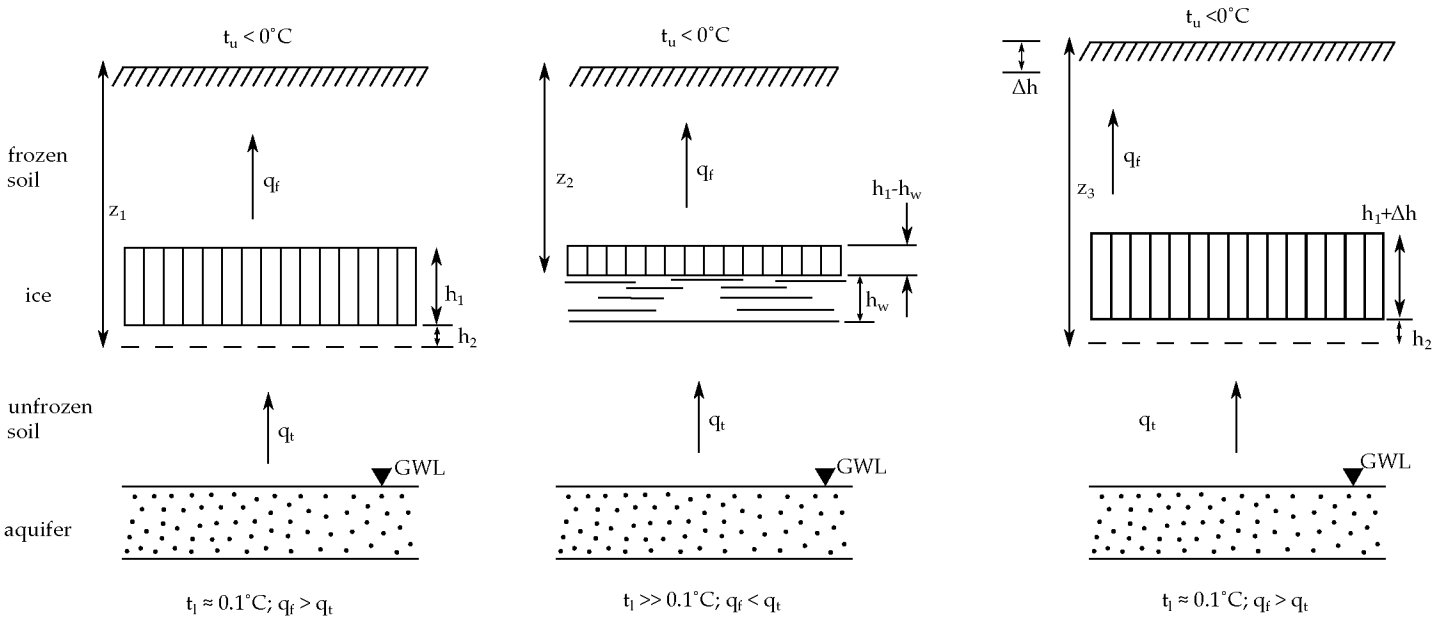

(a) Ice with thickness h_1 forms in the soil during freezing at depth z_1. The surface temperatures are constant at this time. The heat flux due to the phase change in the frozen half (q_f) is greater than the heat flux from the lower surface to the ice interface (q_t). The layer of frozen soil below the ice (h_2) is assumed to be approaching zero thickness.

(b) The temperature at the lower surface is increased. The ice begins to thaw from the bottom up, forming a layer of water (h_w). Due to the water's phase change, there is a subsequent 9% volumetric reduction, which forms a vacuum in the thawed soil, causing seepage of water from the aquifer groundwater level (GWL) to the melting ice.

(c) When the temperature at the lower surface is brought back to near-freezing, the freezing front will once again move downward. The refreezing of the water causes the thickness of the ice to increase by $\Delta h = 0.09h_w$. The surface of the soil also moves upward by Δh if the soil matrix is rigid and not deformable.

Figure 1.2. Vacuum-filtration mechanism during epigenetic freezing of fine grain soils, after Fel'dman (1988b)

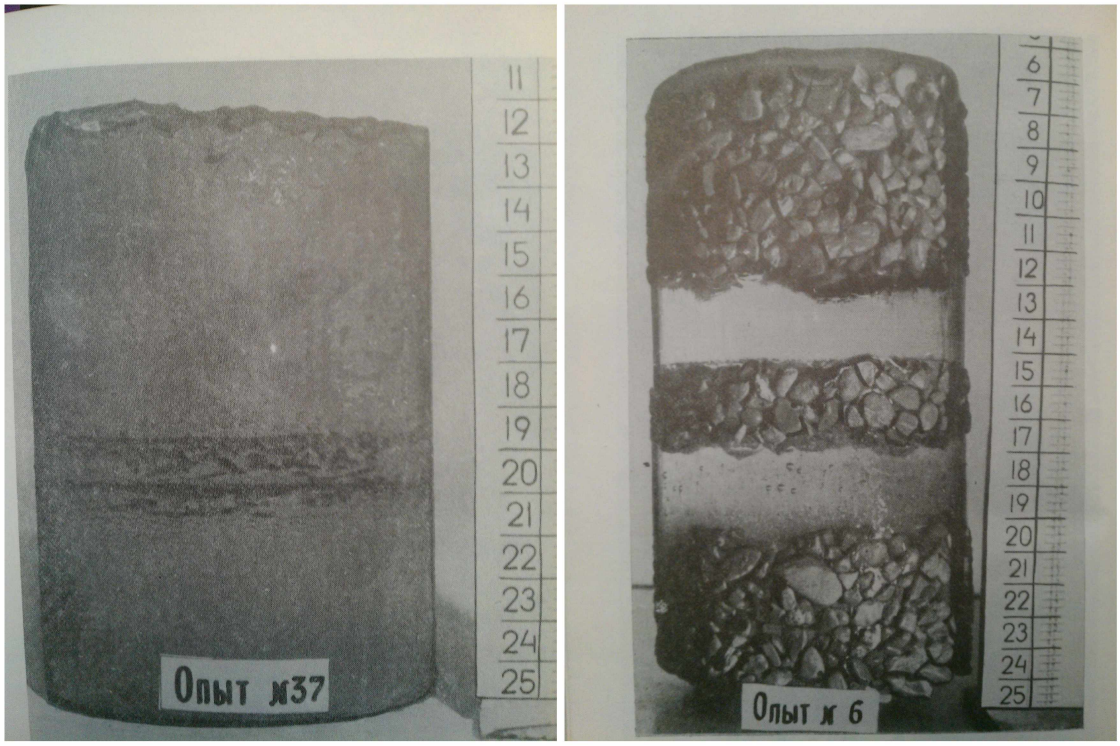

(a) Development of ice in fine-grained soil by vacuum-filtration mechanism

(b) Development of ice in coarse-grained soil by vacuum-filtration mechanism

Figure 1.3. Development of ice in fine- and coarse-grained soils by vacuum-filtration mechanism (Fel'dman, 1988a).

Chapter 2
Methods

2.1 Cyclic frost heave tests

Two custom frost heave cells were utilized to explore the impact of cyclic variation of the frozen-unfrozen boundary on the formation of ice in soils. One of the cells, designed and manufactured at Hokkaido University in Japan (referred to hereafter as the Hokkaido Cell) is constructed of transparent acrylic. The Hokkaido Cell is ideal for testing small soil samples, and was primarily used for tests involving time-lapse photography. The University of Laval in Canada constructed the larger cell (hereafter, the Laval Cell). The Laval Cell provides a larger volume sample size.

2.1.1 Hokkaido Cell

The Hokkaido Cell is a self-contained, custom-made frost heave cell. The transparent nature of the cell allows for immediate and continuous observation of the soil sample. The cell is composed of the acrylic cylinder (60.0 mm diameter, Figure 2.1-A), a metal frame (Figure 2.1-B), and a loading piston (Figure 2.1-C).

The acrylic cylinder fits over a pedestal at the bottom of the cell (Figure 2.1-D). A soil sample rests on top of the pedestal and a highly porous metal plate (Figure 2.1-E) is connected to a water source (Figure 2.1-F) to model open system freezing. The pedestal has inlet and outlet ports through which a thermally controlled fluid circulates (Figure 2.1-G). By connecting a pressurized coolant bath with programmable temperature controls to these ports, the temperature of the pedestal is accurately controlled.

The upper pedestal (Figure 2.1-H) of the cell is identical to the lower pedestal, with one exception: movement is unrestricted in the axial (up/down) direction of the soil sample. This allows for vertical expansion and contraction of the sample, while still maintaining sufficient thermal contact between the soil and the pedestal. The upper pedestal was incrementally loaded with weights to apply a surcharge. The upper pedestal in conjunction with the frictional resistance of the O-ring creates a minimum overburden pressure of 9.1 kPa (Darrow, 2007).

The upper pedestal is free to move with the soil samples' heave and thaw subsidence, and the displacement of the soil surface is measured. This is accomplished by measuring the pedestal displacement with a high precision laser-based linearly variable differential

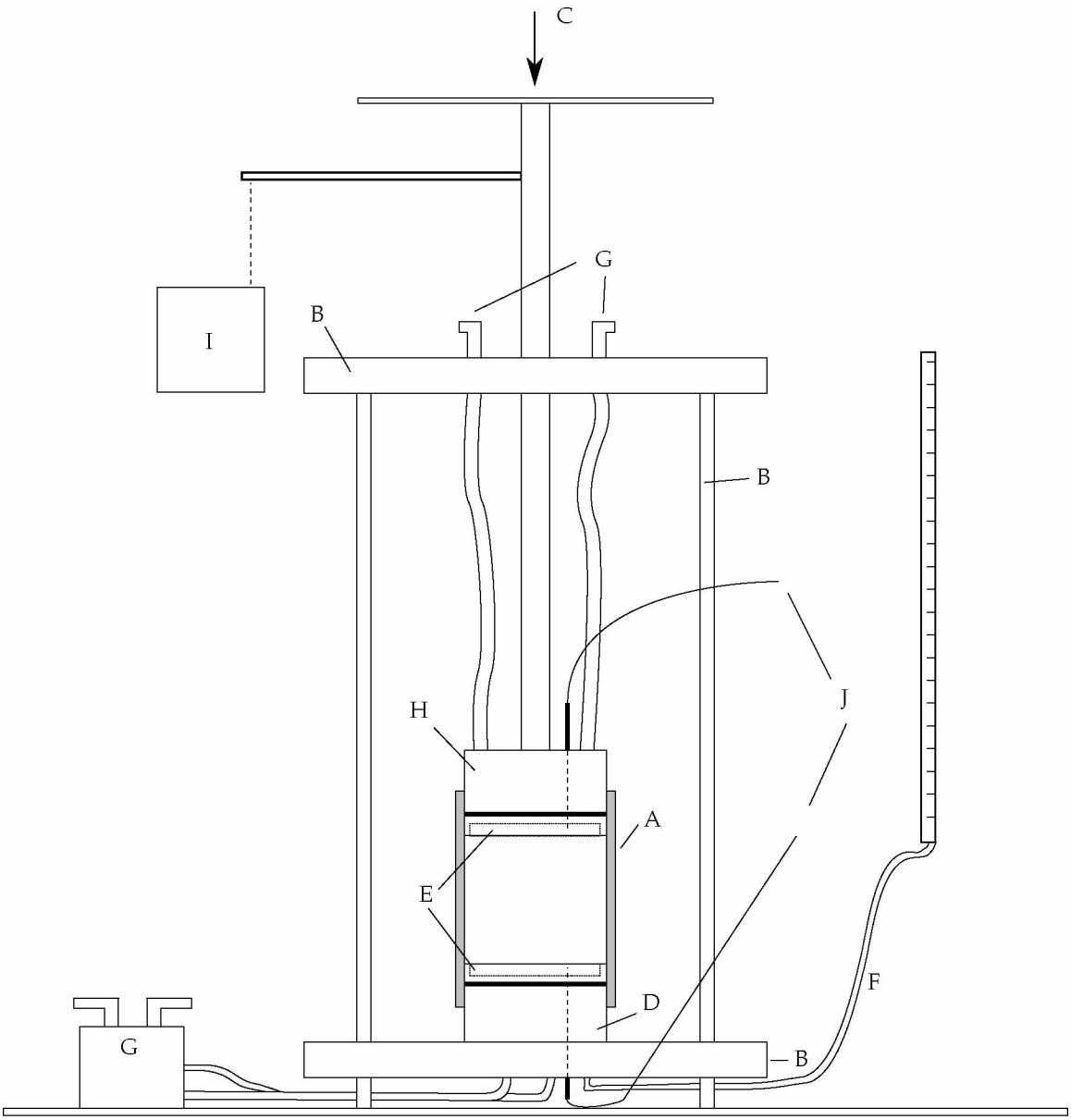

Figure 2.1. Hokkaido Cell schematic.
A – Transparent acrylic cylinder, B – Metal load frame, C – Loading piston, D – Lower pedestal, E – Porous plate, F – Water supply, G – Carrier fluid ports, H – Upper pedestal, I – Laser LVDT, J – RTD temperature sensors
(Not to scale)

transducer (LVDT, Figure 2.1-I). The LVDT used with the Hokkaido Cell has a maximum range of 30 mm and a resolution of 0.003 mm. Both pedestals have drilled holes in which platinum RTDs (resistive thermal devices) are inserted. These temperature sensors are located such that they can measure the temperature of the soil-pedestal interface. The average core volume for this cell is approximately 170 cubic centimeters.

2.1.2 Laval Cell

The Laval Cell is composed of a thick-walled, high-strength plastic 101.2 mm diameter cylindrical cell inside a reaction frame (Figure 2.2).

The pedestal setup in this cell is similar to that of the Hokkaido Cell — independent temperature control and the ability for moisture to pass through the porous stones. As well, the upper pedestal is free to move and able to provide a load via a piston controlled by a positive air manifold. The upper pedestal weight is negligible, providing no significant surcharge to the soil sample. The surface displacement of the soil samples in the Laval Cell is measured with an analog LVDT attached to the upper pedestal. The LVDT has a maximum stroke of 50 mm and a resolution of 0.1 mm. Unlike the Hokkaido Cell, the lower pedestal is permanently fixed to the cylinder sidewalls.

The Laval Cell has a platinum RTD embedded in the upper pedestal, a thermocouple in the lower pedestal, and a series of 7 thermistors along the outer edge of the core. The lowest thermistor is 26 mm from the bottom of the core, with the remaining thermistors at 17 mm intervals upwards along the cell wall. The thermocouple and wall thermistors are stationary sensors, while the platinum RTD in the upper pedestal is always in contact with the upper surface, regardless of heave or subsidence. The thermistor profile allows for determination of the position of the frozen-unfrozen boundary during testing. The average core volume is approximately 1600 cubic centimeters.

2.1.3 Common cell setup features

In general, test methodology did not differ between the two cells. Each cell is placed in a separate refrigerator with a modified compressor to minimize the temperature variation inside. Because the compressor runs at 100% duty-cycle, the temperatures of the refrigerators are regulated by a set of PID (proportional, integral, derivative) controlled 60 Watt to 100 Watt incandescent light bulbs. The bulbs produce waste heat used to control the refrigerated environment. The bulb area is separated from the rest of the refrigerator by

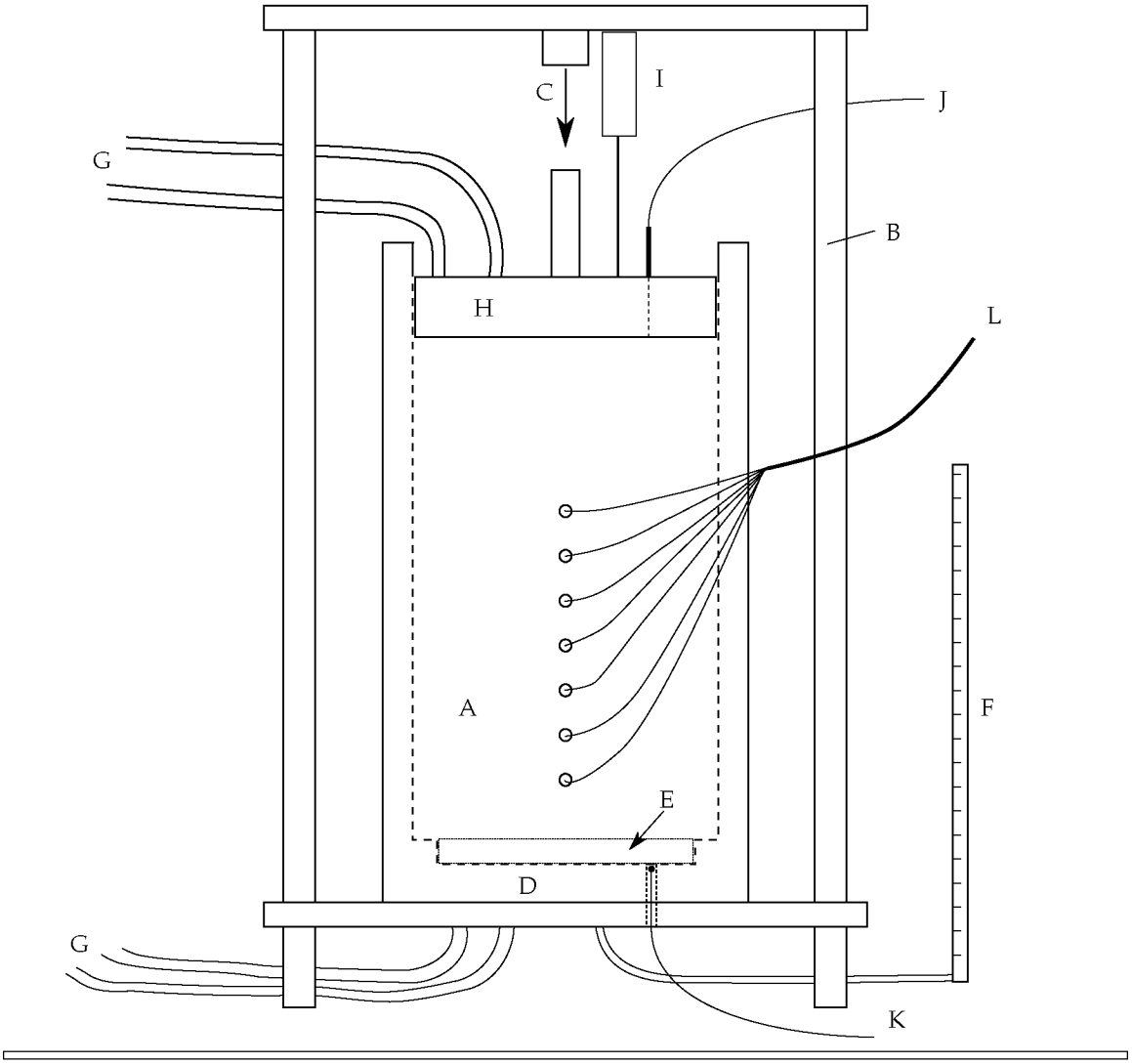

Figure 2.2. Laval Cell schematic.
A – Thick-walled plastic cylinder, B – Metal load frame, C – Loading piston, D – Lower pedestal, E – Porous plate, F – Water supply, G – Carrier fluid ports, H – Upper pedestal, I – Analog LVDT, J – RTD temperature sensor, K – thermocouple temperature sensor, L – thermistor temperature sensors
(Not to scale)

a sheet of reflective insulation, and the air in the refrigerators is circulated via small fans. This setup allowed for relatively accurate control of the ambient air temperature of each frost heave cell with minimal maintenance. The refrigerator temperature set-point is maintained at 1.5°C for all tests, however, the actual ambient air temperature in the chamber fluctuates during testing due to the light bulbs burning out, accumulation of frost on the condenser fins, and from opening and closing the refrigerator door for sample and equipment maintenance. The range of temperatures was typically 0.5°C and 2.5°C, and was generally no greater than -1°C and 10°C for a prolonged period.

Each cell is placed inside its respective refrigerator for the duration of testing. The cells are supplied with water from burettes via a small port on the side of each refrigerator. The sensor lead wires were also routed through the refrigerator ports.

Water levels in the burettes are measured with differential pressure transducers (DPT). The transducers measure the pressure difference between two fixed ports. For these measurements one port is connected to the base of the burette, while the other is left open to atmospheric pressure. As the water level in the burettes rises and falls, the water column pressure is determined from the DPT readings. The impact of atmospheric pressure variations due to meteorological conditions is assumed to be negligible. The DPT range is 1397 mm of water, and the resolution is 3.56 mm.

Each cell's sensors — the temperature, displacement, and pressure — is connected to independent digital multimeter data logging systems. The computer controlled system is polled at predetermined time intervals. Unless otherwise stated, all of the sensor data presented are sampled at 60 second intervals and continually monitored throughout testing.

2.1.4 Soil descriptions

The soil samples were prepared from remolded soils for testing. Five types of soils are utilized throughout the program. Grain size distributions for the soils used are presented in Figure 2.3. The majority of the soil is from Fox, Alaska. The Fox soils were collected from the CRREL Permafrost Tunnel in Fox, Alaska (64° 57.0'N, 147° 37.2'W, Bray et al. (2006)) . Soil was extracted from sloughed material from the tunnel walls (when the ice in the tunnel sublimates, the silt has a tendency to slough off of the walls), and is prepared in several combinations: unscreened Fox silt (Figure 2.4(a), unmodified soil from the tunnel with some gravel and organics present), screened Fox silt (Figure 2.4(b), organics, gravel, and coarse sand screened off from above 300 μm), and Fox sand (Figure 2.4(c), the sand

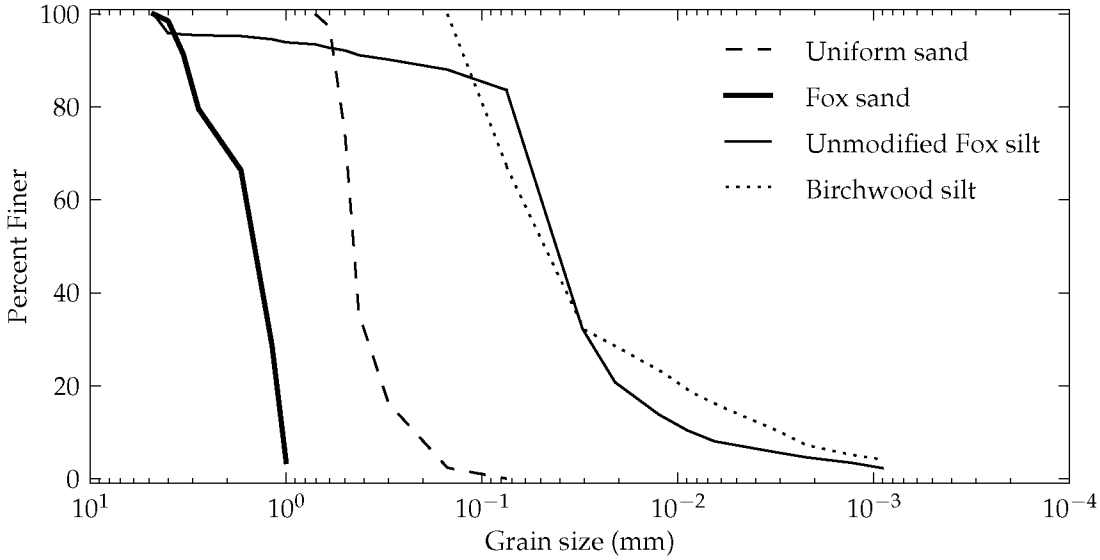

Figure 2.3. Grain size distributions. Average grain sizes: Fox sand – 1.85 mm, Uniform sand – 0.43 mm, Unscreened Fox silt – 0.05 mm, Birchwood silt – 0.06 mm

fraction extracted from the Fox silt stock). The soil obtained from the tunnel was already mostly dry when collected, due to the sublimation of the ice.

In addition to the Fox soils, two other soil types are utilized. A uniform sand (Figure 2.4(d)) was prepared from an industrial bag of sand-blasting silica sand. Birchwood silt (Figure 2.4(e)) was used from continuous cores drilled Birchwood, Alaska (61° 23'N, 149° 33'W, Krzewinski et al., 2006). The Birchwood soil was oven dried, pulverized, and screened. The resulting material that was utilized was the silt passing the 300 μm sieve.

2.2 Time-lapse photography

For visual monitoring, a digital camera is placed in the refrigerator in front of the Hokkaido Cell. The camera is programmed for image capture at a regular interval, typically 60 seconds. In post-processing, the images are rescaled and matched with the temperature data collected from the sensors, and rendered to a unique frame (Figure 2.5). Each frame displays the photo snapshot at a given time, temperatures at the top and bottom pedestals, and a rotated progress bar that shows the elapsed and remaining test time (gray bar behind temperature plot in Figure 2.5). When quickly played back in sequential order, these frames form a time-lapse video for each test performed in the Hokkaido Cell (see Appendix A). For all tests, the frame rate of the final rendered video is 60 frames per

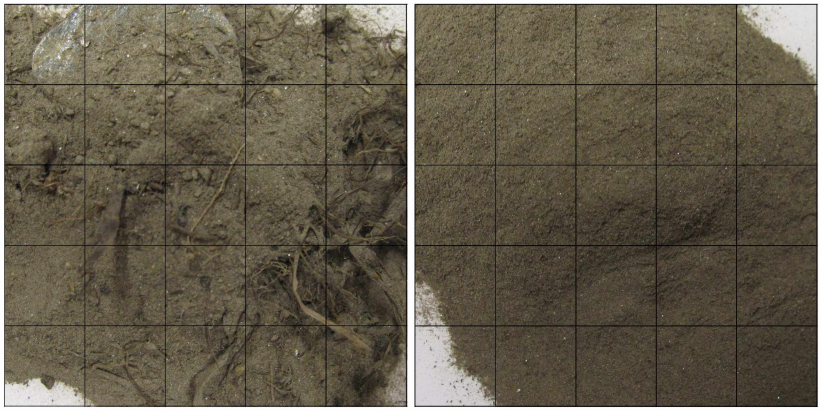

(a) Unscreened Fox silt (b) Screened Fox silt $< 300\ \mu$m

(c) Fox sand (d) Uniform sand

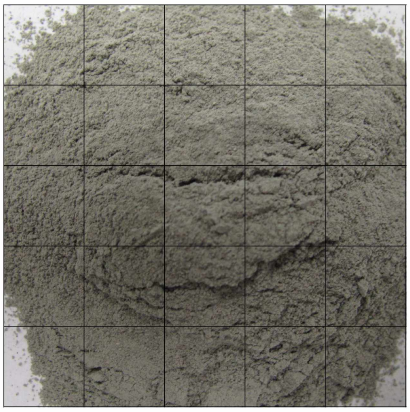

(e) Birchwood silt $< 300\ \mu$m

Figure 2.4. Soils utilized for testing (image side lengths are 50 mm)

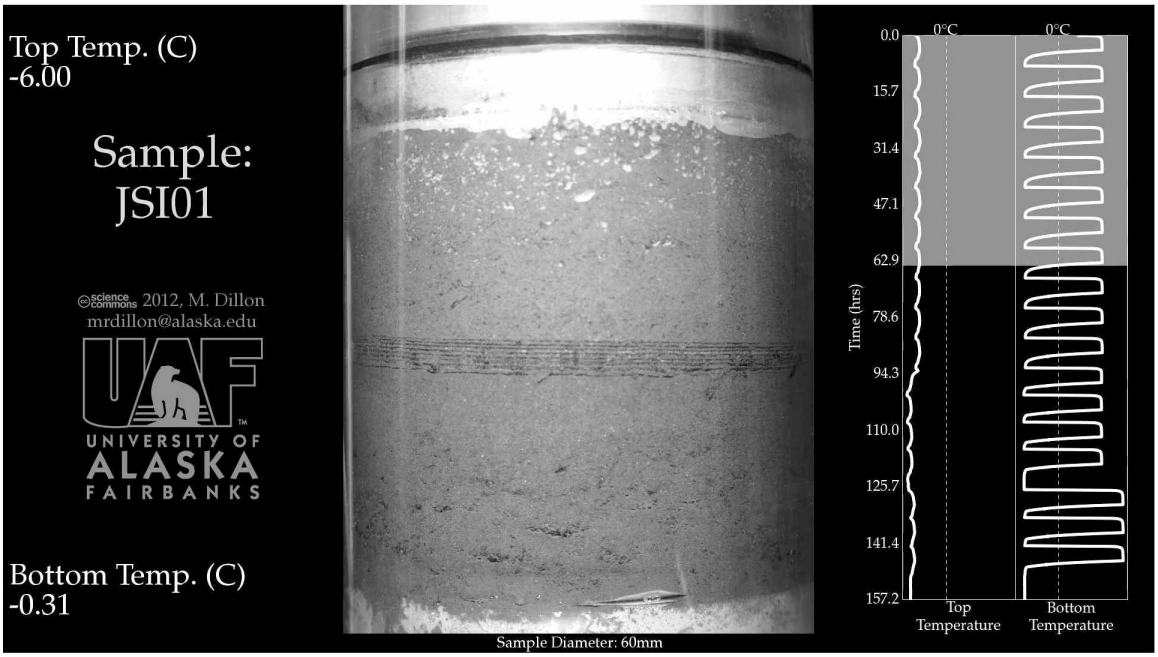

Figure 2.5. Sample frame from Hokkaido Cell time-lapse video

second, compressing 1 hour of actual test time into 1 second of video.

2.3 Micro-computed tomography

Select samples are scanned (while still frozen) in an x-ray micro-computed tomographic (μCT) acquisition system following frost heave testing. The μCT scans allow for 3 dimensional (3D), non-destructive imaging of the internal structure of the soil samples. It is possible to identify and differentiate between ice, minerals, gas, and organic materials with μCT methods (Dillon et al., 2008). For this study, the primary goal of the μCT analysis is to characterize the region of the sample where the ice bodies form.

The scans are acquired with a Skyscan 1172^{TM}. The scanner is equipped with a stationary camera and x-ray source, and a rotating sample stand. Scans are performed in a walk-in freezer to ensure that the excessive heat generated by the X-ray source did not induce any thawing of the soil. The samples are imaged with an 80 kV/100 μA x-ray source. The scanner acquires an x-ray image of the core every 0.3° rotation. The x-ray exposure time per rotation step is 1264 ms. Scan datasets are processed and analyzed with several techniques: raw x-ray images, reconstructed cross-sections, and 3D volumetric renderings.

The scanner produces x-ray images of a sample by rotating the sample stage by a given

degree interval, exposing the sample to x-ray energy, and measuring the amount of x-ray energy that passes through the sample with a high-resolution scintillation sensor. Figure 2.6(a) is an example of this type of x-ray image. The scintillation sensor measures the attenuation of the x-ray energy, and dense materials will attenuate more than non-dense materials. In the images, this corresponds to darker pixels (dense, more energy attenuation) and lighter pixels (less dense, less energy attenuation). The resulting dataset from a scan is a series of x-ray images, such as Figure 2.6(a). Each image represents a 0.3° rotation step, out of a 360° domain (1200 images total). Each pixel represents a single 34.46 μm by 34.46 μm area of the sample. The pixel values are representative of integer values ranging from 0 to 254 (Figure 2.7).

Scan reconstruction is the process of taking raw images and interpolating pixel values to determine the internal structure of the scanned sample. This process is automated, and the interpolation is performed with a proprietary software package that is included with the Skyscan 1172. Figure 2.6(b) represents one horizontal layer of pixels (34.46 μm thick) from the summation of the images in the dataset from which Figure 2.6(a) is sampled.

Once re-sampled, the reconstructed x-ray cross-sections are loaded into a 3D array with a computer. Advanced volumetric rendering techniques are utilized to manipulate and view the datasets. The pixel values in Figure 2.6(c) are not the same as the original pixel values (Figure 2.7(a)); this is to facilitate interpretation. Original μCT data are scaled from 0 to 254 (less dense to more dense material, part (a), unit-less values). Two separate functions were utilized for this study — one for 2D cross-sections (Figure 2.7(b)), and one for 3D reconstructions (Figure 2.7(c)). By generating a density value histogram, an appropriate cutoff between sediment and non-sediment is selected for each scan (value "X" in Figure 2.7). The 2D color transfer function outputs a binary image to highlight the boundaries and area occupied by the sample constituents. The 3D color transfer function varies both the opacity and the shade of the pixel value. Gas and organics are depicted as shades of black and dark gray, ice as white. The sediment cutoff value has a step-wise increase in shade, with the least dense sediment rendered in black, while the most dense sediment is rendered in a mid-tone gray. The opacity increases with density, and is overall more opaque than the non-sediment values.

Maximum density projections are created by sorting the array data in a manner that produced one frame of data for the entire scan dataset, where each pixel value represented the maximum density value found in the single pixel's representative row. This image is

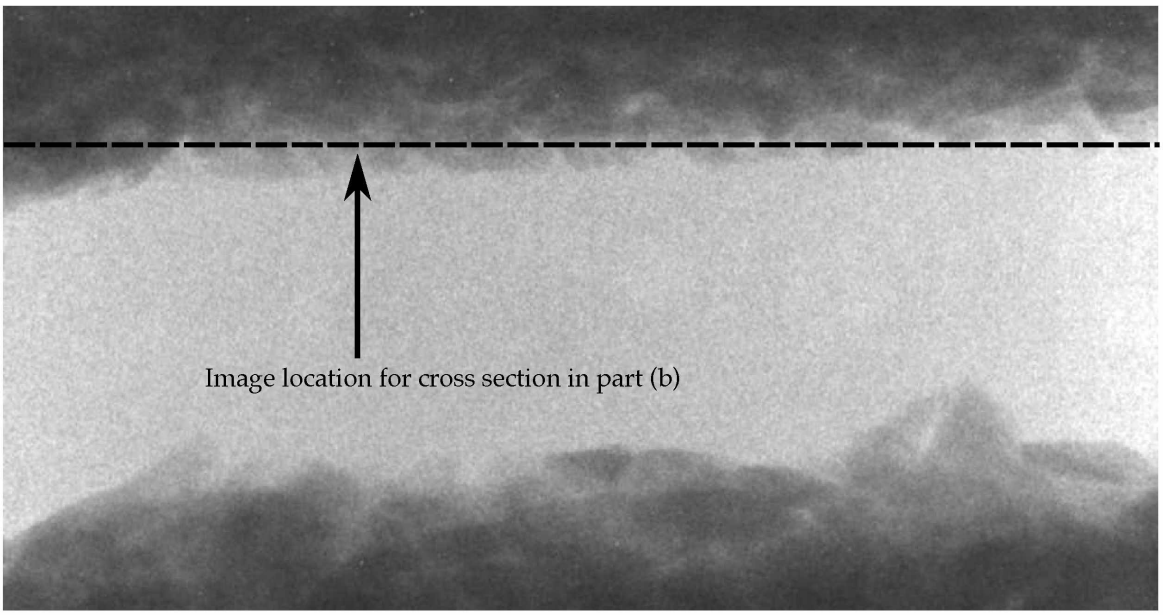

(a) Raw x-ray μCT image (core oriented vertically, image take from the side, 18.1 mm tall)

(b) Reconstructed cross-section image (perpendicular slice from dashed line in part (a), 34.5 mm diameter)

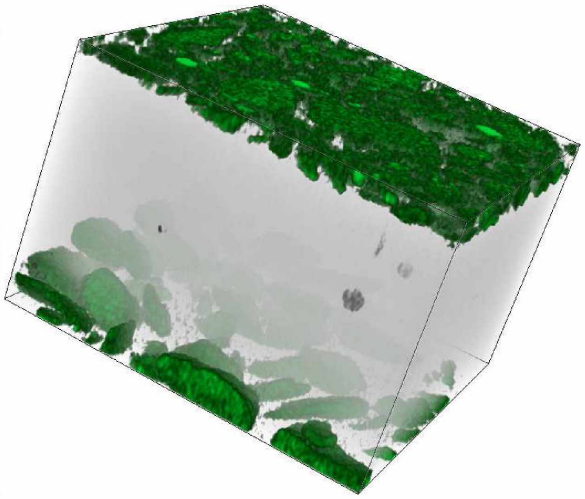

(c) 3D volumetric rendering, sub-sampled from center of core (white is ice, black is gas, green is sediment)

Figure 2.6. Sample images of x-ray μCT scan data.

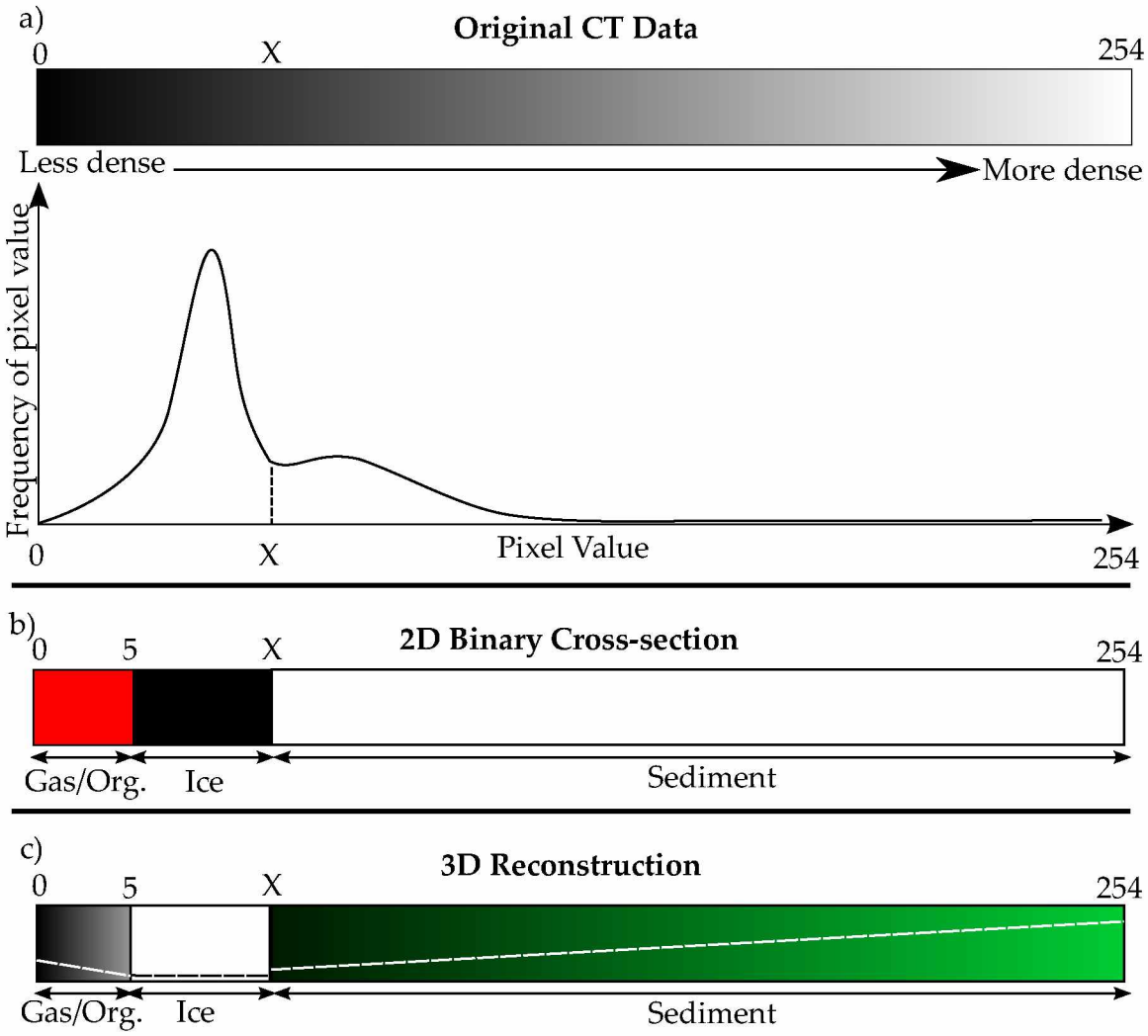

Figure 2.7. X-ray μCT color transfer function. Original μCT data is scaled from 0 to 254 (less dense to more dense material, part a, unit-less values). Two separate functions are utilized for this study — one for 2D cross sections (b), and one for 3D reconstructions (c). Cutoff parameter "X" determined on a per-sample basis.

similar to a traditional x-ray image; however the results are high resolution, and specifically represent the highest density values.

2.4 General testing procedures & testing program

Table 2.1 contains a summary of general test descriptions. All soils were prepared from dry stock, by saturating either in-place in the cell, or saturating in an external saturation cell. Samples prepared with homogeneous fine-grained soils were mixed into a slurry, which was allowed to settle out, and the supernatant water was drained off. If the sample was prepared with homogeneous sand, or a base layer of sand, the dry soil was placed directly in the cell, and was saturated from the bottom. If the soil was prepared in the external cell, an appropriately sized sample was cut from the larger sample by pressing a thin-walled pipe with a sharpened edge into the soil. The pipe was extracted, removing the soil plug with it. The plug was extruded into the cell for testing. Once the saturated soil was placed into the cell, the refrigerators and circulating baths were turned on and set to initial temperatures close to 0°C. While the equipment was cooling, the samples were consolidated in place by applying an axial load. The minimum consolidation pressure applied was 30 kPa. The consolidation was considered complete when no further displacement of the soil was observed with the LVDT.

Once consolidated, the sample was frozen for testing, by setting both pedestals to -5°C. This allowed for relatively fast pre-freezing of the sample. Once pre-frozen, the consolidation load was removed, and the frozen-unfrozen boundary cycling tests were started. The cycle tests were conducted by varying the temperatures applied to the top and the bottom of the frost heave cells. By applying a subfreezing temperature to the top of the sample, and temperature above freezing to the bottom, the sample was subject to partial freezing (only the upper portion). By varying the upper pedestal temperature, or the lower pedestal temperature (and for some tests, varying both), the thermal conditions caused the frozen-unfrozen boundary to move up and down in the sample. Applied thermal parameters were varied on a per-test basis. The applied soil temperatures are described in Chapter 3 for each test.

At the conclusion of the thermal cycling testing, both pedestal temperatures were lowered below freezing if they were not there already, to freeze the entire sample for extraction. Once frozen, the upper and lower pedestals were briefly warmed in order to break the bond of the frozen soil and the pedestals. The sample was extracted from the cell,

and photographed, wrapped in plastic wrap and aluminum foil, and stored in a freezer for additional testing. Select samples were sliced into thin sub-samples at the conclusion of a freezing test, and were tested for moisture content and organic content, per ASTM procedures (2007a; 2007b). A schedule of the testing program is listed in Table 2.2.

Table 2.1. General test descriptions

Test Name	Soil(s) used (see Figure 2.4)	Sample Composition	Test Length (hrs)	Cell Used
CSA01	uniform sand (d*)	Homogeneous	118	Laval
CSI01	unscreened Fox silt (a)	Homogeneous	262	Laval
JCL01	Birchwood silt w/ uniform sand (e/d)	Silt with sand as base layer	337	Hokkaido
JCL02	screened Fox silt (a)	Homogeneous	15	Hokkaido
JGR01	Fox sand (c)	Artificial initial ice layer	277	Hokkaido
JSA01	uniform sand (d)	Homogeneous	110	Hokkaido
JSA02	uniform sand (d)	Homogeneous	470	Hokkaido
JSA04	uniform sand (d)	Homogeneous	72	Hokkaido
JSI01	unscreened Fox silt (a)	Homogeneous	174	Hokkaido
JSI02	screened Fox silt w/ uniform sand (b/d)	Silt with sand layer at base	255	Hokkaido
JSI03	unscreened Fox silt w/ uniform sand (a/d)	Silt with sand layer at base	54	Hokkaido
JSI04	screened Fox silt w/ uniform sand (b/d)	Silt with sand layer at base	338	Hokkaido
JSI05	screened Fox silt w/ uniform sand (b/d)	Silt with sand layer at base	526	Hokkaido
JSI08	screened Fox silt (d)	Homogeneous	607	Hokkaido

*Letter represents respective subfigure in Figure 2.4

Table 2.2. Testing schedule

Test Name	Freezing Test	Time-lapse	μCT Scan	Moisture Content	Organic Content
CSA01	●	○	●	●	○
CSI01	●	○	○	●	●
JCL01	●	●	●	●	○
JCL02	●	●	○	○	○
JGR01	●	●	●	●	○
JSA01	●	●	●	●	○
JSA02	●	●	○	○	○
JSA04	●	●	○	○	○
JSI01	●	●	●	●	●
JSI02	●	●	●	●	○
JSI03	●	●	○	○	○
JSI04	●	●	○	○	○
JSI05	●	●	○	○	○
JSI08	●	●	●	●	○

○ = Test not performed

● = Test performed

Chapter 3
Results

Fourteen temperature controlled tests were conducted to study the impact of cyclic variation of the frozen-unfrozen boundary on the formation of ice in soils, as well as controlled variations on freezing front direction and amplitude on several types of soils (Figure 2.4). The following sections are separated into the two major soil types tested: coarse-grained soils (medium and coarse sand), and fine-grained soils (homogeneous silt and silt with a coarse-grained base layer). Two general testing regimes were performed: open-system warming and cooling, and closed-system cooling with open-system warming.

Several test parameters were recorded throughout each test progression. The parameters include temperatures at the upper and lower pedestals, the displacement at the top of the sample, and the water movement in and out of the sample. The displacement is presented as the frost heave ratio (FHR) — the ratio of the displaced length of the sample to the original length of the sample. The water flux is the volume of water moved into or out of the cell, normalized by the cross-sectional area of the sample. Heave and water flux rates were determined for each test by calculating the first derivative of the FHR and water flux, respectively.

For clarity, several components of this chapter are presented in the Appendices: Time-lapse videos – Appendix A, Test progression image sequences – Appendix B, Supplementary tests – Appendix C, and μCT rendering videos – Appendix D. The time-lapse videos and 3D renderings of the μCT rendering videos may be found on the DVD-ROM in the pocket.

3.1 Experiments with fine-grained homogeneous soils

Fine-grained soils tested included unscreened Fox silt (Figure 2.4(a)), screened Fox silt (less than 300 microns, Figure 2.4(b)), and Birchwood silt (Figure 2.4(e)). Tests in this category include: JSI08, JSI01, CSI01, and JCL02. Table 3.1 is a summary of all of the testing conducted on fine-grained homogeneous soils, and sample JCL02 test data is presented in Appendix C.

Table 3.1. Test parameters for experiments with fine-grained homogeneous soils

Sample Name	Test Type*	Start Time (hrs)	End Time (hrs)	T_{top} Min. (°C)	T_{top} Max. (°C)	T_{bottom} Min. (°C)	T_{bottom} Max. (°C)	Cycle Length (hrs)	Number of Cycles
JSI08	h	0	148	-7	-3.5	2	2	20	4
	h	148	420	-7.5	-3	2	2	36	7
	h	420	610	-3.5	-2	2	2	varies	8
JSI01	s	0	126	-7	-6	-7.5	10	8	15
	s	126	150	-8.5	-7	-7.5	15	8	3
CSI01	s	0	262	-10	-10	-7.5	12	10	25
JCL02	r	80	97	-7	-1	1	7	4	4
	r	97	150	-5	-1	3	7.5	4	12

* s = "stepped", r = "ramped", h = "hybrid" (stepped and ramped)

3.1.1 Open-system cooling and warming

3.1.1.1 Sample JSI08

Sample JSI08 was composed of screened Fox silt, initially consolidated, saturated, and frozen in the Hokkaido Cell prior to testing as described in Section 2.4. The test was split into three distinct phases (Table 3.1). The bottom temperature was held constant at approximately 2.5°C for the duration of the test, while the top temperature was varied step-wise from -7.5°C to -3°C (Figure 3.1(a,b), Table 3.1). The thermal conditions ensured that the sample was under open-system conditions while warming and cooling, because the water supply at the bottom of the sample was always able to enter the soil matrix.

Figure A.1 (Appendix A) is a condensed time-lapse video of the total test progression for sample JSI08. Select stills from the video are in Appendix B, Figure B.1.

The initial freezing of the sample did not produce any segregated ice in the sample. The test produced a thin zone of excess ice in the soil sample. The total FHR at the conclusion of the test, prior to refreezing the bottom of the sample, was 2.0%. Water was taken in during the upward movement of the frozen-unfrozen boundary, and was expelled from the sample during the downward movement of the freezing front (Figure 3.1(d)). A simi-

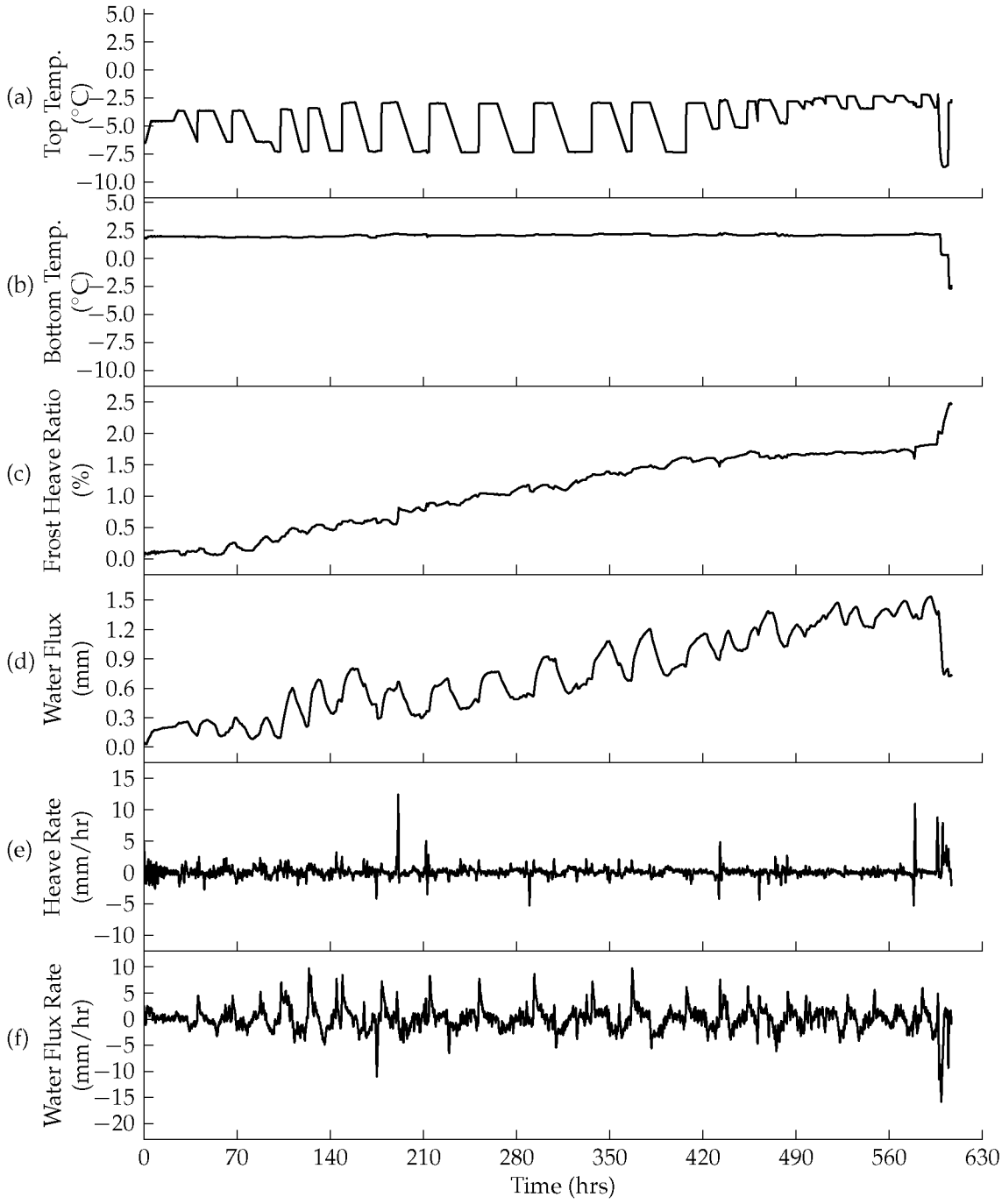

Figure 3.1. JSI08 soil temperatures (a,b), frost heave ratio (c), water flux (d), heave rate (e), and water flux rate (f).

lar trend is seen in the FHR wherein the sample length decreases slightly during warming (Figure 3.1(c)). This indicates that the soil was frozen to the cell walls. However, because of the construction of the cell, which allowed for vertical movement of the cell wall (Figure 2.1–A), the effect is the same as if the sample was not frozen to the sidewalls. Implied freezing to the cell walls was a chief complaint against the Benkleman group's experiments, and detracted from their hypothesis because they had no data to prove that it was not occurring in their experiments.

A moisture content profile for sample JSI08 was determined at the termination of the test (Figure 3.2). The sub-sample from 23 mm to 33 mm contained the ice lens. The moisture content below the ice lens was slightly higher than that immediately above, 46.3% versus 43.1%, respectively.

A μCT scan was performed (Figures 3.3, 3.4, D.1). The scan is a sub-sample of the test sample, imaged along the vertical axis of the core, centered across the ice layer in the sample. Results are presented in two formats – two-dimensional cross-sections and three-dimensional volumetric renderings. Individual soil grains are smaller than the pixel size of the scan, hence the homogeneous appearance of the soil mass in Figures 3.3 and 3.4. The main ice body is easily identified in the 3D renderings (Figure 3.4). A second, thin ice layer just below the main ice lens is identifiable in scan data, but was not apparent from visual observations of the sample. The second ice layer was created by a brief, rapid increase in temperature on the upper pedestal immediately prior to refreezing the remainder of the sample at the end of the test. No gas was identified in the scans.

The μCT-derived relative density of the sample was plotted as a function of height (Figure 3.5). Figure 3.5(a) indicates three distinct regions: below the ice layer (higher density), the ice layer (lower density), followed by above the ice layer. The small decrease in density near the bottom of the scanned region is the thin ice layer noted earlier. Figure 3.5(b) shows that the majority of the scanned region of the sample was composed of high density material – mostly silt.

3.1.2 Closed-system cooling and open-system warming

3.1.2.1 Sample JSI01

Sample JSI01 was composed of unscreened Fox silt, initially consolidated, saturated, and frozen in the Hokkaido Cell prior to testing, as described in Section 2.4. The test was

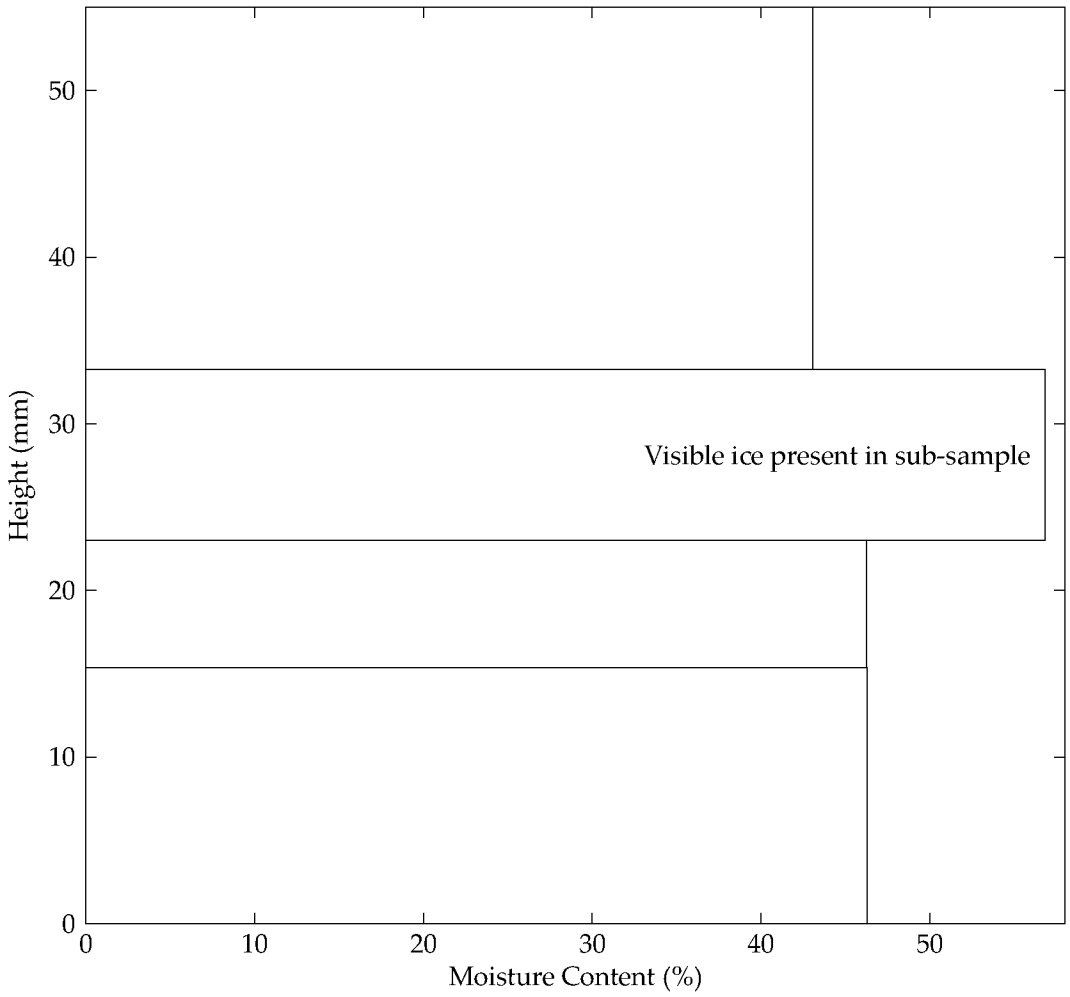

Figure 3.2. JSI08 moisture content variation with height.

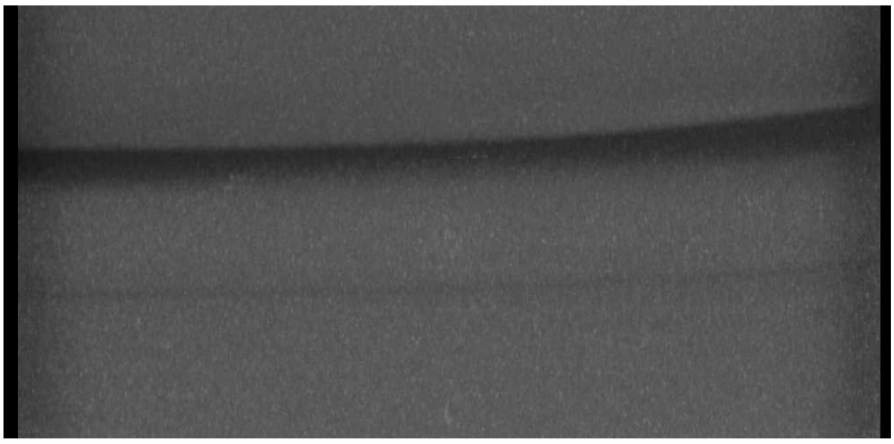

(a) Maximum density projection, vertical profile, height = 16.82 mm, diameter = 34.46 mm, silt with two ice layers.

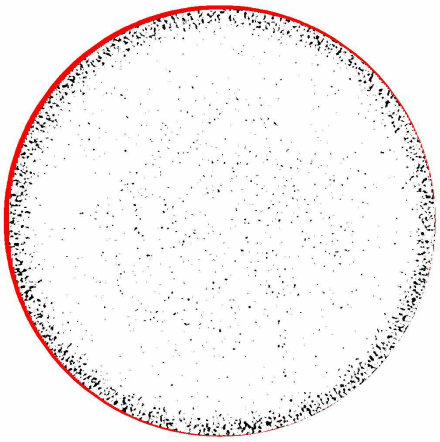

(b) Horizontal plane at height of 0.55 mm

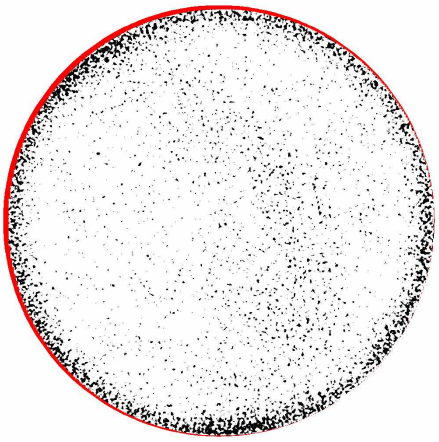

(c) Horizontal plane at height of 6.48 mm

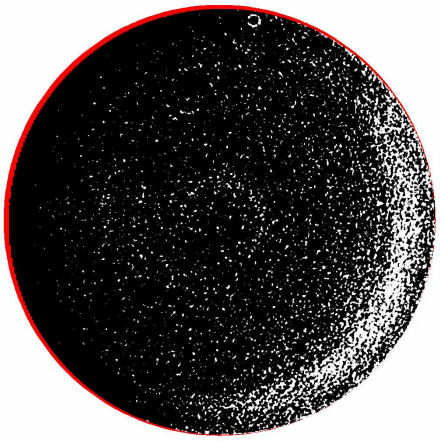

(d) Horizontal plane at height of 11.58 mm

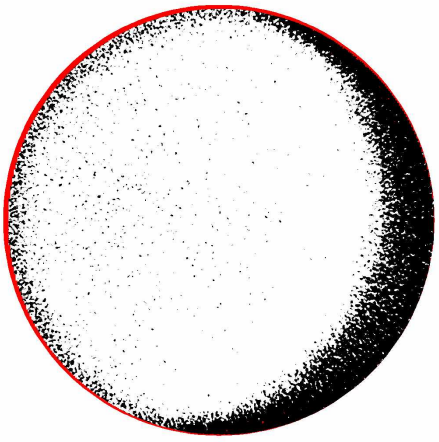

(e) Horizontal plane at height of 12.99 mm

Figure 3.3. JSI08 X-ray μCT cross-sections. See Figure 3.5 for threshold value. Threshold methods discussed in Section 2.3

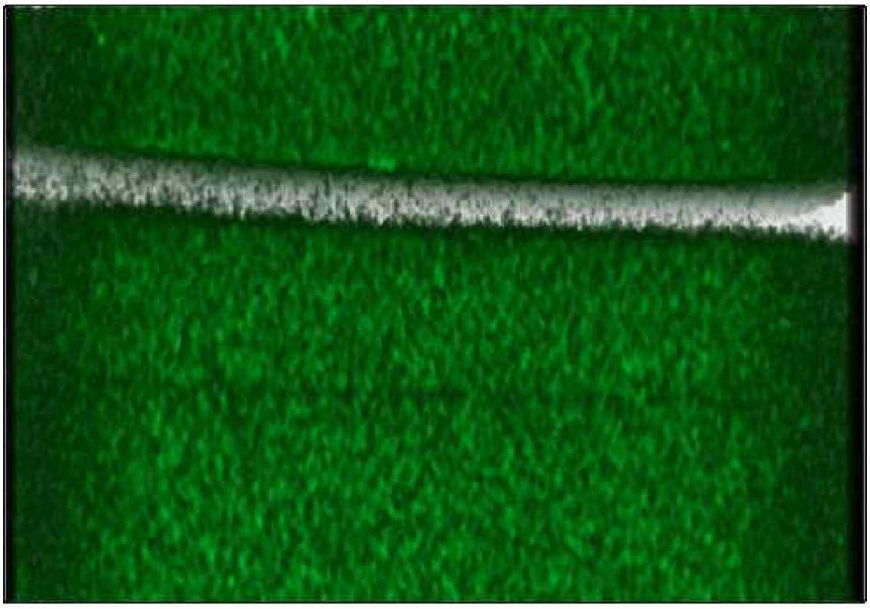

(a) Rendering view 1

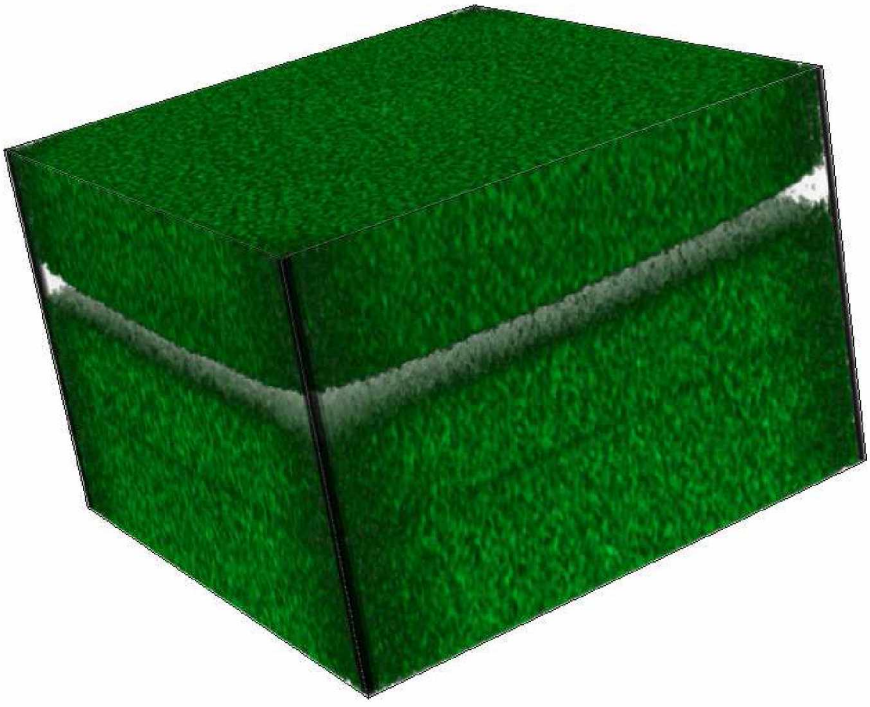

(b) Rendering view 2

Figure 3.4. JSI08 μCT soil renderings. Sub-sample is 16.82 mm tall, 24.26 mm wide and deep. See Figure 2.7 for color transfer function.

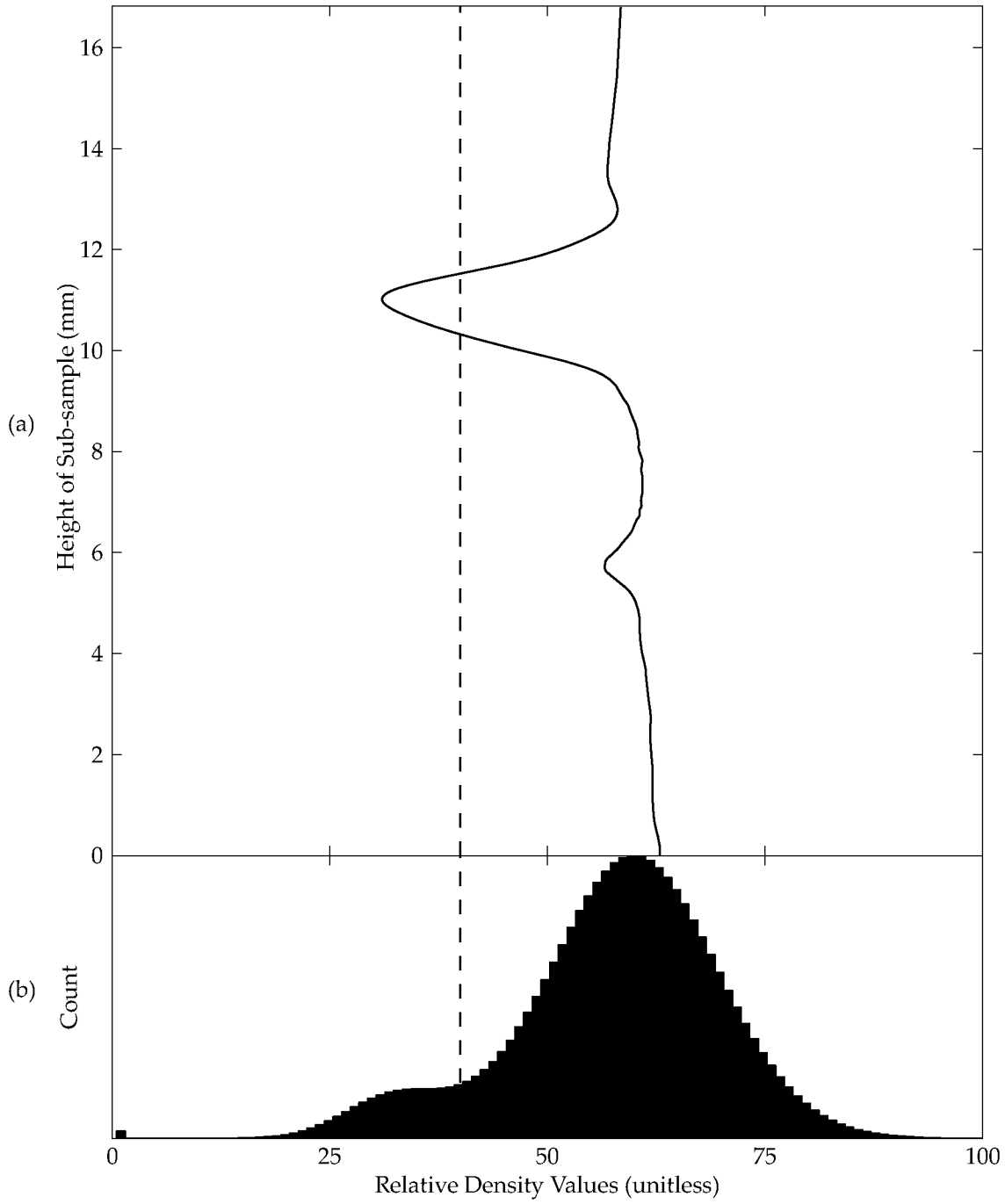

Figure 3.5. JSI08 μCT-derived relative density profile (a) and density histogram (b). Threshold value of 40 selected for scan data. See Section 2.3 and Figure 2.7 for information regarding density values.

divided into two distinct phases of testing (Table 3.1). The top temperature was held constant at approximately -7°C for the duration of the test, while the bottom temperature was varied step-wise from -8.5°C to 15°C (4 hours warming, 4 hours cooling, Figure 3.6(a,b), Table 3.1). These thermal conditions ensured that the sample was under closed-system conditions while cooling and open-system conditions while warming. The free water supply at the bottom of the sample was blocked from entering the sample during cooling due to the presence of pore ice, but free to enter the sample during warming when the ice was no longer preventing liquid transport.

Figure A.2 (Appendix A) is a condensed time-lapse video of the total test progression for sample JSI01. Select stills from the video are in Appendix B, Figure B.2. The initial freezing of the sample did not produce any segregated ice. Movement of the frozen-thawed interface was visible during the first warming cycle. As the frozen-thawed interface advanced upward, a small void formed at the bottom of the sample and increased as the interface moved. When the first cycle began to refreeze, a thin horizontal line across the sample was visible as the water turned to ice.

The advance of the freezing front from the top and bottom of the sample was visible. The point where the two freezing fronts intersected was several centimeters below the initial ice layer. The maximum extent of the thawed soil for the following 10 cycles was several millimeters below the previous ice layer, creating an alternating section of silt and ice, each layer 1 to 2 mm thick. The location of the frozen-thawed interface was visible during each warming period – the upward progress of the warming soil was slowed due to the increased moisture content at this location. After 11 cycles (93 hours), the increased moisture content tipped the thermal equilibrium such that the maximum extent of thaw was several centimeters below the previous intersection point. This cycle marked the second phase of ice accumulation for this test.

Thaw loosening of the lower half of the sample was apparent throughout the test, and became more exaggerated after the 11th cycle. The following four cycles accumulated more ice than the previous 11, and the presence of gas bubbles was noted. Upon refreezing, the silt was compressed upwards as the freezing front advanced from the bottom of the sample. The final three cycles were cycled to 14.5°C during the warming stage. The LVDT stroke maxed out at approximately 126 hours – no displacement data is available after that time for the test. Significant accumulation of organics near the ice/water layer was noted; the organic debris floated to the top of the thawed zone during each of the last

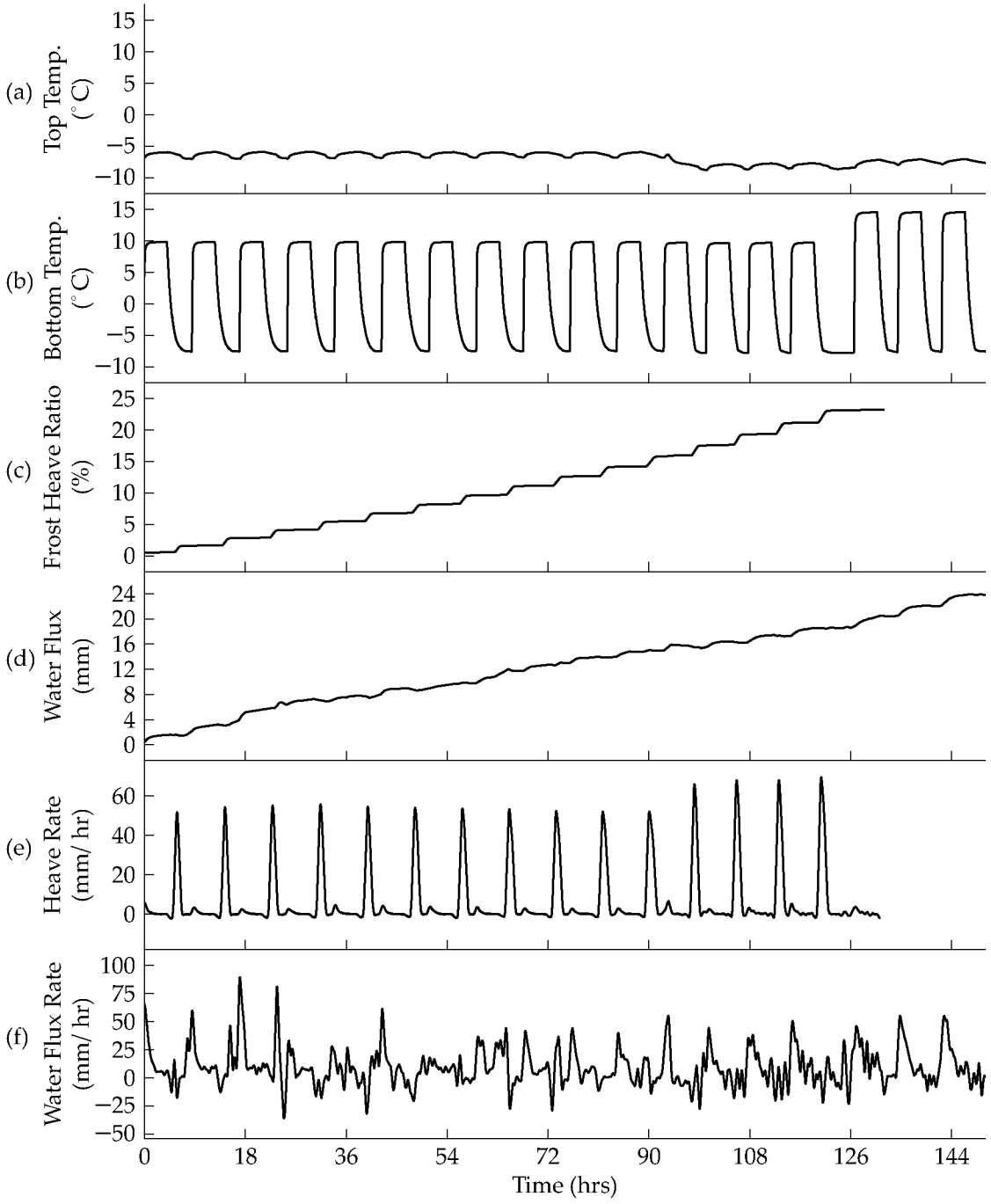

Figure 3.6. JSI01 soil temperatures (a,b), frost heave ratio (c), water flux (d), heave rate (e), and water flux rate (f).

three cycles. The thawed organics released gas during this portion of the test, which was visible as bubbles at the top of the water layer. The bubbles were frozen in place between warming cycles.

Throughout the duration of the test approximately 24 mm of water (area normalized) was transported into the sample, and over 25 mm of surface displacement occurred. The water flux rate (Figure 3.6(f)) indicates that at the moment just before the warming cycles began water was expelled into the water reservoir. This expulsion is due to the formation of ice in the lower pedestal and supply line. The heave rate indicates brief rapid increases in surface displacement – between 50 and 60 mm/hr, followed by a slower brief rise in heave rate (2 to 5 mm/hr), which coincided with the start of the warming cycle (Figure 3.6).

A moisture content profile for sample JSI01 was determined at the termination of the test (Figure 3.7). The sub-sample from 23 mm to 38 mm contained the ice lens. The moisture content immediately below the ice lens was higher than that directly above it. Similarly, an organic content profile was determined for the sample (Figure 3.8). The organic content was determined after the moisture content, and is presented as a percentage of the dried sample mass that was lost on ignition. The sub-sample with the ice layer had the highest organic content, corresponding with the observation of floating organics in the time-lapse video. The organic content below the ice sub-sample is slightly lower than those above, due to the upward migration of organics during warming.

A μCT scan was performed on sample JSI01 (Figures 3.9, 3.10, D.2). The alternating layers of ice and silt are visible at the top of the scanned region. Several dense grains of sand are visible in Figure 3.9(a). The dark zone below the alternating layers is primarily ice and gas. A significant layer of entrained gas bubbles is visible near the bottom of the scanned volume, which is likely where the maximum extent of the frozen-thawed interface reached during the final warming cycle of the test.

The μCT-derived relative density of the sample was plotted as a function of height (Figure 3.11). Figure 3.11(b) shows that the majority of the sample was composed of low density material – primarily ice. Slight fluctuations in the density profile in Figure 3.11(a) correlate with the alternating layers of silt and ice.

3.1.2.2 Sample CSI01

Sample CSI01 was composed of unscreened Fox silt, initially consolidated and saturated in an external cell. The sample was prepared by saturating in an acrylic cell, and

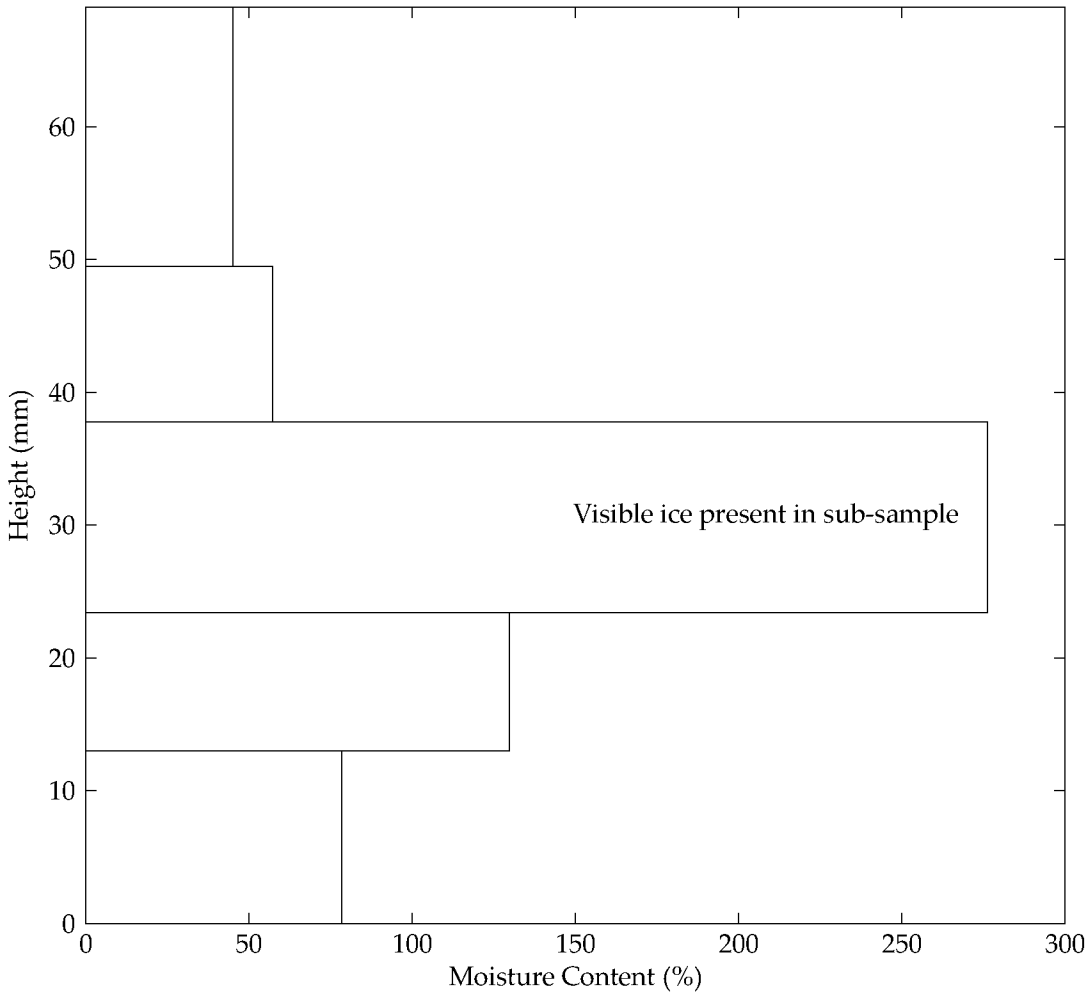

Figure 3.7. JSI01 moisture content variation with height.

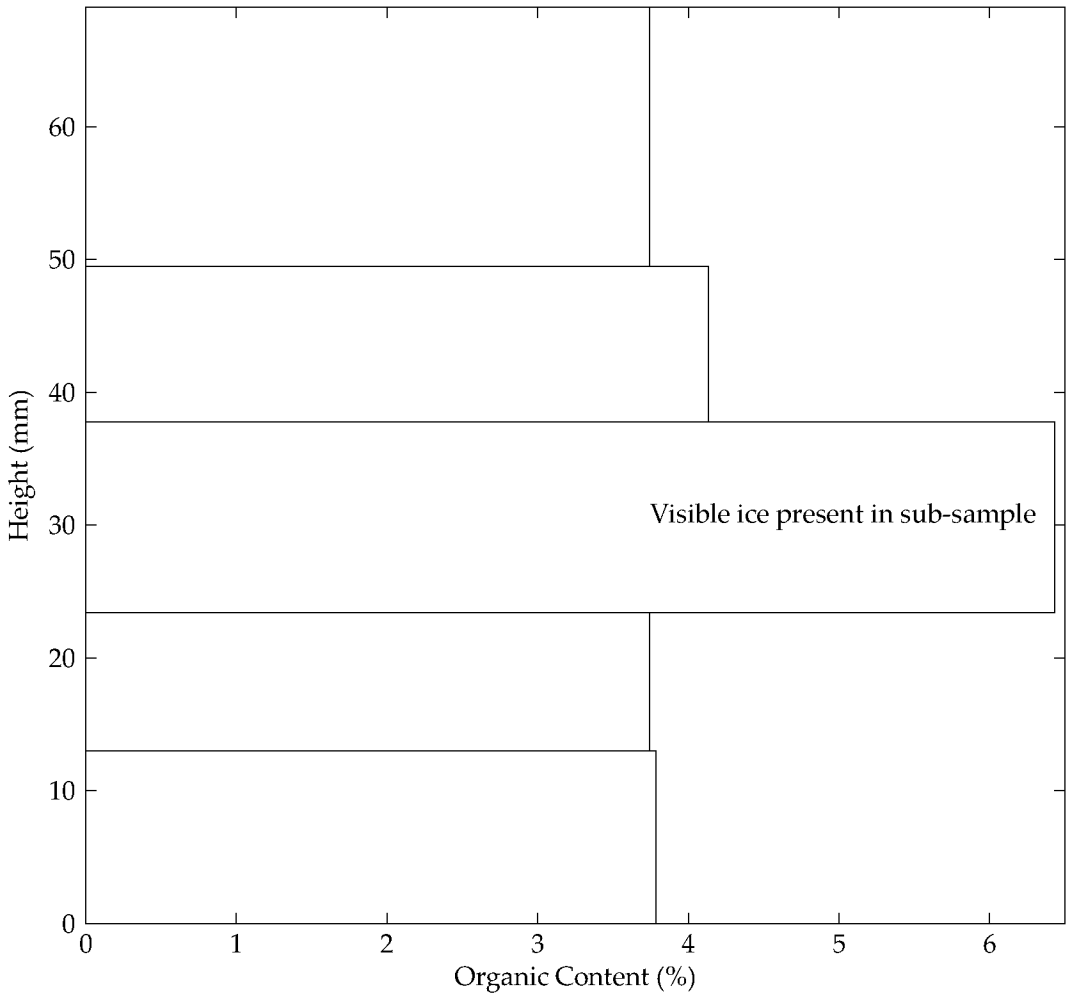

Figure 3.8. JSI01 organic content variation with height.

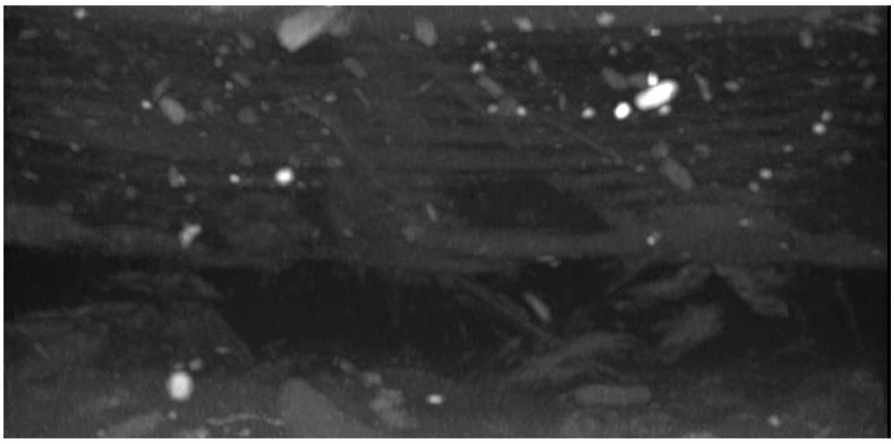

(a) Maximum density projection, vertical profile, height = 16.82 mm, diameter = 34.36 mm, ice with organics and gas, silt at top and bottom of sub-sample.

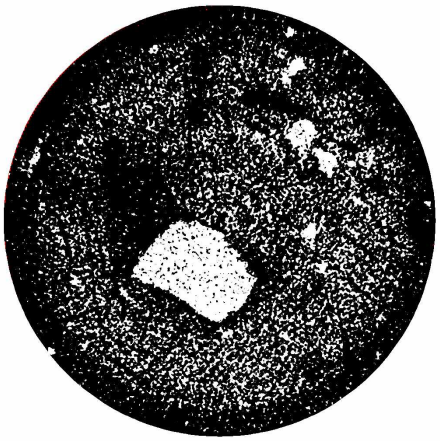

(b) Horizontal plane at height of 0.55 mm

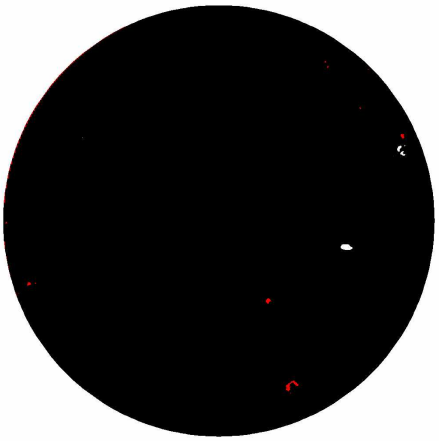

(c) Horizontal plane at height of 6.93 mm

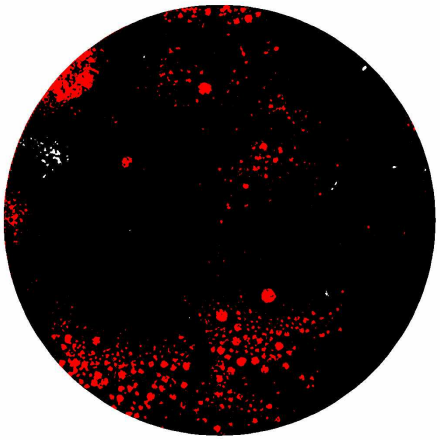

(d) Horizontal plane at height of 8.44 mm

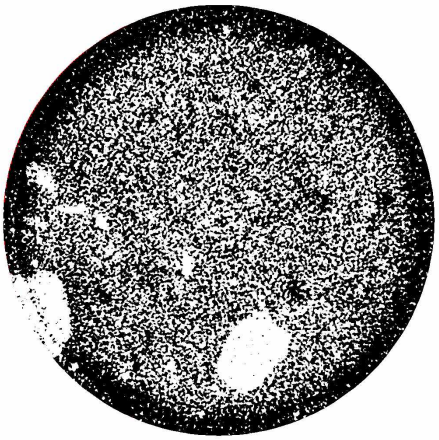

(e) Horizontal plane at height of 20.09 mm

Figure 3.9. JSI01 X-ray μCT cross-sections. See Figure 3.11 for threshold value. Threshold methods discussed in Section 2.3

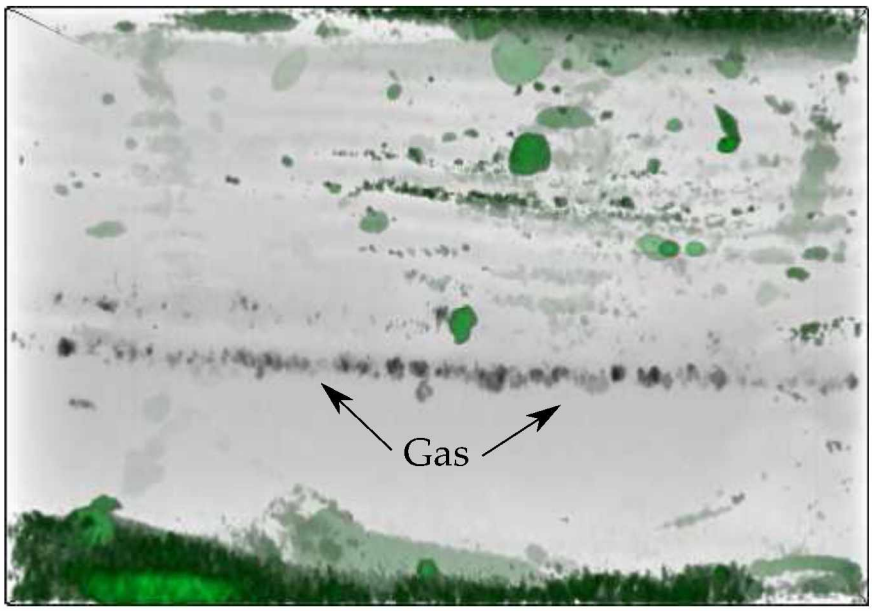

(a) Rendering view 1

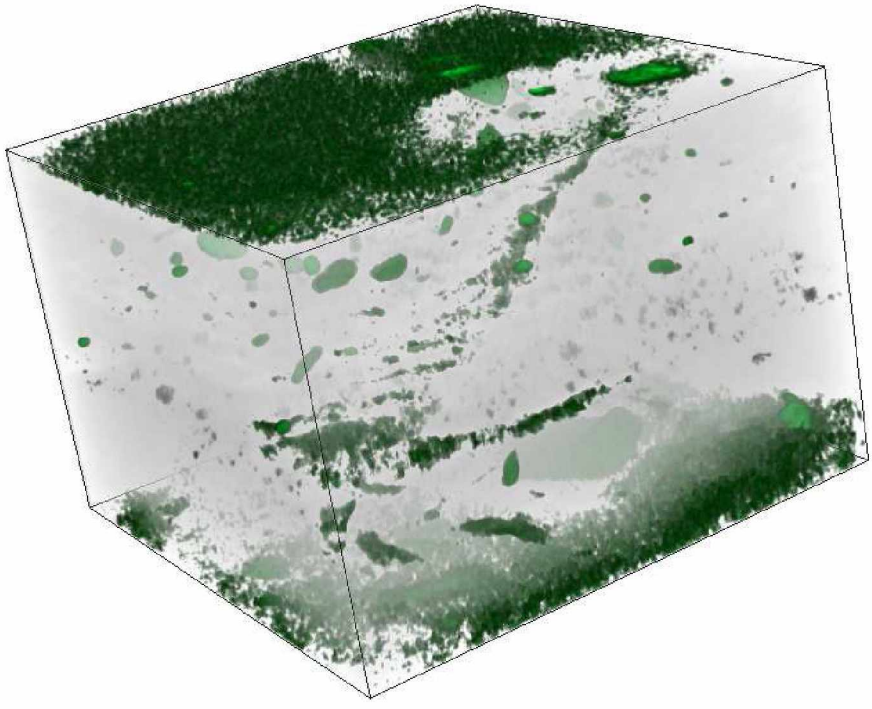

(b) Rendering view 2

Figure 3.10. JSI01 μCT soil renderings. Sub-sample is 16.82 mm tall, 24.26 mm wide and deep. See Figure 2.7 for color transfer function.

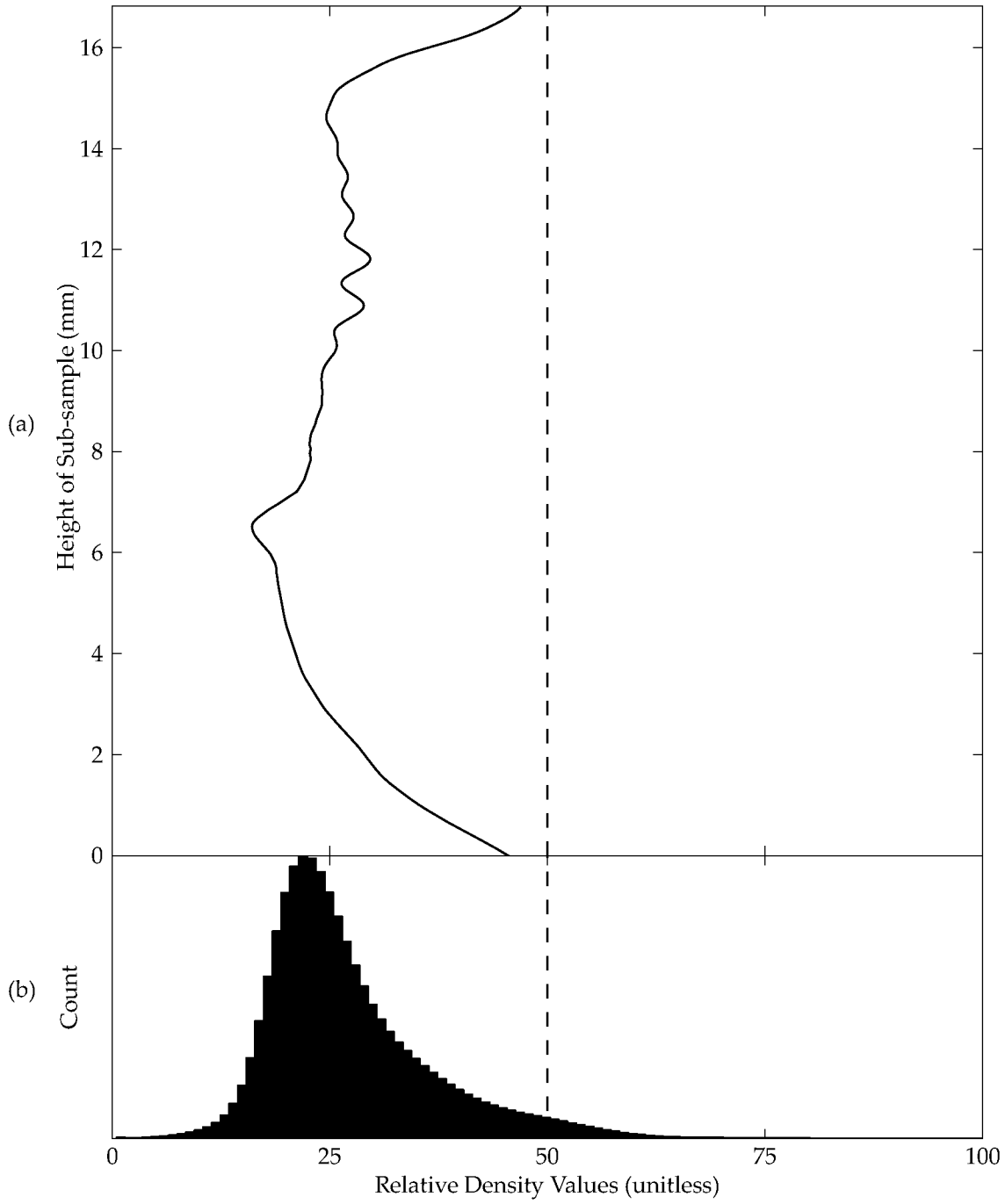

Figure 3.11. JSI01 μCT-derived relative density profile (a) and density histogram (b). Threshold value of 50 selected for scan data. See Section 2.3 and Figure 2.7 for information regarding density values.

was allowed to naturally grade while saturating. When the sample was transferred to the Laval Cell, the vertical orientation was accidentally switched, placing the larger diameter soil at the top of the sample, and the fine-grained material at the bottom. The sample was transferred to the Laval Cell, and pre-frozen prior to testing, as described in Section 2.4. The top temperature was held constant at approximately -10°C for the duration of the test, while the bottom temperature was varied step-wise from -7.5°C to 12°C (5 hours warming, 5 hours cooling, Figure 3.12(a,b), Table 3.1). These thermal conditions ensured that the sample was under closed-system conditions while cooling and open-system conditions while warming, similar to sample JSI01.

The initial freezing of the sample did not produce any segregated ice. Sample CSI01 (Figures 3.13, 3.14) developed ice in a manner similar to sample JSI01, by cutting off the water supply during cooling (closed-system). The sample experienced vertical displacement due to the phase change of the water into ice. During warming from the bottom, the sample was under open-system conditions, and was able to take water into the sample (Figure 3.12(d)).

A moisture content profile for sample CSI01 was determined at the termination of the test (Figure 3.15). The sub-samples from 32 mm to 56 mm contained the ice lens. The moisture content immediately below the ice lens was higher than that directly above. Similarly, an organic content profile was determined for the sample (Figure 3.16). The organic content was determined after the moisture content – the organic content is presented as a percentage of the dried sample mass that was lost on ignition. The sub-sample with the lowest ice layer had the highest organic content.

3.1.3 Summary of experiments on fine-grained homogeneous soils

During pre-freezing, none of the samples produced segregated ice. In general, the sample length was found to increase slightly during the initial freezing, but no visible ice was formed. When subjected to open-system cooling and warming conditions, Fox silt developed a small horizontal layer of ice in the sample, as well as an increase in moisture content in the portion of the sample that experienced freeze-thaw cycles. When the cooling was initiated from the bottom to simulate closed-system cooling, the accumulation of ice in the sample was significantly greater. During the initial freezing of samples in this category, it was noted that no segregated ice formed, or significant surface displacement occurred. However, during closed-system cooling and open-system warming phases of the test, the

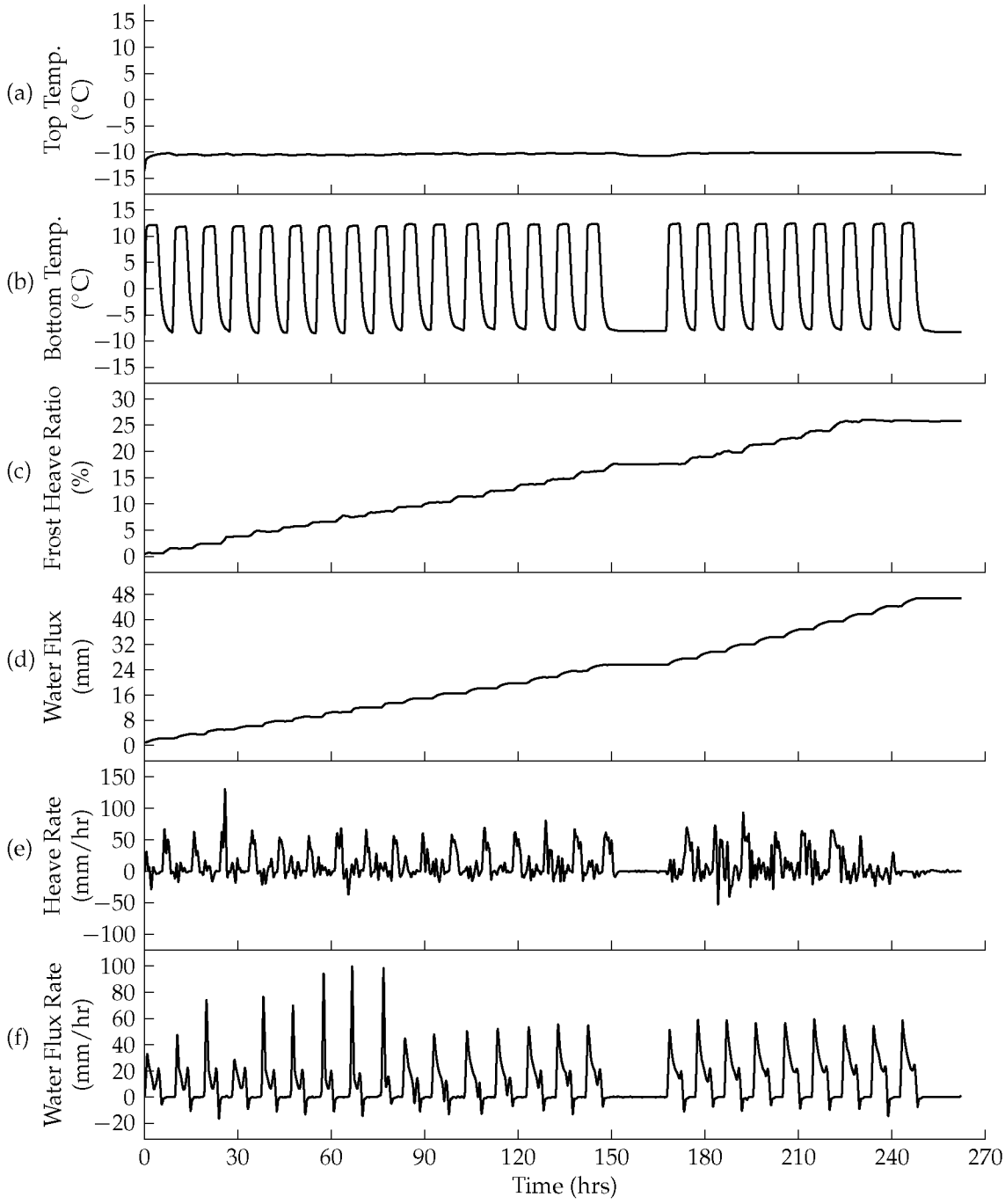

Figure 3.12. CSI01 soil temperatures (a,b), frost heave ratio (c), water flux (d), heave rate (e), and water flux rate (f).

Figure 3.13. Post-frost heave test photograph of sample CSI01.

Figure 3.14. Post-frost heave test photograph of vertical section of sample CSI01. Sample was graded due to preparation and saturation process; sample was accidentally inverted during transfer to the Laval Cell (coarse-grained material overlying fine-grained material).

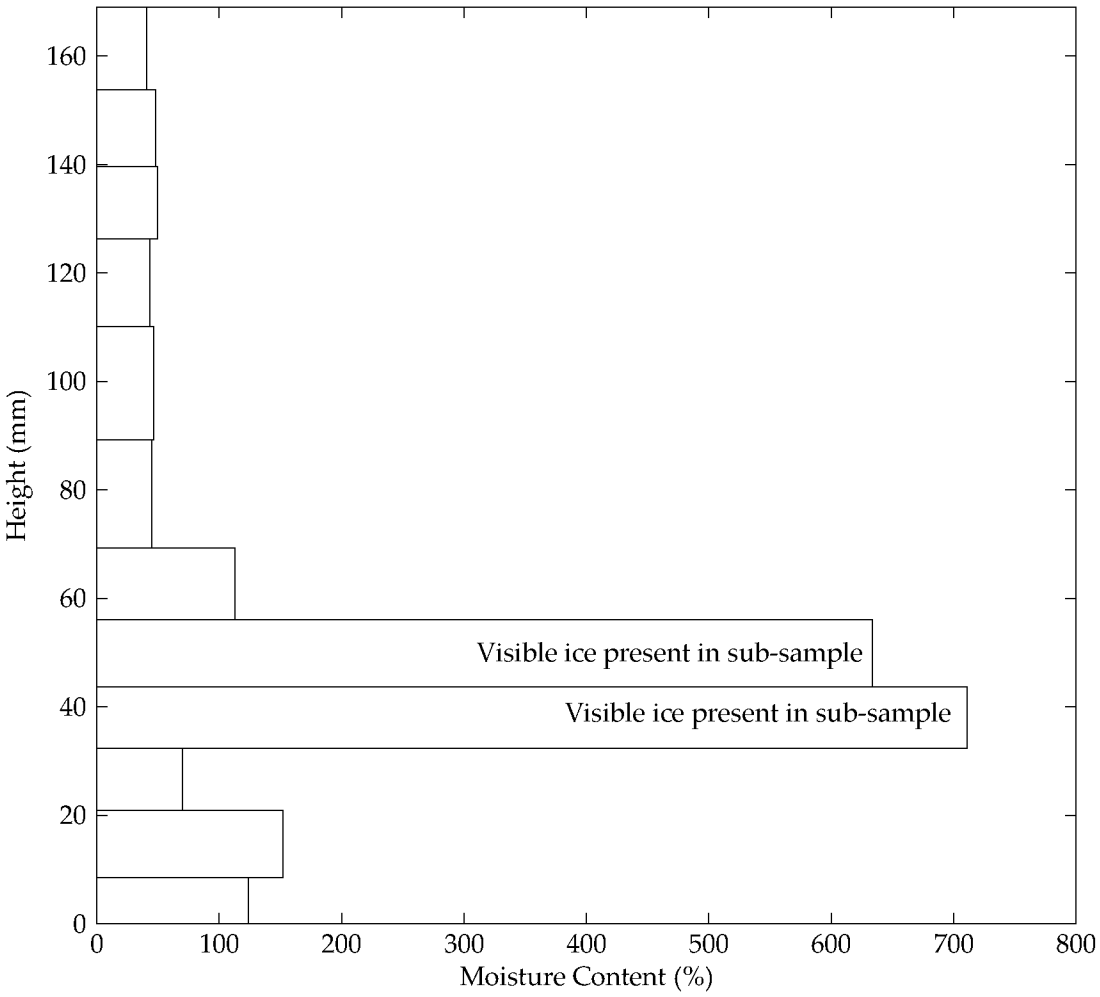

Figure 3.15. CSI01 moisture content variation with height.

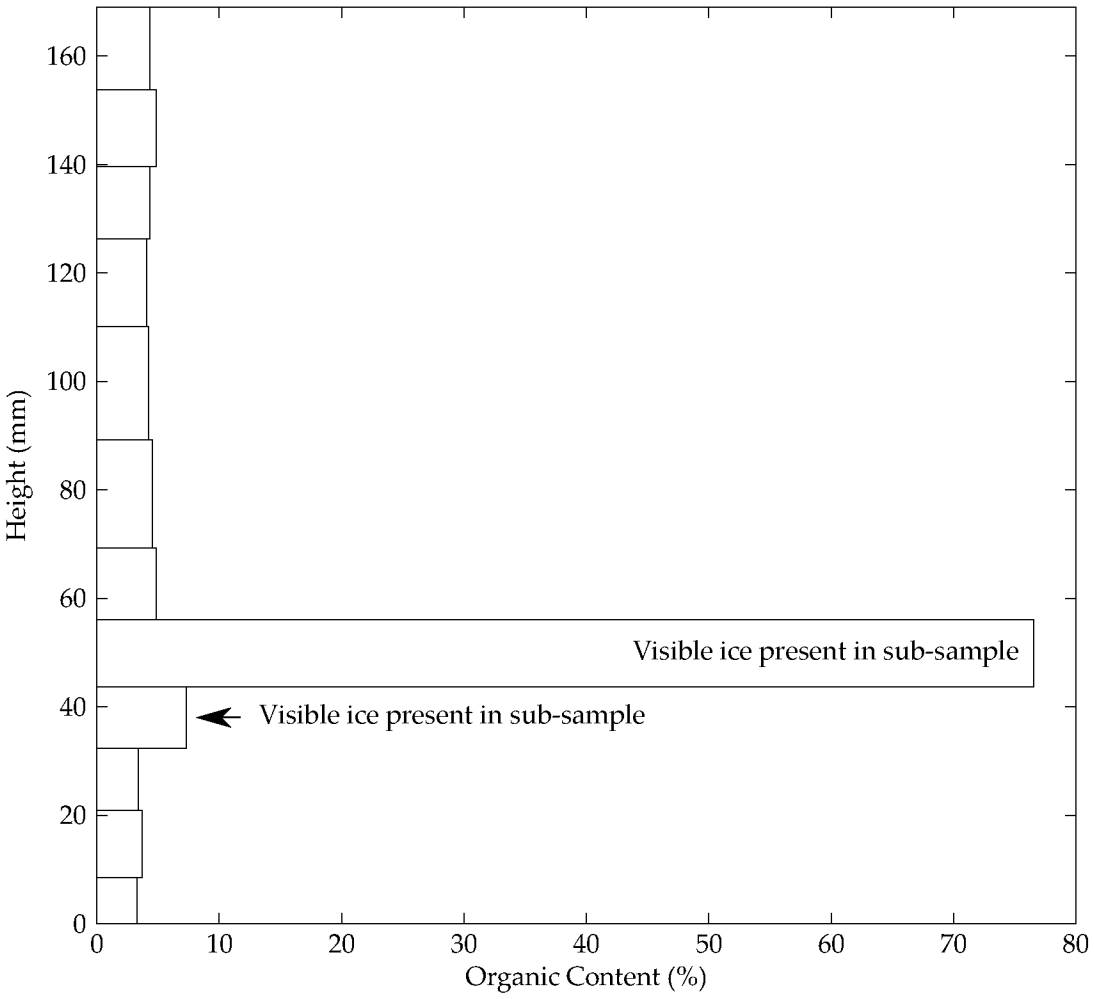

Figure 3.16. CSI01 organic content variation with height.

total FHR ranged from 20% to 25%.

3.2 Experiments with fine-grained soils with coarse-grained base layer

Fine-grained soils tested included screened Fox silt (less than 300 microns, Figure 2.4(b)), uniform sand (Figure 2.4(d)) and Birchwood silt (Figure 2.4(e)). Tests in this category include: JCL01, JSI02, JSI03, JSI04, and JSI05 (Table 3.2). Test data from samples JSI03, JSI04, and JSI05 are presented in Appendix C.

3.2.1 Open-system cooling and warming

3.2.1.1 Sample JCL01

Sample JCL01 was composed of Birchwood silt over a layer of uniform sand, initially consolidated, saturated, and frozen in the Hokkaido Cell prior to testing as described in Section 2.4. The test was divided into two distinct phases of testing (Table 3.2). The bottom temperature was held constant at approximately 3°C for the duration of the test, while the top temperature was varied linearly from approximately -6.5°C to -1°C for most of the test (Figure 3.17(a,b), Table 3.2). These thermal conditions ensured that the sample was under open-system conditions while cooling and warming.

Figure A.4 (Appendix A) is a condensed time-lapse video of the total test progression for sample JCL01. Select stills from the video are in Appendix B, Figure B.4. The first 35 hours of testing accidentally had two cycles at the top pedestal varying from -7°C to 8°C, which thawed the sample from the top down, and allowed the bottom of the sample to expand upward. After this error was noted, the programming was corrected and several cycles from -3°C to -7°C were applied to the sample, which initiated surface displacement of the sample. Each cycle following this phase saw upward displacement of the sample during cooling, and downward displacement during warming (Figure 3.17(c,e)). Visible ice was noted after approximately 70 hours of elapsed test time. A second layer of ice was noted after approximately 90 hours. A third layer of ice was noted after approximately 105 hours. A fourth layer of ice developed after approximately 140 hours, and then merged with the third layer over the next several cycles. After approximately 206 hours the surface displacement halted. From 222 hours to 248 hours, the camera malfunctioned and did not capture images, however the test continued. Image capture resumed after 248 hours. At 275 hours the top temperature was increased to -2.5°C. During this extended warming,

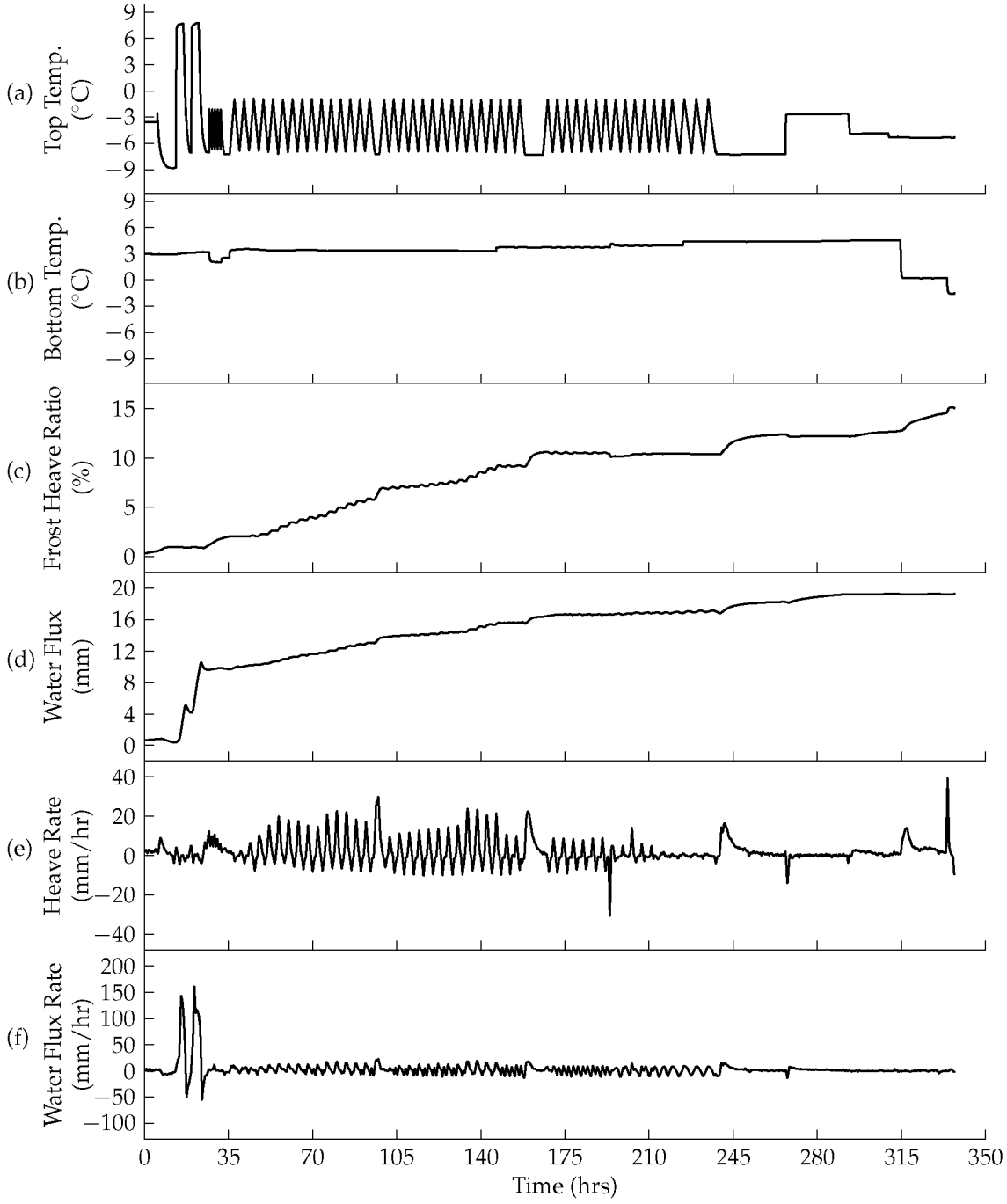

Figure 3.17. JCL01 soil temperatures (a,b), frost heave ratio (c), water flux (d), heave rate (e), and water flux rate (f).

Table 3.2. Test parameters for experiments with fine-grained soils with coarse-grained base layer

Sample Name	Test Type*	Start Time (hrs)	End Time (hrs)	T_{top} Min. (°C)	T_{top} Max. (°C)	T_{bottom} Min. (°C)	T_{bottom} Max. (°C)	Cycle Length (hrs)	Number of Cycles
JCL01	r	27	35	-6.5	-2	2	3	1	5
	r	35	238	-6.5	-1	3	4	4	47
	s	238	314	-7	-2.5	0	4.5	24	1
JSI02	r	0	22	-4.5	-0.5	0.5	3	12	2
	r	22	236	-4.5	-1.5	0.5	2	12	17
	r	236	270	-5.5	-2	0.5	1.5	12	1.5
JSI03	r	0	54	-5	-1.5	1.5	2.5	24	2
JSI04	r	0	313	-4	-1	1.5	1.5	24	13
JSI05	r	0	457	-6.5	-3	1	3	24	19

* s = "stepped", r = "ramped", h = "hybrid" (stepped and ramped)

the ice/water void moved upward. When the upper layer of silt thawed and particles moved downward, the water-filled void became cloudy with suspended particles. During refreezing, the suspended silt was pushed downward ahead of the freezing ice.

A moisture content profile for sample JCL01 was determined at the termination of the test (Figure 3.18). The sub-sample from 44 mm to 51 mm contained the ice lens. The moisture content immediately below the ice lens was lower than that directly above, however the lowest sub-sample had the second largest moisture content.

A μCT scan was performed on sample JCL01 (Figures 3.19, 3.20, D.3). Several high density grains are visible in Figure 3.19(a). The ring visible in the center of the scan data is an artifact of the scanning procedure, and is not an actual feature of the sample (Figures 3.19, 3.20). Elongated gas bubbles were identified in the 3D rendering, and are visible as well in Figure 3.19(c). The bubbles likely came from the last warming cycle, which was significantly longer than the previous cycles. Refreezing was slow, and the freezing front appeared to push the bubbles downward, stretching them out.

The μCT-derived relative density of the sample was plotted as a function of height

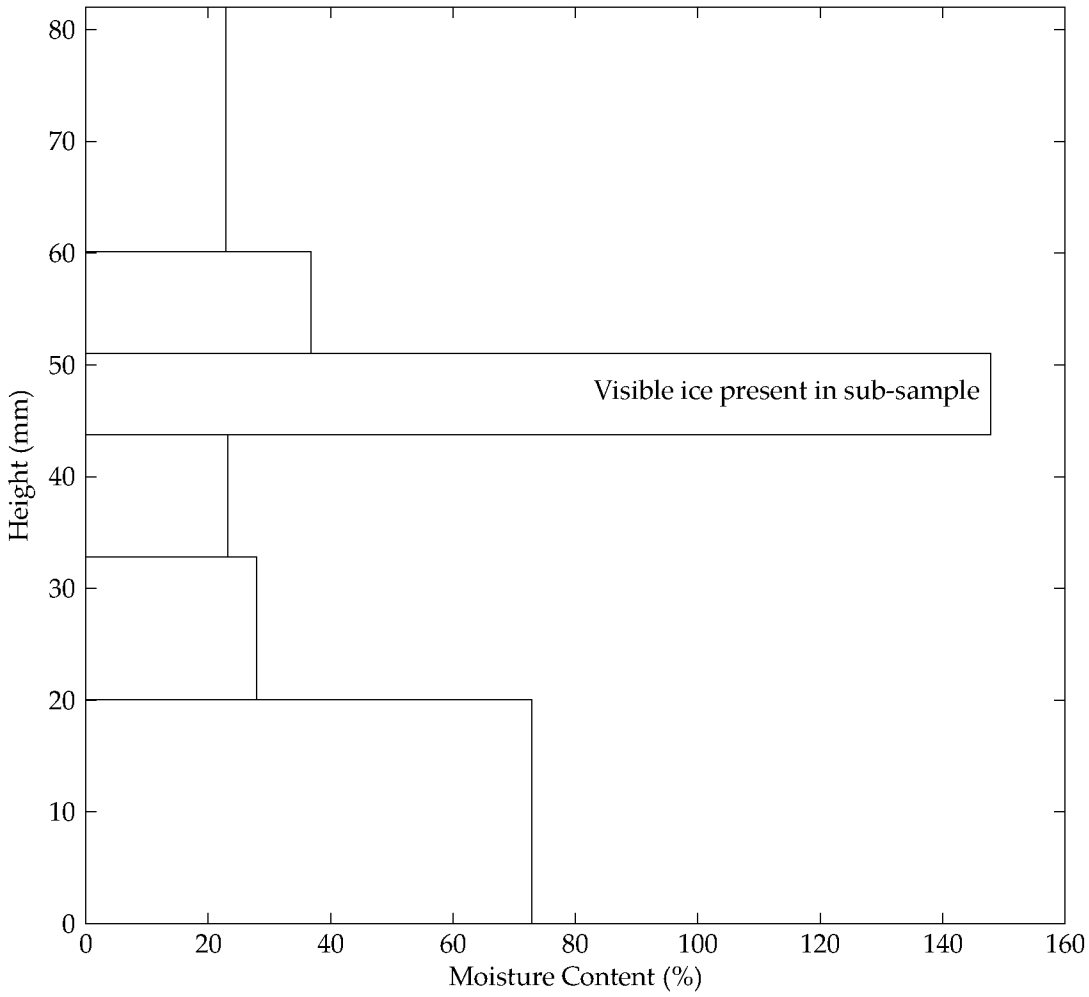

Figure 3.18. JCL01 moisture content variation with height.

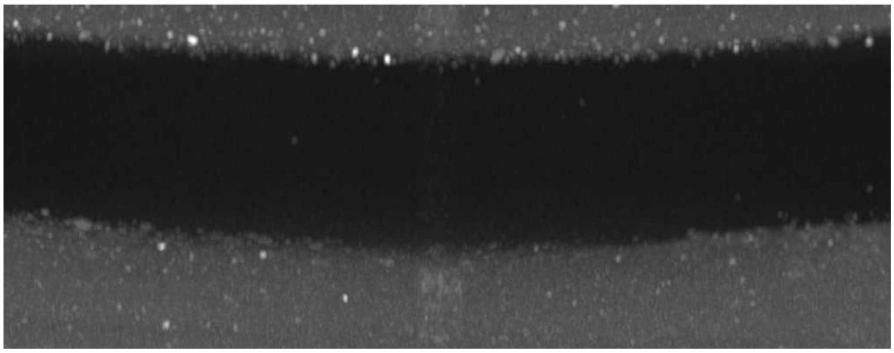

(a) Maximum density projection, vertical profile, height = 16.82 mm, diameter = 34.46 mm, silt with trace coarse-grained sand, ice layer in center.

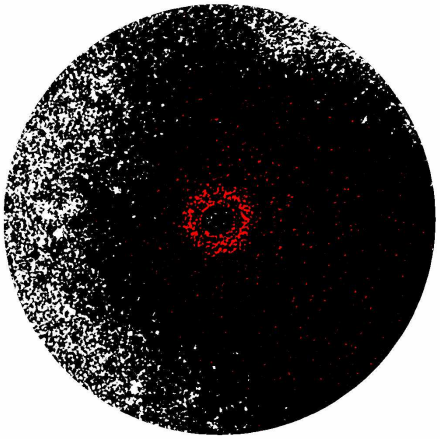

(b) Horizontal plane at height of 3.62 mm

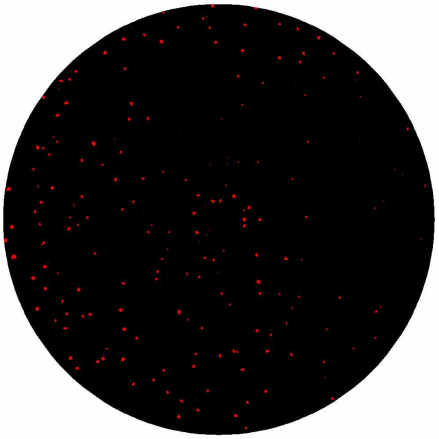

(c) Horizontal plane at height of 6.20 mm

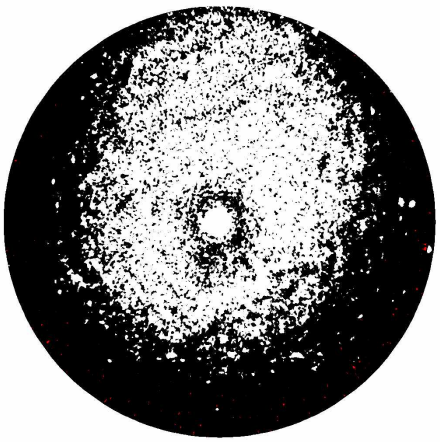

(d) Horizontal plane at height of 11.85 mm

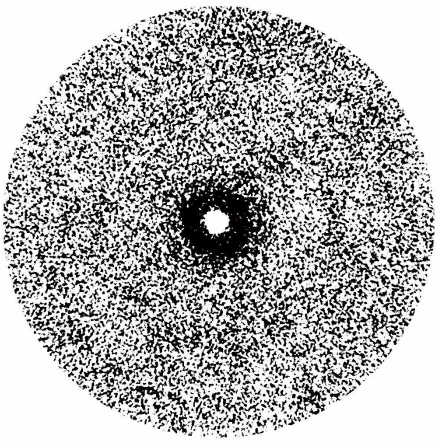

(e) Horizontal plane at height of 13.30 mm

Figure 3.19. JCL01 X-ray μCT cross-sections. See Figure 3.21 for threshold value. Threshold methods discussed in Section 2.3. Ring artifact visible at center of cross-sections due to scanner settings, not an actual feature of the sample.

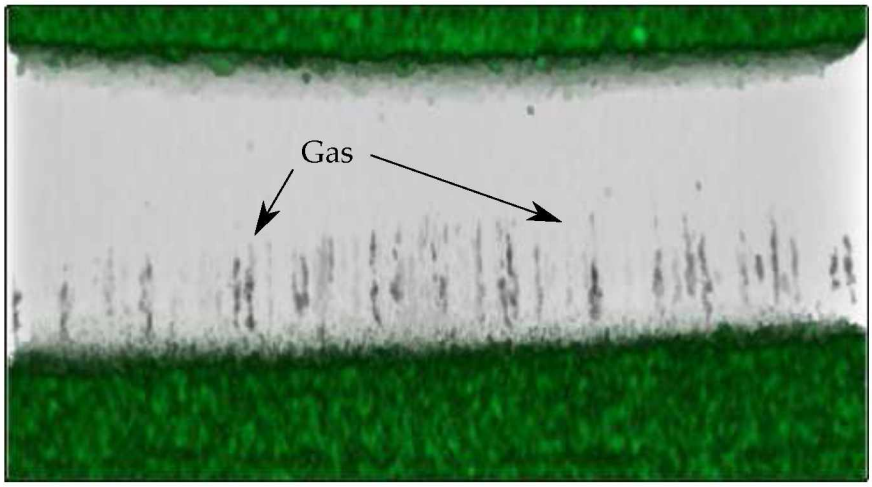

(a) Rendering view 1

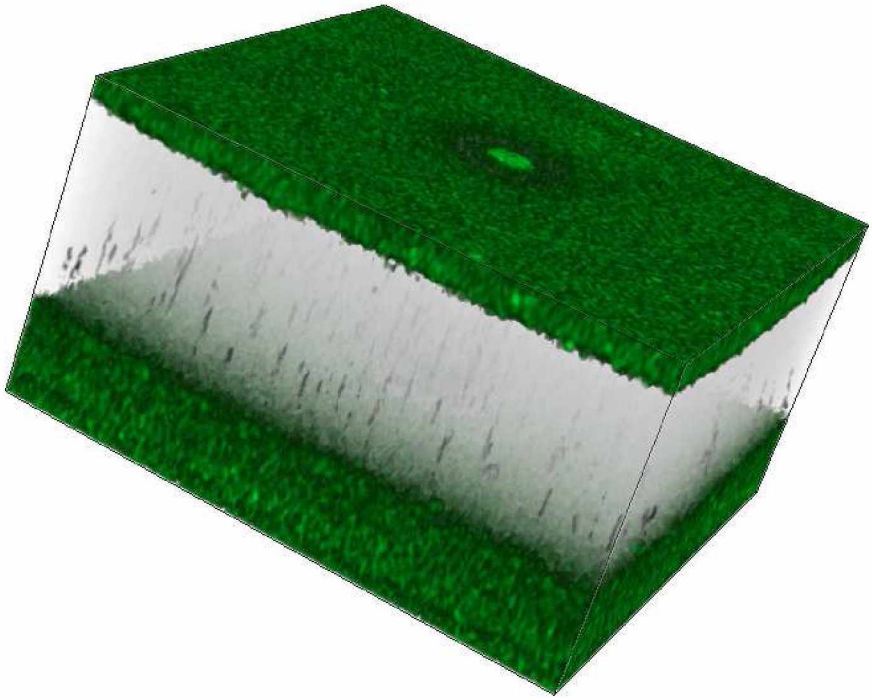

(b) Rendering view 2

Figure 3.20. JCL01 μCT soil renderings. Sub-sample is 16.82 mm tall, 24.26 mm wide and deep. See Figure 2.7 for color transfer function. Ring artifact visible at center of renderings due to scanner settings, not an actual feature of the sample.

(Figure 3.21). Figure 3.21(b) shows that part of the sub-sample was composed of high density material – primarily soil, while a significant amount of low density material (ice and organics) was present in the center of the sub-sample.

3.2.1.2 Sample JSI02

Sample JSI02 was composed of screened Fox silt over a layer of uniform sand, initially consolidated, saturated, and frozen in the Hokkaido Cell prior to testing as described in Section 2.4. The test was divided into 3 distinct phases of testing (Table 3.2). The top temperature was linearly varied from approximately -4.5°C to -1.5°C for most of the test, while the bottom temperature was varied linearly from approximately 0.5°C to 3°C (6 hours warming, 6 hours cooling, Figure 3.22(a,b), Table 3.2). The sample was under open-system conditions while cooling and warming.

The initial freezing of the sample prior to testing did not produce any segregated ice. Total surface displacement was effectively zero at the conclusion of the test, however several millimeters of ice were formed near the center of the sample. Approximately 2.5 millimeters of water (area normalized) were taken in by the sample during testing. The water flux rate cycled between positive and negative during testing, indicating that water was being expelled from the system during the downward movement of the freezing front (Figure 3.22(f)).

Figure A.5 (Appendix A) is a condensed time-lapse video of the total test progression for sample JSI02. Select stills from the video are in Appendix B, Figure B.5. The ice layer did not begin forming until approximately 75 hours into the test, due to the changing thermal equilibrium from the temperature cycles. Several thin layers were started in the upper portion of the sample, but each subsequent cycle advanced the freezing front to a height below the last cycle, therefore not thawing the previously accumulated ice. Once the sample reached equilibrium the accumulation of ice was visible upon each cooling and warming cycle. Gas bubbles became visible in the ice layer during the final several cycles, increasing with each successive cycle.

A moisture content profile for sample JSI02 was determined at the termination of the test (Figure 3.23). The sub-sample from 23 mm to 34 mm contained the ice lens. The moisture contents below and above were 33% and 62%, respectively.

A μCT scan was performed on sample JSI02 (Figures 3.24, 3.25, D.4). Figure 3.24(a) shows the distribution of coarse-grained of sand in the sample. There is a higher con-

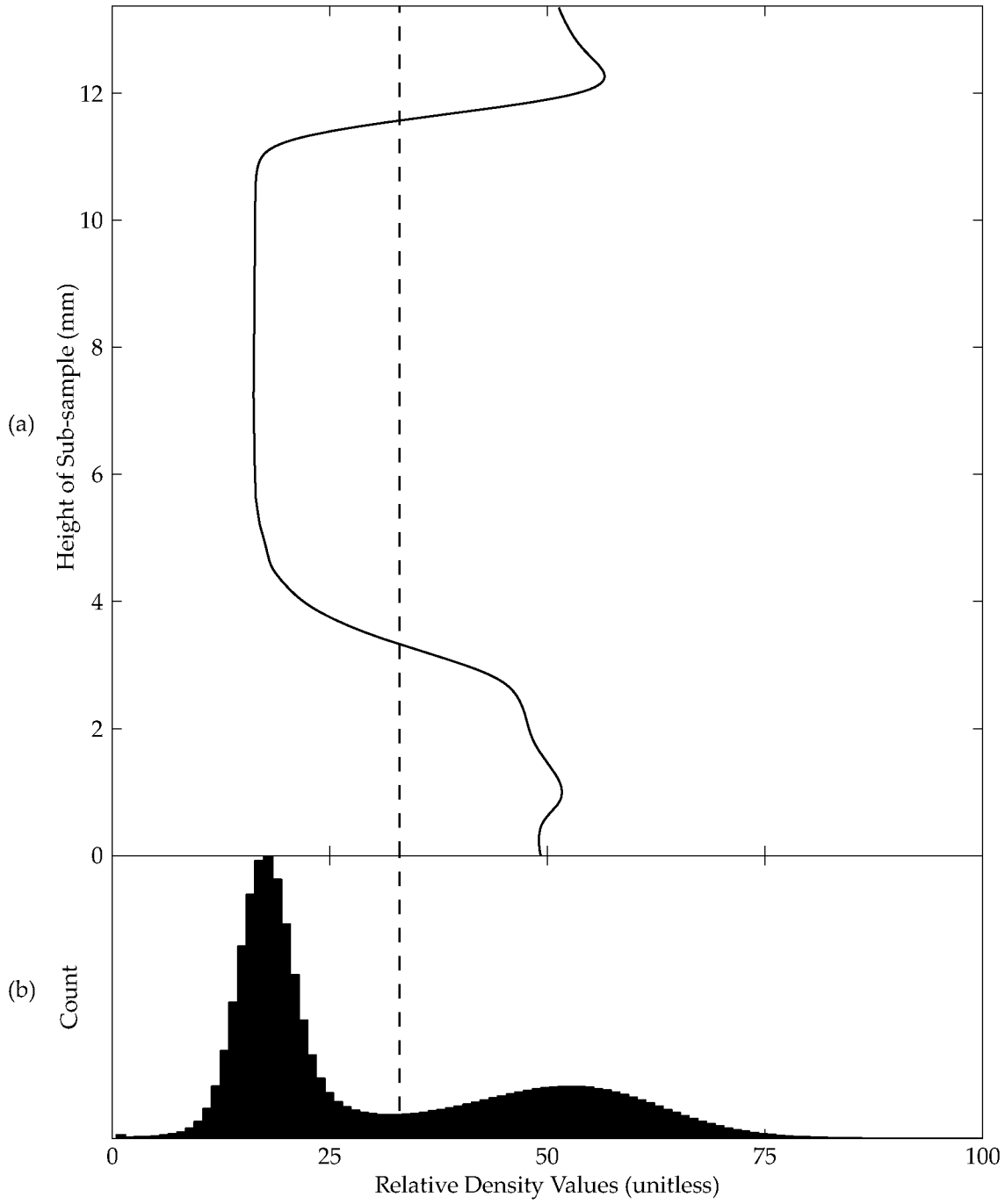

Figure 3.21. JCL01 μCT-derived relative density profile (a) and density histogram (b). Threshold value of 33 selected for scan data. See Section 2.3 and Figure 2.7 for information regarding density values.

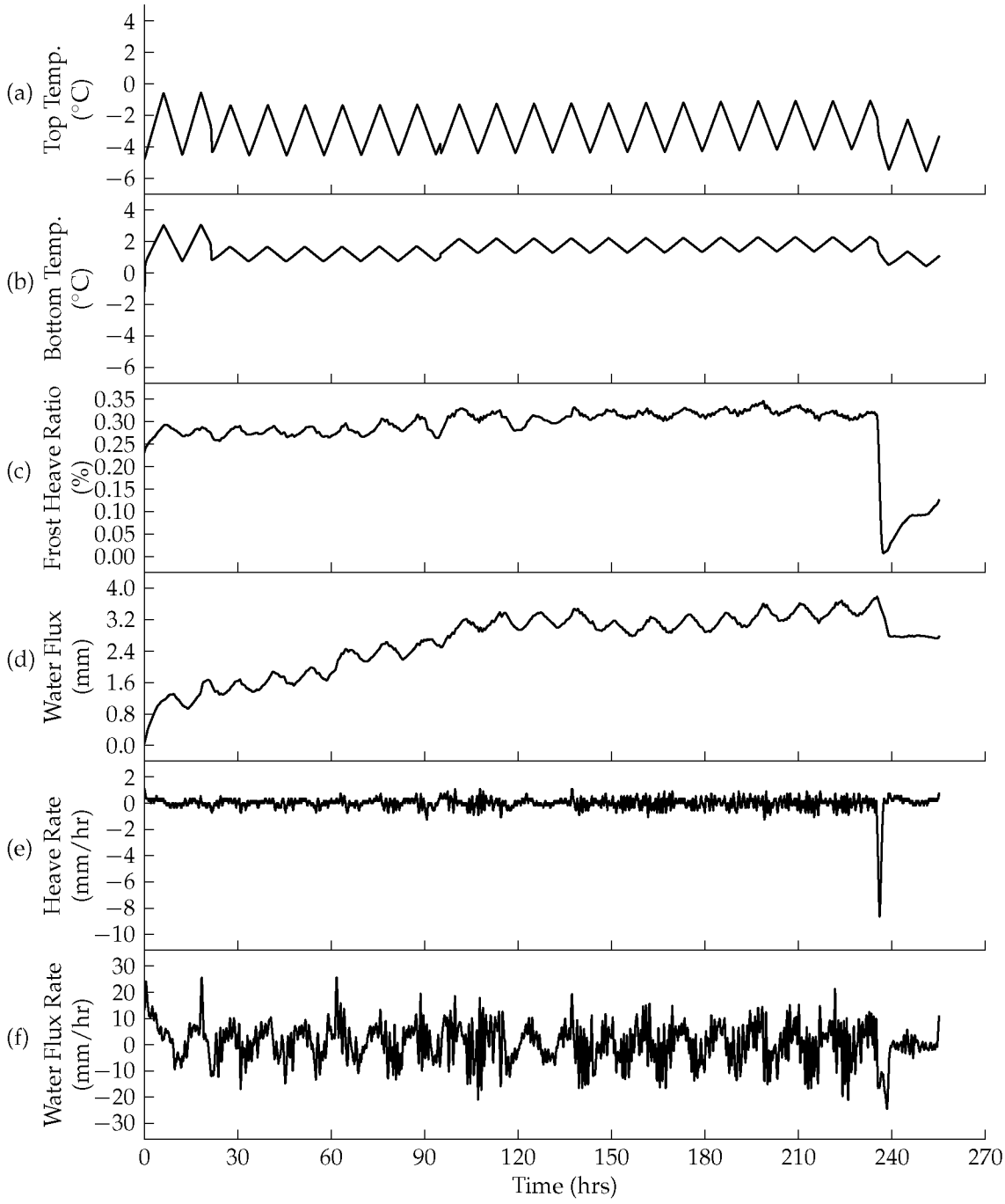

Figure 3.22. JSI02 soil temperatures (a,b), frost heave ratio (c), water flux (d), heave rate (e), and water flux rate (f).

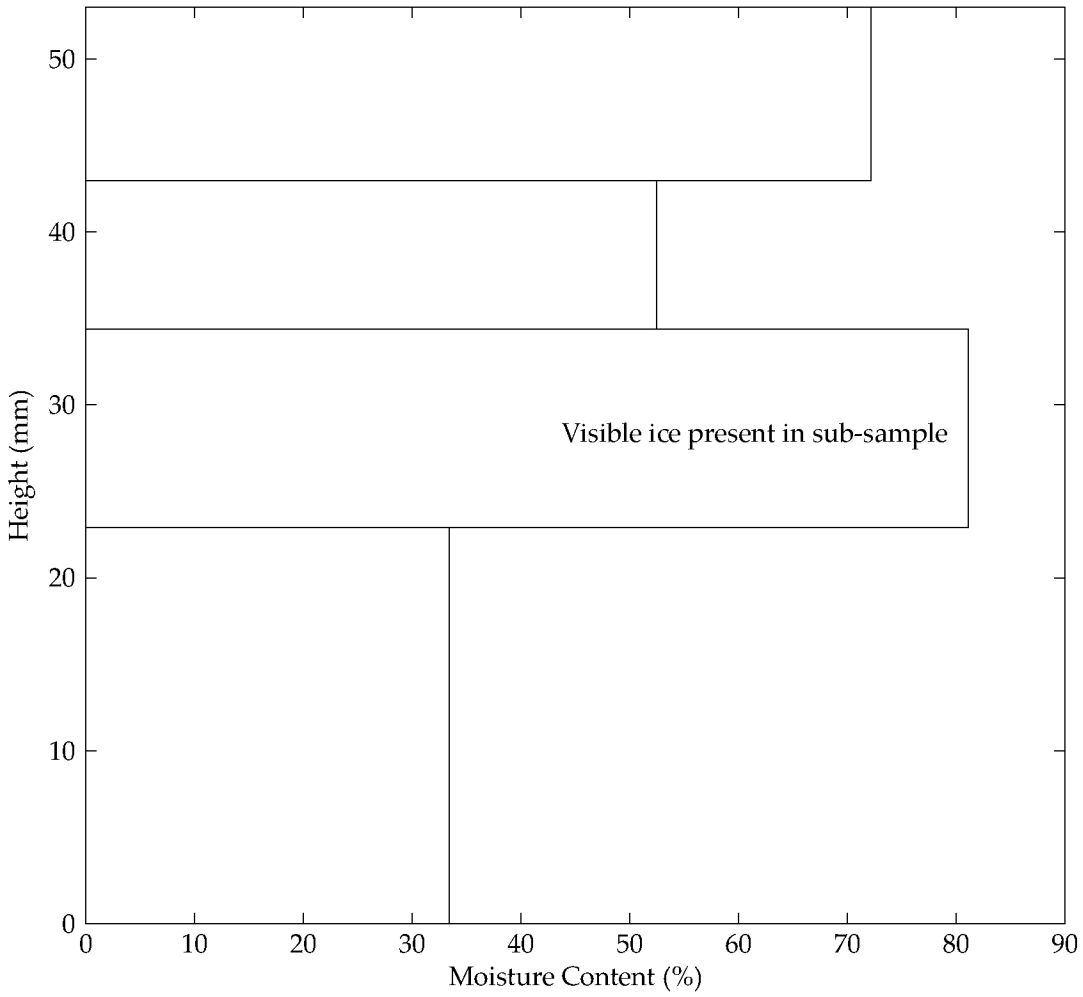

Figure 3.23. JSI02 moisture content variation with height.

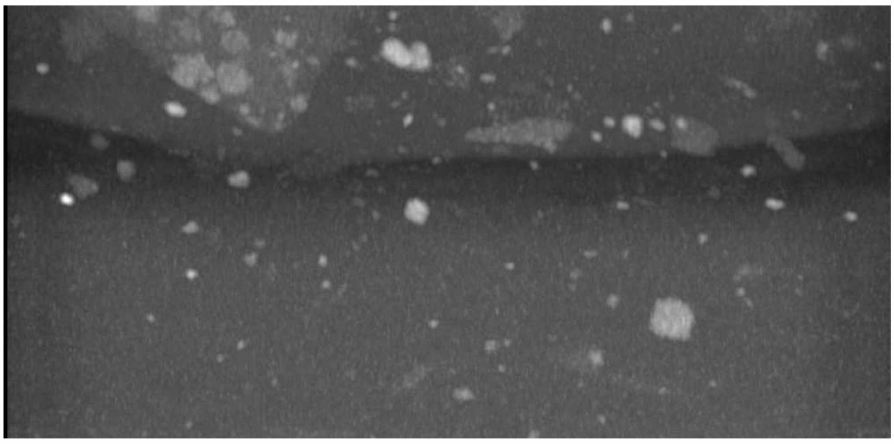

(a) Maximum density projection, vertical profile, height = 16.82 mm, diameter = 34.46 mm, silt with trace coarse-grained sand, ice layer in center.

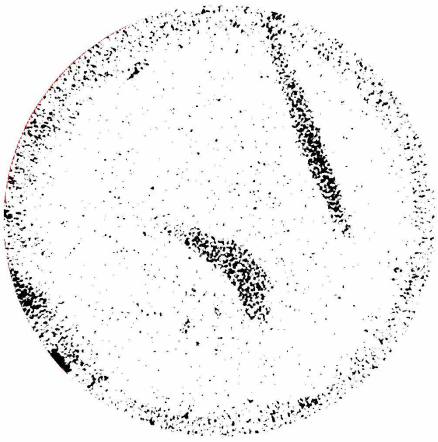

(b) Horizontal plane at height of 0.55 mm

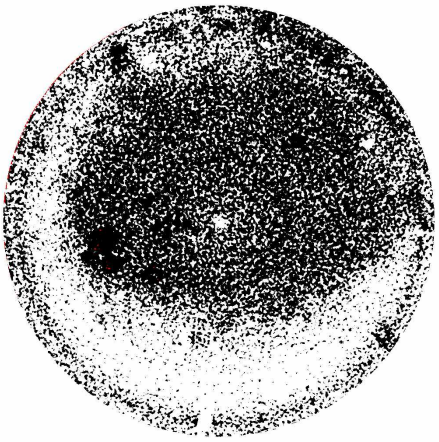

(c) Horizontal plane at height of 9.24 mm

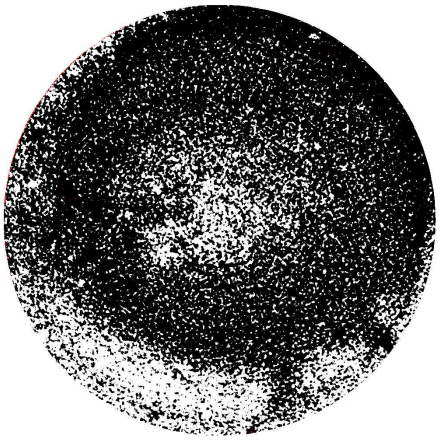

(d) Horizontal plane at height of 9.99 mm

(e) Horizontal plane at height of 12.65 mm

Figure 3.24. JSI02 X-ray μCT cross-sections. See Figure 3.26 for threshold value. Threshold methods discussed in Section 2.3

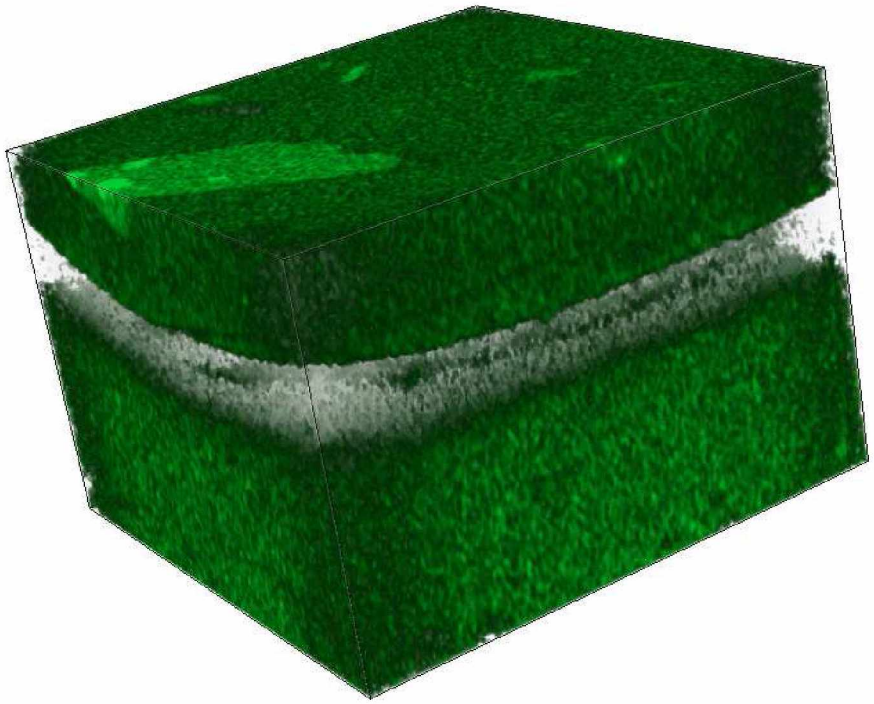

(a) Rendering view 1

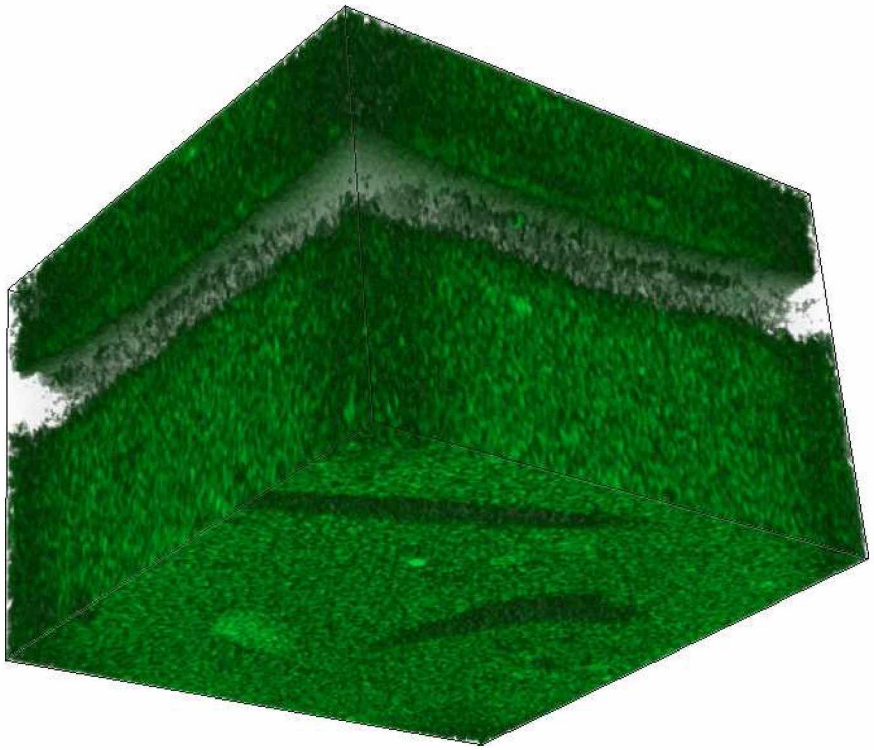

(b) Rendering view 2

Figure 3.25. JSI02 μCT soil renderings. Sub-sample is 16.82 mm tall, 24.26 mm wide and deep. See Figure 2.7 for color transfer function.

centration of grains above the ice layer compared to below, likely due the downward displacement of the heavier particles during the times that the lower portion was thawed. The μCT-derived relative density of the sample was plotted as a function of height (Figure 3.26). Figure 3.26(b) shows that the majority of the sample was composed of high density material – primarily soil, while low density material (ice) was present in lesser quantities (at the location of the sub-sample). No organics were detected in in the μCT data.

3.2.2 Summary of experiments on fine-grained soils with coarse-grained base layer

The addition of a layer of coarse-grained material at the base of the sample was an attempt to increase the hydraulic conductivity, to allow additional water to flow in and out of the sample. During open-system cooling, the silt between the frozen-thawed interface and the coarse-grained layer was enough of a hydraulic break to prevent significant outflow of water. This was similar to what was seen in sample JSI08, where no coarse-grained base layer was present. The addition of the coarse-grained layer at the base appears to have no significant effect on the accumulation of ice in the fine-grained soils above it.

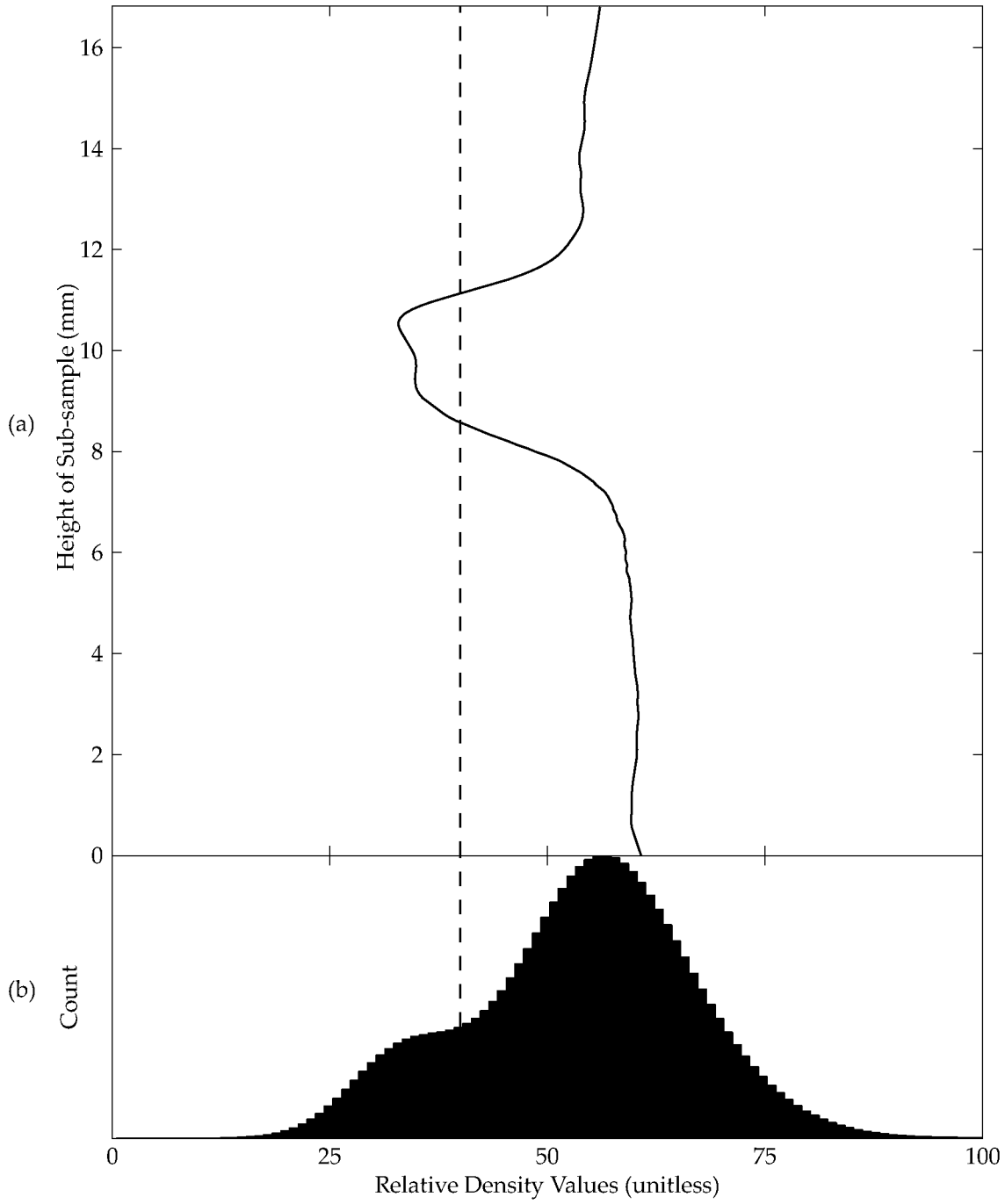

Figure 3.26. JSI02 μCT-derived relative density profile (a) and density histogram (b). Threshold value of 40 selected for scan data. See Section 2.3 and Figure 2.7 for information regarding density values.

3.3 Experiments with coarse-grained soils

Coarse-grained soils tested include uniform sand (Figure 2.4(a)) and Fox sand (Figure 2.4(c)). Tests in this category include: JSA02, JSA01, CSA01, JSA04, and JGR01 (Table 3.3).

3.3.1 Open system during cooling and warming

3.3.1.1 Sample JSA02

Sample JSA02 was composed of uniform sand, initially compacted, saturated, and pre-frozen in the Hokkaido Cell prior to testing as described in Section 2.4. The bottom temperature was held constant at approximately 2.5°C for the duration of the test, while the top temperature was varied linearly from -5°C to -3°C (12 hours warming, 12 hours cooling, Figure 3.27(a,b), Table 3.3). The sample was under open-system conditions while cooling and warming, and the free water supply at the bottom of the sample was always available to enter the soil matrix.

This test produced no excess ice in the soil sample. The total FHR at the conclusion of the test was 0.04% – effectively zero. This is because this sample had a relatively high hydraulic conductivity, permitting the water to flow freely in and out of the soil matrix. During cooling, the expulsion of water was evident in the water flux (Figure 3.27(d)) and in the water flux rate (Figure 3.27(f)). Approximately 4.5 mm of water (water volume has been normalized to the sample cross-sectional area) was absorbed by the sample during testing. This is most likely due to incomplete saturation of the sample at the onset of testing, and not related to the test procedures.

Figure A.9 (Appendix A) is a condensed time-lapse video of the total test progression for sample JSA02. Select stills from the video are in Appendix B, Figure B.9. Movement of the freezing front was barely perceptible during the initial and final freezing, however, movement was not identifiable during the majority of the test. This is to be expected when compared to data presented in Figure 3.27, where negligible vertical movement was observed during the cooling and warming cycles.

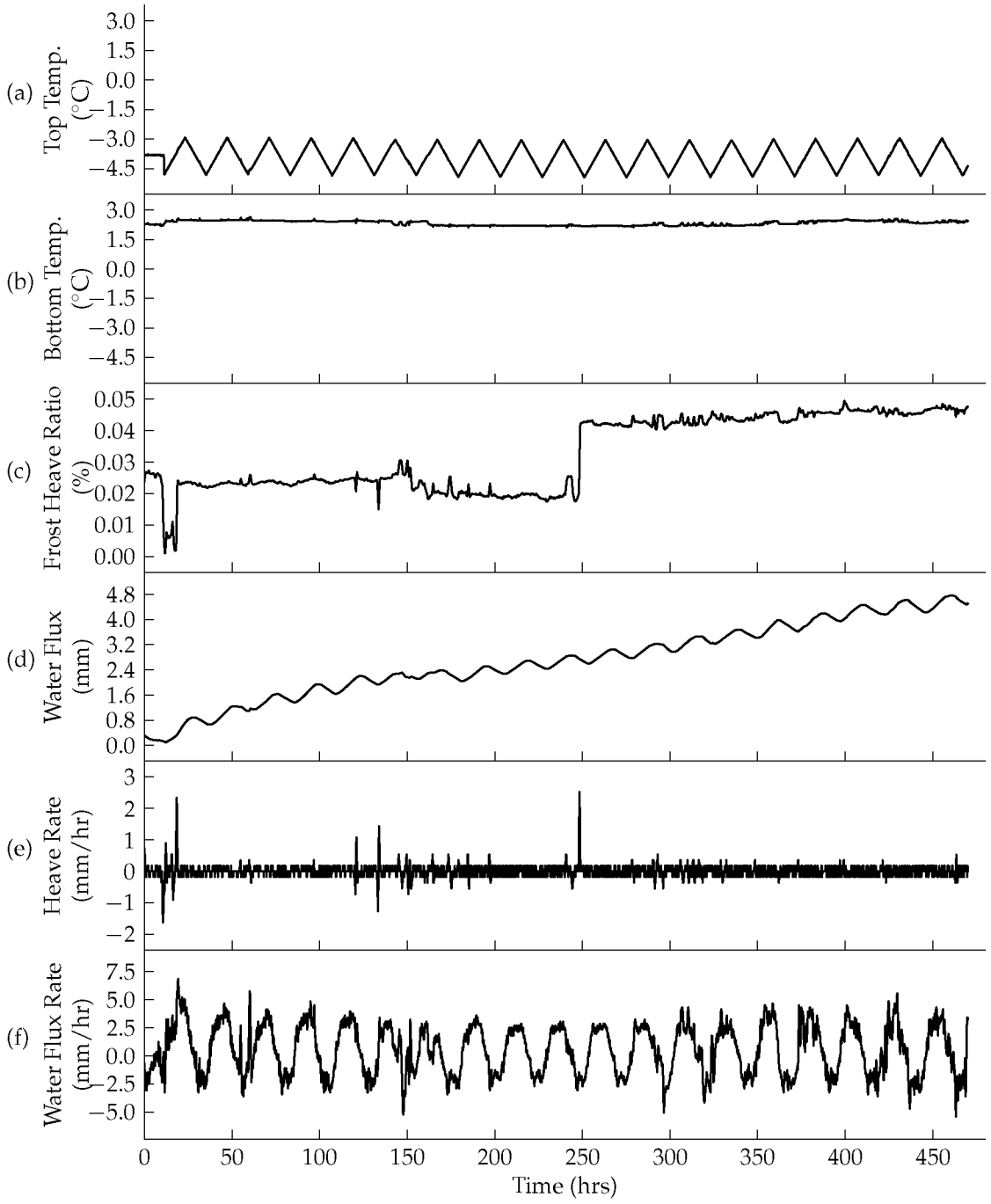

Figure 3.27. JSA02 soil temperatures (a,b), frost heave ratio (c), water flux (d), heave rate (e), and water flux rate (f).

Table 3.3. Test parameters for experiments with coarse-grained soils

Sample Name	Test Type*	Start Time (hrs)	End Time (hrs)	T_{top} Min. (°C)	T_{top} Max. (°C)	T_{bottom} Min. (°C)	T_{bottom} Max. (°C)	Cycle Length (hrs)	Number of Cycles
JSA02	r	0	480	-5	-3	2.5	2.5	24	19
JSA01	s	20	115	-7	-6	-7	10	8	10
CSA01	s	0	40	-7.5	-5.5	-6.5	12	9	9
JSA04	r	0	38	-6.5	-6.5	3	7	8	4
	r	38	56	-6.5	-6.5	2	8.5	8	4
JGR01	h	0	258	-4	-1	1.5	1.5	varies	9

* s = "stepped", r = "ramped", h = "hybrid" (stepped and ramped)

3.3.2 Freezing-induced closed-system cooling and open-system warming

3.3.2.1 Sample JSA01

Sample JSA01 was composed of uniform sand initially compacted and saturated in the Hokkaido Cell prior to testing as described in Section 2.4. The first 43 hours of testing were spent ensuring the testing equipment was functioning properly and pre-freezing the sample. The top temperature was held constant at approximately -6.5°C for the duration of the test, while the bottom temperature was varied step-wise from -7°C to 10°C (4 hours warming, 4 hours cooling, Figure 3.28(a,b), Table 3.3). These thermal conditions ensured that the sample was under closed-system conditions while cooling and open-system conditions while warming. The free water supply at the bottom of the sample was blocked from entering the sample during cooling due to the presence of pore ice, and free to enter the sample during warming when the ice was no longer preventing moisture migration.

Figure A.10 (Appendix A) is a condensed time-lapse video of the total test progression for sample JSA01. Select stills from the video are in Appendix B, Figure B.10. Movement of the frozen-unfrozen boundary was visible during the first warming cycle after 24 hours. A small void formed at the bottom of the sample, and as the frozen-thawed interface advanced upward, the thickness of the water-filled void increased. When refreezing after the first temperature cycle, a thin horizontal line across the sample was visible as the water

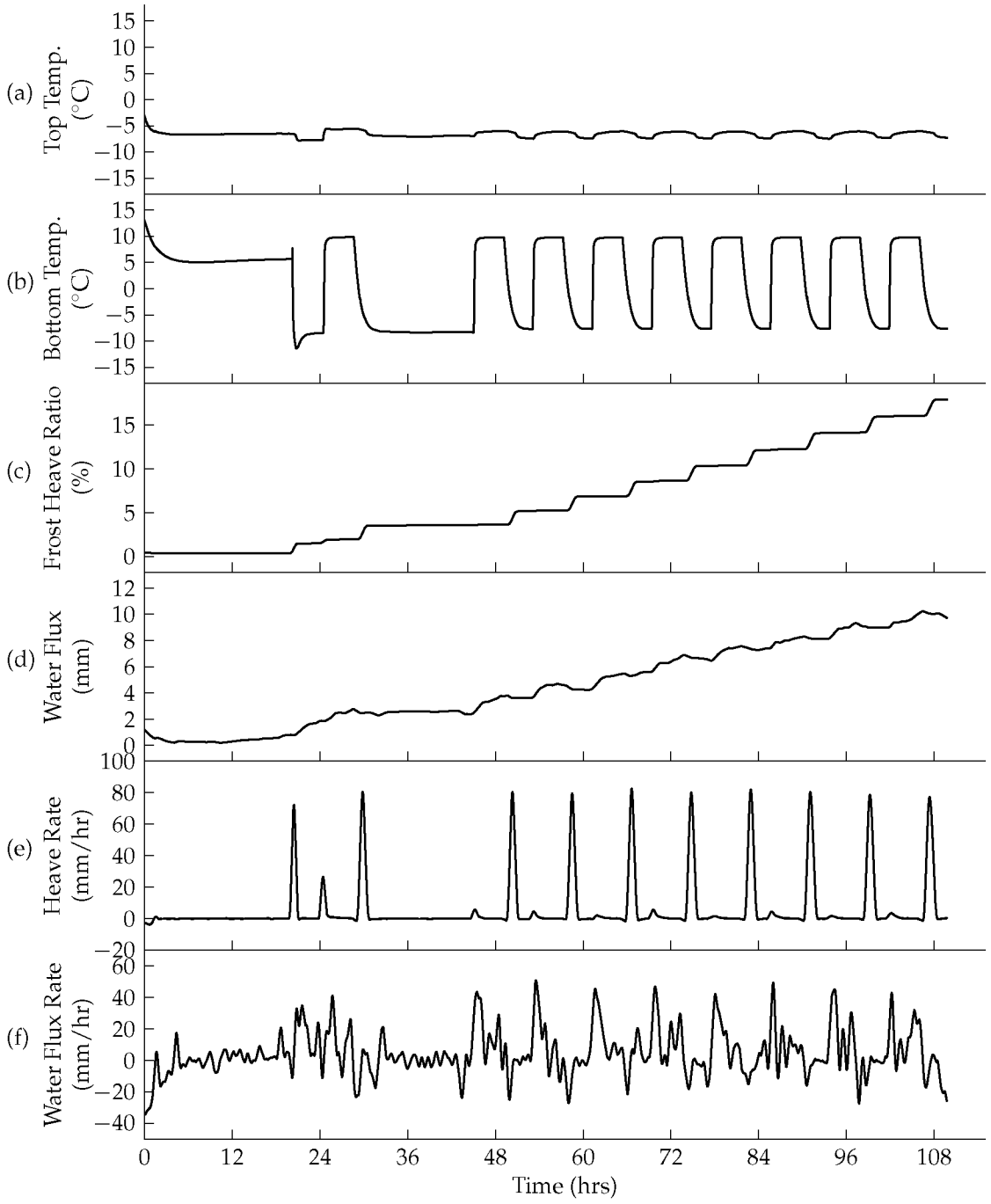

Figure 3.28. JSA01 soil temperatures (a,b), frost heave ratio (c), water flux (d), heave rate (e), and water flux rate (f).

turned to ice.

During refreezing of the first cycle, it is evident in the time-lapse video that the freezing front began advancing from the top and the bottom of the sample concurrently. Since freezing was occurring from opposite directions, the water was forced to the midpoint (below the initial cycle ice line) from the bottom of the sample, and is visible on the time-lapse video.

The heave rate during this first cycle rapidly peaked from 0 mm/hr to approximately 75 mm/hr, and quickly dropped back to 0 mm/hr. This was caused by the sample being completely frozen at this point, with no additional vertical displacement possible.

A small, positive peak in heave rate (approximately 5 mm/hr) was observed during the initial warming stages of each cycle, indicating a minor increase in the sample length. This increase is not apparent in the frost heave ratio. During these small increases in heave rate, a marked increase in water flux rate is visible, indicating that water is quickly entering the sample. While the water supply was not at a significant head, the pressure of the water column was enough to slightly raise the upper (frozen) portion of the sample during the initial stages of testing. This is due to the water head from the burette, situated approximately one meter above the cell, which was acting against the base of the frozen portion of the sample (likely less than 100g, depending on the thickness of the section, which varied throughout the test). This force balance was verified mathematically. Additional mass of the upper portion was accumulated by ice formation, which caused the water level in the burette to drop. This process caused the force balance to eventually prevent any uplift forces from acting on the sample.

The expulsion of water is evident in the water flux rate subplot (Figure 3.28(d)) during the refreezing periods, where the heave rate peaks. This is due to ice nucleation at the soil-cell interface at the bottom pedestal (see discussion in Section 3.1.2.1) and subsequent ice buildup out of the Hokkaido Cell and into the water supply line, pushing any additional water back into the external storage reservoir, from which the water flux was measured.

The temperature cycle at 40 hours did not advance the water-filled void to the same extent as the first cycle, because the temperatures and cycle lengths were adjusted slightly between cycles. The subsequent cycles, however, did advance up to the location where the second cycle terminated, and accumulated ice with each cycle. Gas bubbles and sand grains were seen at the interface of the liquid water and ice during several of the cycles, which then became trapped in the ice matrix during refreezing.

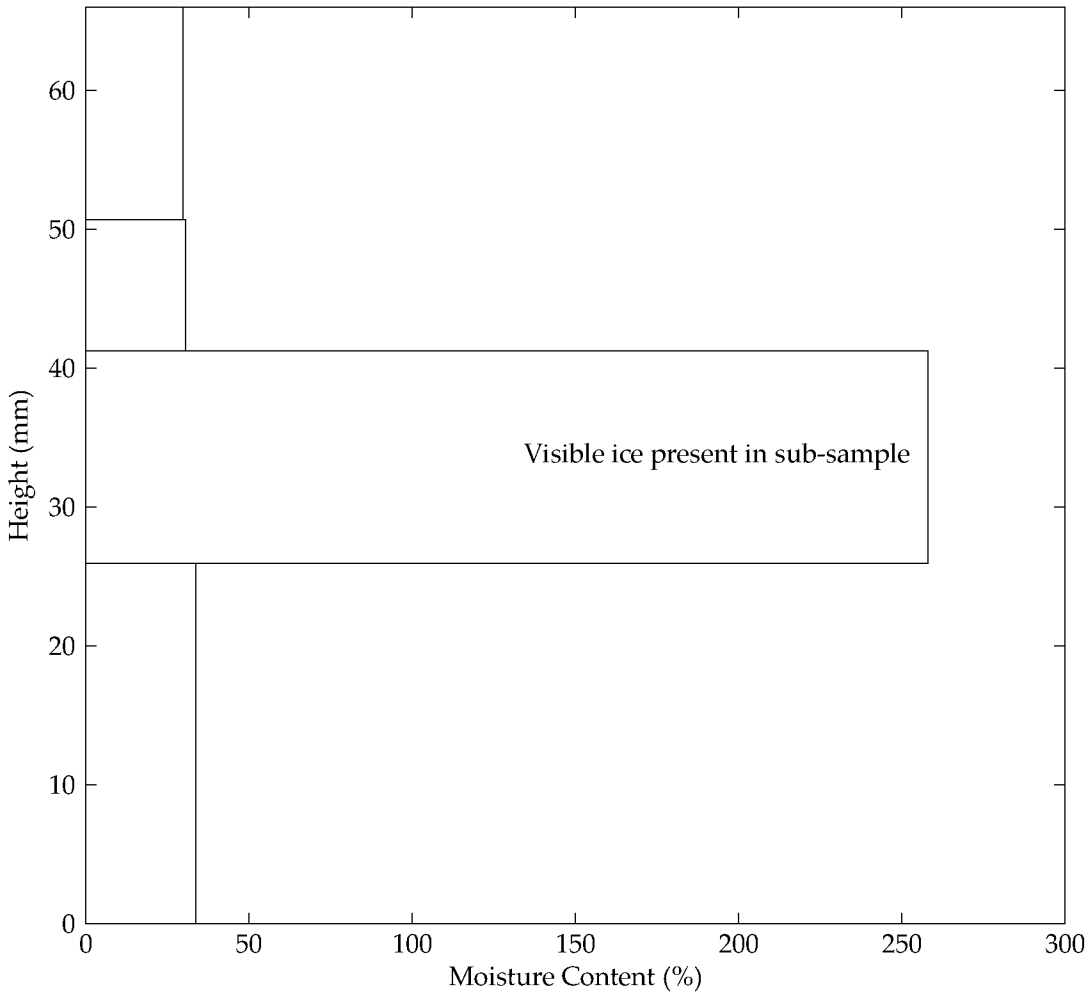

Figure 3.29. JSA01 moisture content variation with height.

A moisture content profile for sample JSA01 was determined at the termination of the test (Figure 3.29). The sub-sample from 26 mm to 41 mm contained the ice lens. The moisture content immediately below the ice lens was slightly higher than that directly above, 33.8% versus 29.7%, respectively. This is most likely due to the influx of water upon warming during each temperature cycle.

A μCT scan was performed with a sub-sample. Individual soil grains are easily identified in Figures 3.30, 3.31, and D.5. A second, thin ice layer just above the main ice lens is identifiable in scan data, but is not apparent with traditional photography. Several grains of sand in the ice are visible in Figures 3.30(e) and 3.31(a), centered vertically in the sample. These grains appear to have been at the interface of the bottom half of the sample and the ice layer during the first part of the test, and did not become dislodged from the ice lens upon warming, subsequently trapping these grains in the ice layer.

The μCT-derived relative density of the sample was plotted as a function of height (Figure 3.32). Figure 3.32(a) shows three distinct regions: below the ice layer (higher density), the ice layer (lower density), and then above the ice layer (higher density). The small decrease in density near the top of the scanned region is the thin ice layer noted earlier. The density of this region is not as low as the main ice layer, mainly because the core was not oriented perfectly vertically when scanned in the μCT scanner.

3.3.2.2 Sample CSA01

Sample CSA01 was composed of uniform sand, initially compacted, saturated, and frozen in the Laval Cell prior to testing as described in Section 2.4. The top temperature was held constant at approximately -6.5°C for the duration of the test, while the bottom temperature was varied step-wise from -6.5°C to 12°C (4.55 hours warming, 4.5 hours cooling, Figure 3.33(a,b), Table 3.3). These thermal conditions ensured that the sample was under closed-system conditions while cooling and open-system conditions while warming, similar to sample JSA01.

Ice formation in sample CSA01 was similar to that described in sample JSA01. By cutting off water expulsion from coarse-grained soil during cooling (closed-system), the sample experienced vertical displacement due to the phase change of the water into ice. During warming from the bottom, the sample was under open-system conditions, and was able to take water into the sample, as seen in Figure 3.33(d).

Figure 3.34 shows the extracted sample at the conclusion of test CSA01. Figure 3.35 is

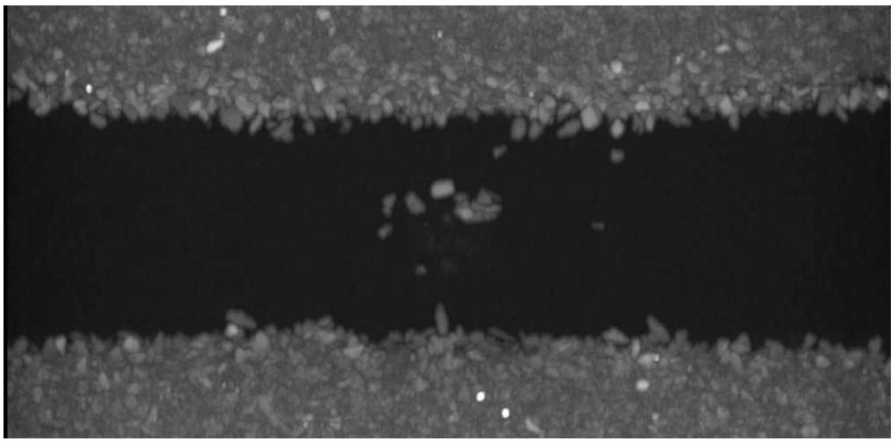

(a) Maximum density projection, vertical profile, height = 16.82 mm, diameter = 34.46 mm. Sand at top and bottom, center black layer is ice.

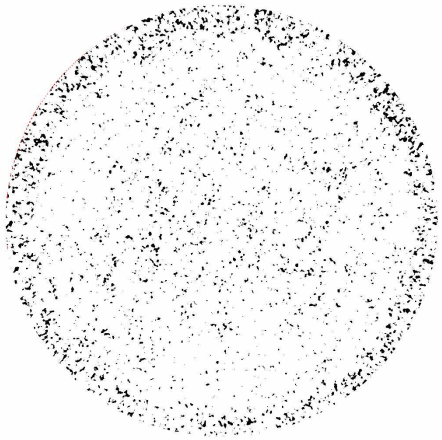

(b) Horizontal plane at height of 0.55 mm

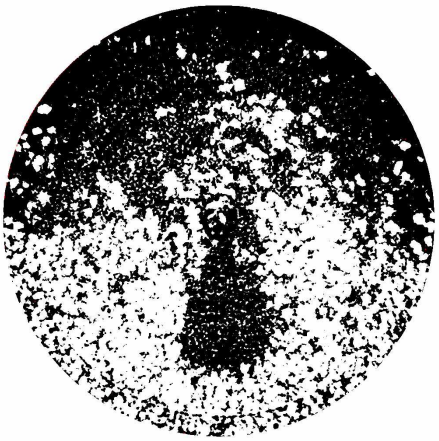

(c) Horizontal plane at height of 3.51 mm

(d) Horizontal plane at height of 9.61 mm

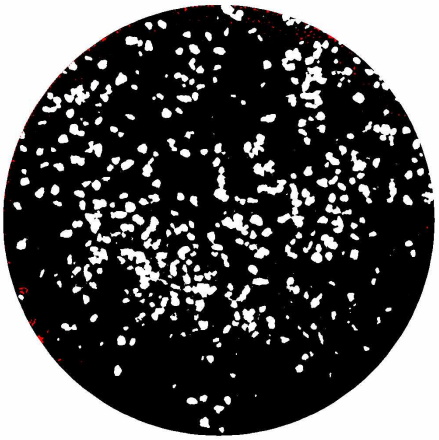

(e) Horizontal plane at height of 13.44 mm

Figure 3.30. JSA01 X-ray μCT cross-sections. See Figure 3.32 for threshold value. Threshold methods discussed in Section 2.3

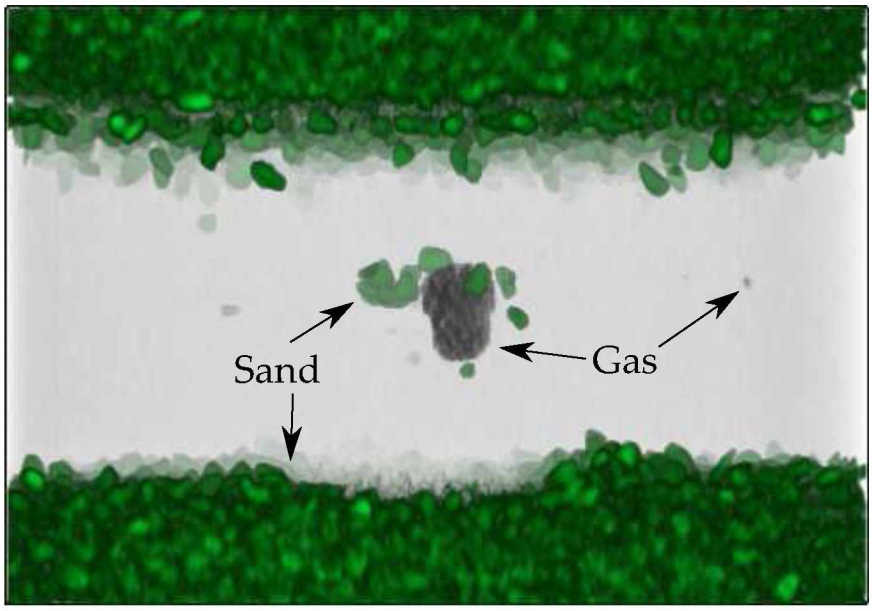

(a) Rendering view 1

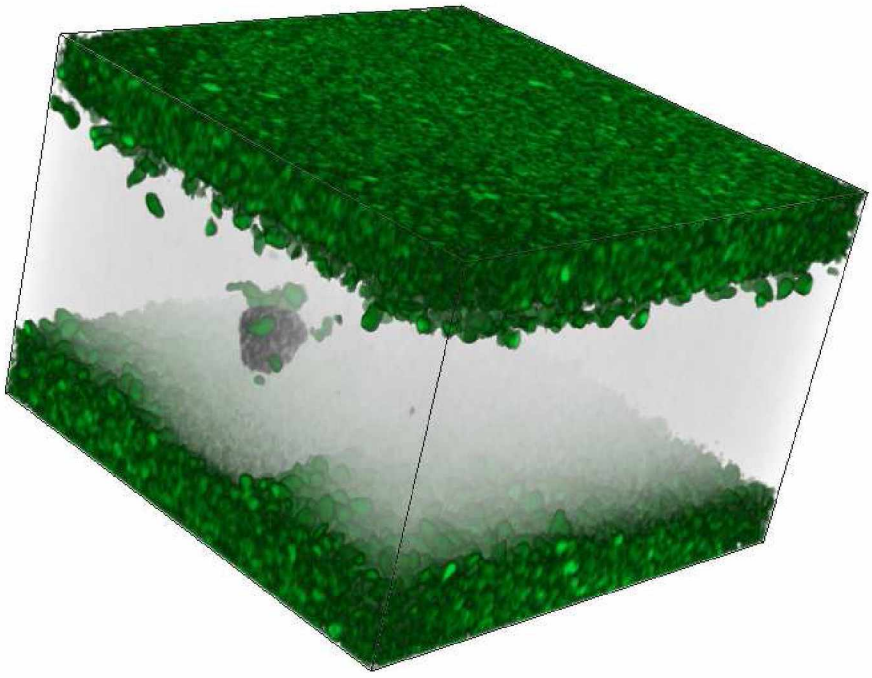

(b) Rendering view 2

Figure 3.31. JSA01 μCT soil renderings. Sub-sample is 16.82 mm tall, 24.26 mm wide and deep. See Figure 2.7 for color transfer function.

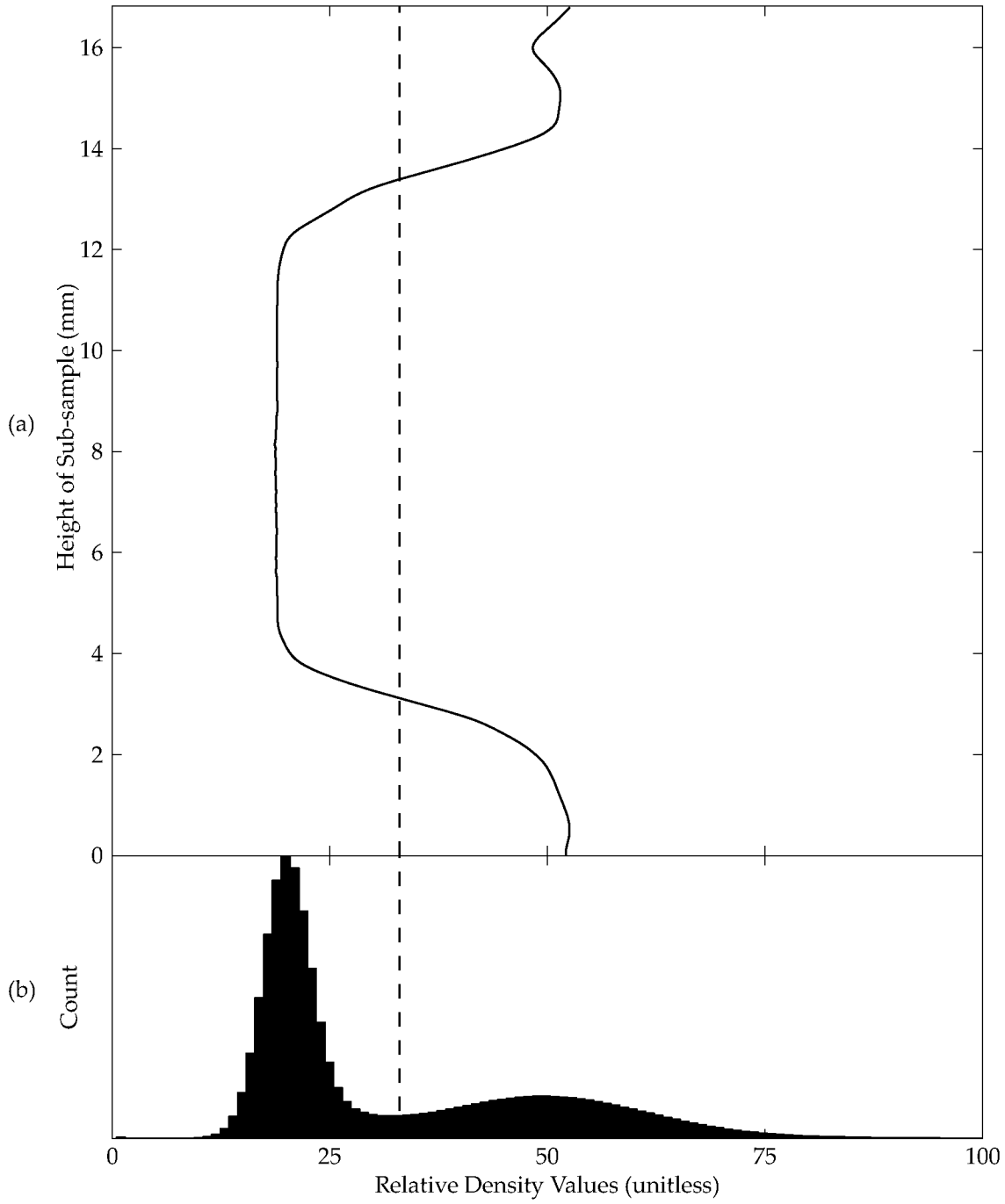

Figure 3.32. JSA01 μCT-derived relative density profile (a) and density histogram (b). Threshold value of 33 selected for scan data. See Section 2.3 and Figure 2.7 for information regarding density values.

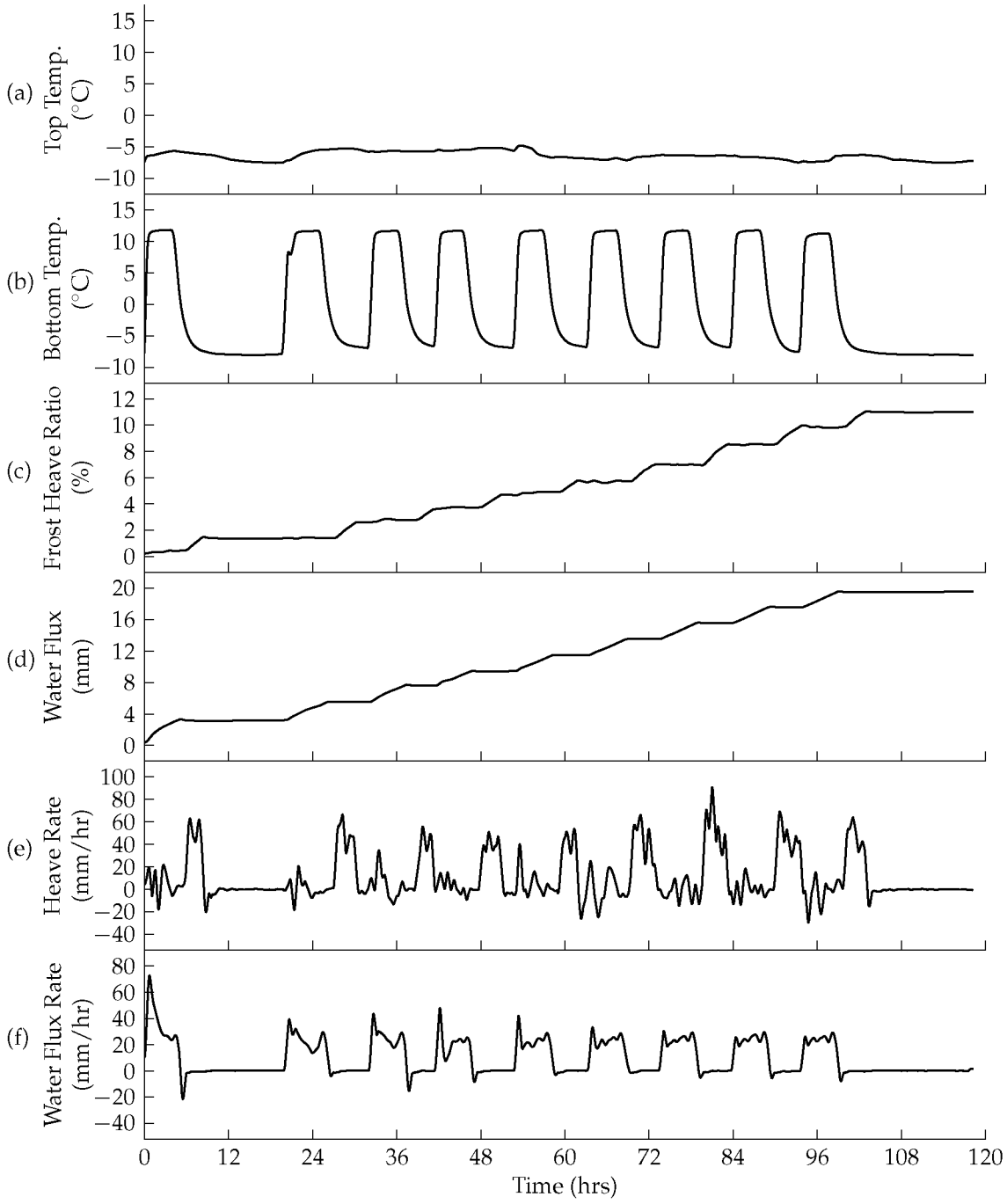

Figure 3.33. CSA01 soil temperatures (a,b), frost heave ratio (c), water flux (d), heave rate (e), and water flux rate (f).

Figure 3.34. Post-frost heave test photograph of sample CSA01.

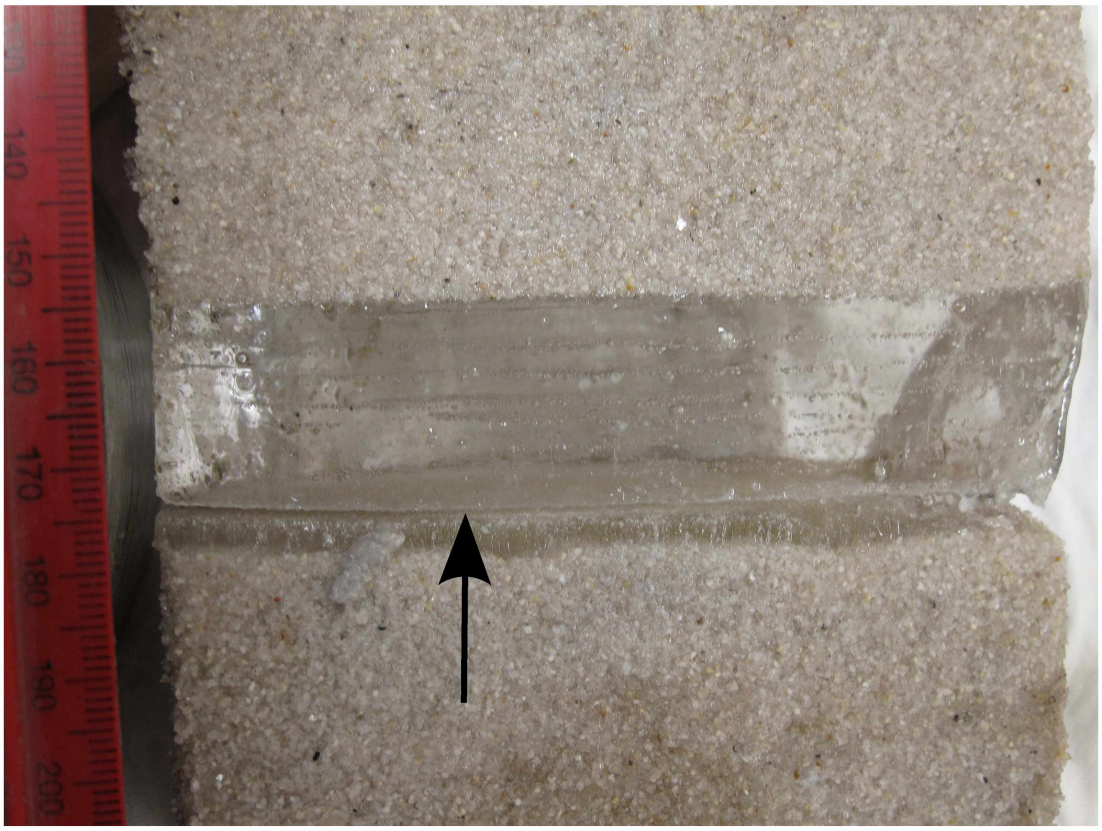

Figure 3.35. Close-up of soil/ice interface of sample CSA01. Fractured surface identified by arrow is not a result of the test, but due to mishandling the sample during photographing.

a close-up of the ice lens in sample CSA01. The ice at the top of the sample in Figure 3.34 was not formed through the testing procedures outlined – it was created during the initial freezing of the sample prior to testing, by filling the cell with water sufficient to cover the top of the thawed soil. In Figure 3.35 several horizontal striations are visible – each of these were formed during a successive temperature cycle. The crack at the bottom of the ice was due to mishandling of the post-test sample, and is not related to the processes occurring in the soil during testing.

A moisture content profile for sample CSA01 was determined at the termination of the test (Figure 3.36). The sub-sample from 45 mm to 79 mm contained the ice lens. Unlike sample JSA01, the moisture content immediately below the ice lens was slightly lower than that directly above, 29.9% versus 35.8%, respectively.

A μCT scan was performed (Figures 3.37, 3.38, D.6). The scan is a sub-sample of the test sample, imaged along the vertical axis of the core, centered across the ice layer in the sample. The sample was not perfectly vertical when scanned, therefore dark wedges are visible at the top and the bottom of the scan in Figure 3.38 due to the lack of sub-sample in that portion of the scanner caddy. There are at least seven distinct layers of gas bubbles, corresponding to the extent of the frozen-unfrozen interface during temperature cycles (the gas bubbles float to the top of the liquid portion of the void formed upon thawing, and are impeded from further advance). The gas bubbles in the layer near the top of the sub-sample represent the oldest extent of the frozen-unfrozen interface, while the ice between the lowest layer of bubbles and the sediment was the last ice to form during testing.

The μCT-derived relative density of the sample was plotted as a function of height (Figure 3.39). Figure 3.39(a) shows two distinct regions: below the ice layer (higher density) and the ice layer (lower density).

3.3.3 Artificially-induced closed-system cooling and open-system warming

3.3.3.1 Sample JSA04

Sample JSA04 was composed of uniform sand, initially compacted, saturated, and frozen in the Hokkaido Cell prior to testing as described in Section 2.4. The test was divided into two distinct phases (Table 3.3). The top temperature was held constant at approximately -6.5°C for the duration of the test, while the bottom temperature was varied linearly from 2°C to 8.5°C (Figure 3.40(a,b), Table 3.3). The thermal conditions are

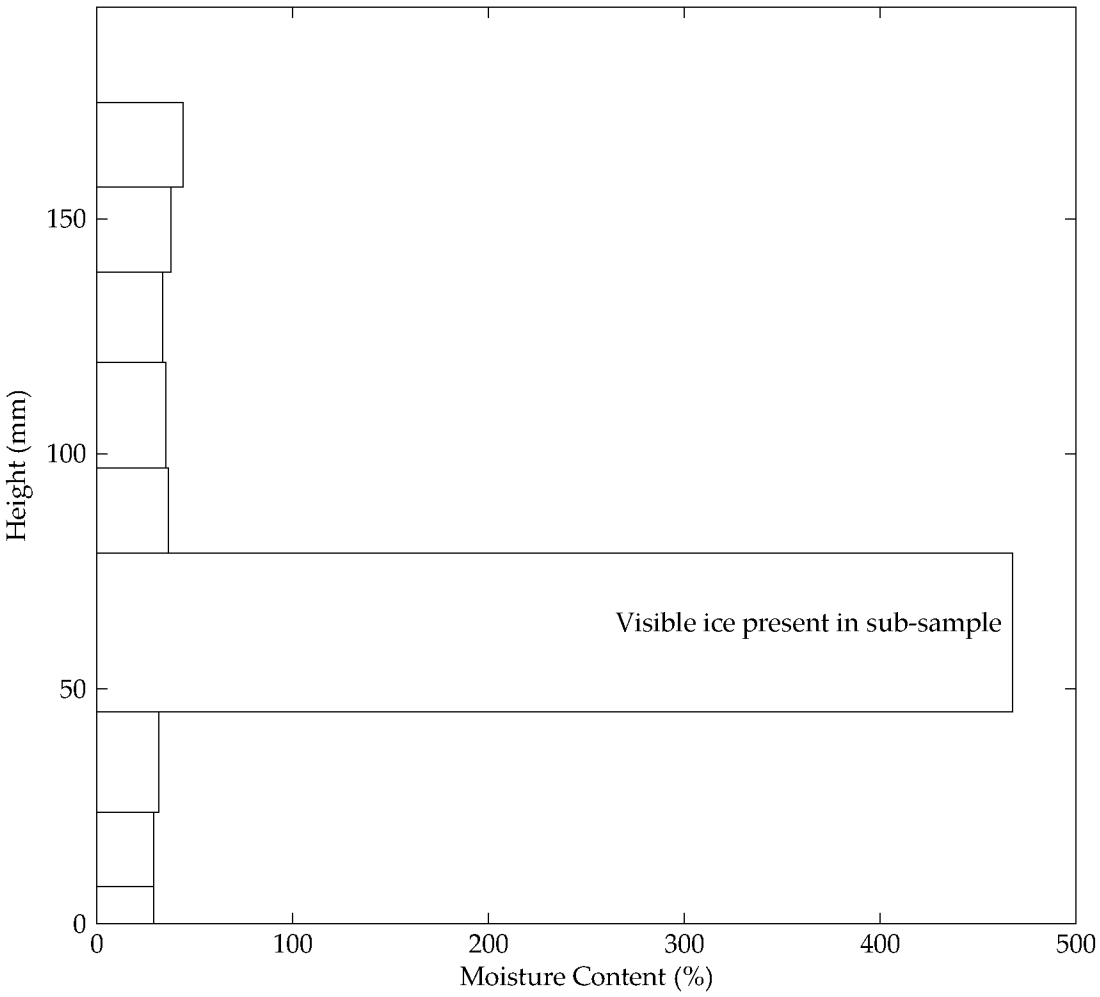

Figure 3.36. CSA01 moisture content variation with height.

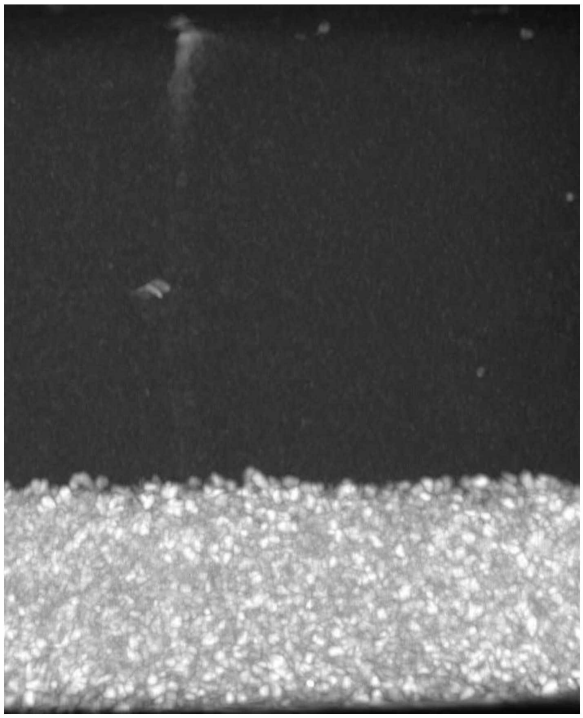

(a) Maximum density projection, vertical profile, height = 29.88 mm, uniform sand at bottom

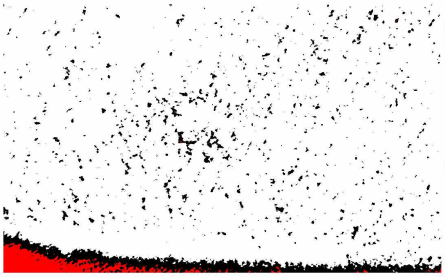

(b) Horizontal plane at a height of 3.72 mm

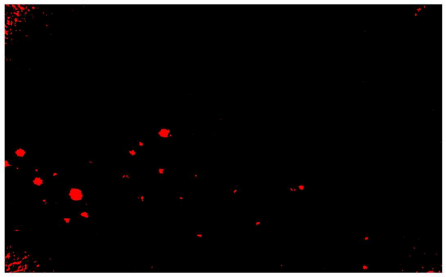

(c) Horizontal plane at a height of 13.99 mm

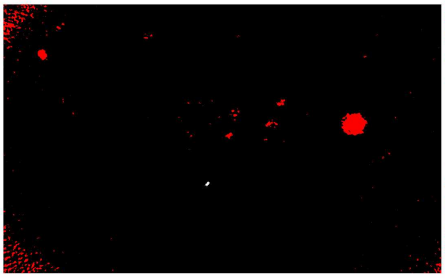

(d) Horizontal plane at a height of 18.26 mm

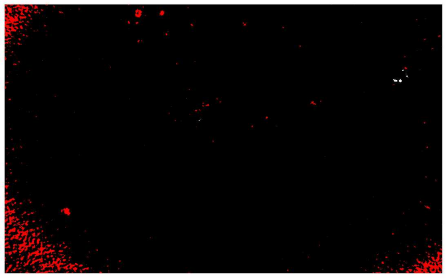

(e) Horizontal plane at a height of 24.88 mm

Figure 3.37. CSA01 X-ray μCT cross-sections. See Figure 3.39 for threshold value. Threshold methods discussed in Section 2.3

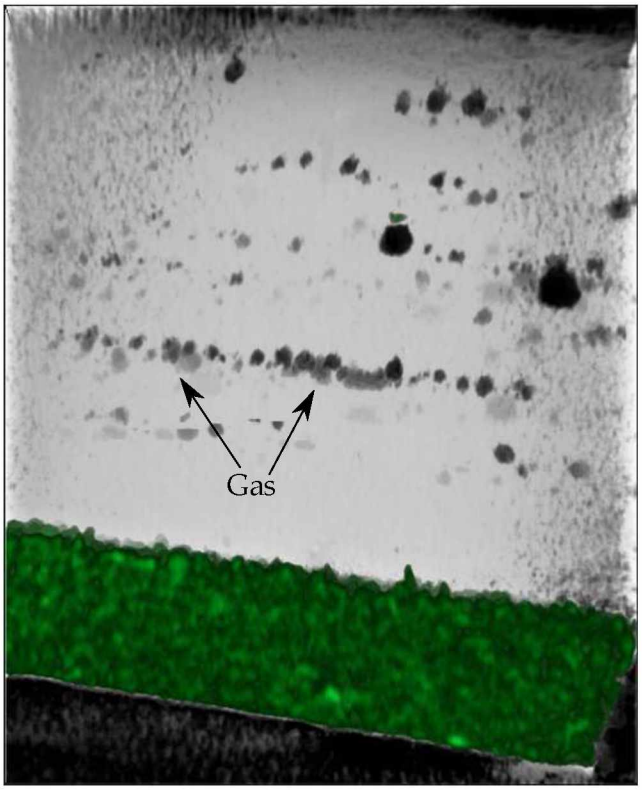

(a) Rendering view 1

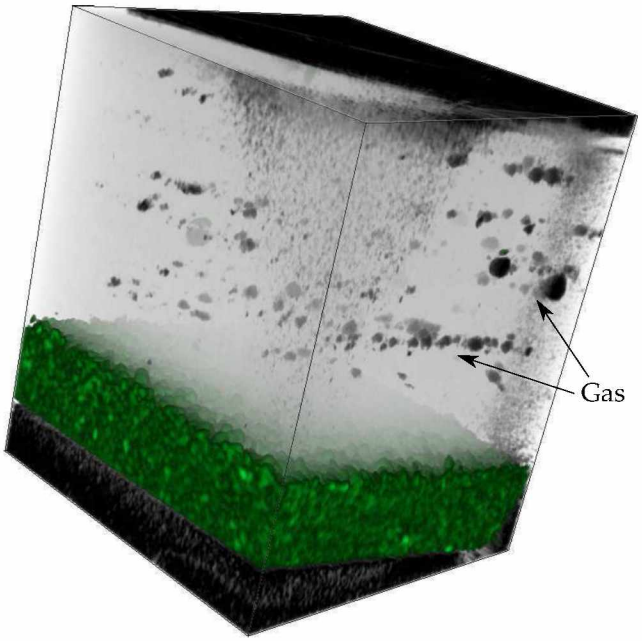

(b) Rendering view 2

Figure 3.38. CSA01 μCT soil renderings. Sub-sample is 29.88 mm tall, 24.26 mm wide and deep. See Figure 2.7 for color transfer function.

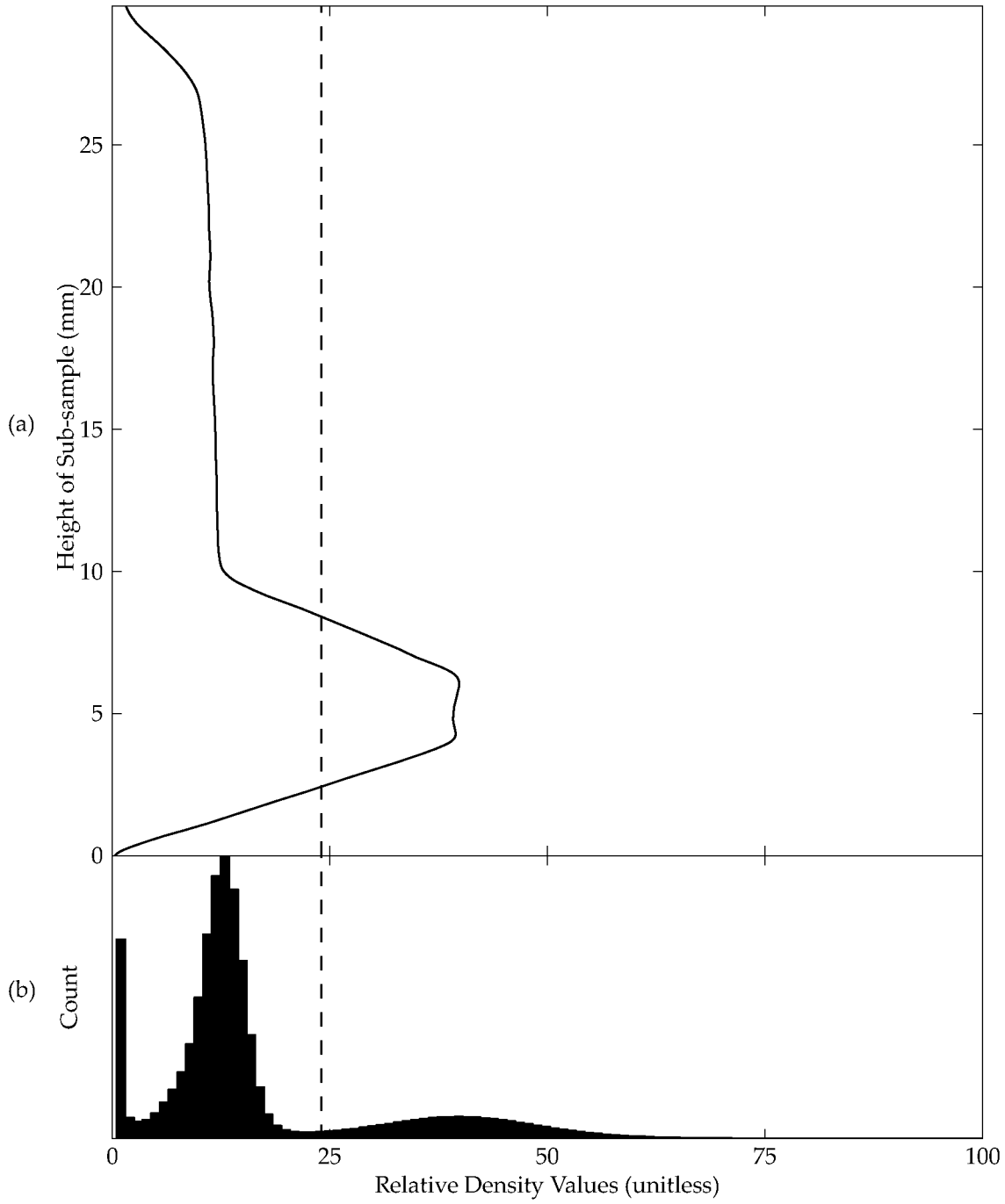

Figure 3.39. CSA01 μCT-derived relative density profile (a) and density histogram (b). Threshold value of 24 selected for scan data. See Section 2.3 and Figure 2.7 for information regarding density values.

similar to JSA02, in that the soil at the bottom of the sample was frozen and thawed under open-system conditions. To force closed-system cooling conditions, the water inlet valve was opened and closed during the testing program, to prevent the outflow of water from the sample during cooling.

Figure A.11 (Appendix A) presents a condensed time-lapse video of the total test progression for sample JSA04. Select stills from the video are in Appendix B, Figure B.11. Upward movement of the frozen-unfrozen boundary was visible during the first 17 hours of the test. The second cooling stage of the test produced the first visible ice layer, which was approximately 1 mm thick. Over the next 30 hours, the maximum height of the frozen-thawed interface gradually moved upward with each successive warming and cooling cycle, indicating that thermal equilibrium for the sample was not stable during the first part of the test. At approximately 40 hours into the test, the amplitude of the temperature cycles were increased in an attempt to increase the thickness of the ice layer. The valve was left open during the last half of the test, and no additional ice was accumulated at the freezing front.

The heave rate (Figure 3.40(e)) indicates several heave (upward surface displacement) events throughout the test, as well as several decreases in sample length during the first half of the test, when the water inflow valve was closed periodically. During the second half of the test, excluding the final freezing of the sample, there was effectively no change in heave rate.

3.3.3.2 Sample JGR01

Sample JGR01 was composed of Fox sand, initially compacted, saturated, and frozen in the Hokkaido Cell prior to testing as described in Section 2.4. This sample was created with an initial layer of ice inserted into the middle of the sample by compacting and freezing the sample in two layers, the bottom layer of sand with standing water above it, which was frozen, and then an additional layer of sand was place above that, saturated, then frozen. The ice was inserted to create a sample that had a significant amount of ice present to immediately thaw and freeze. The bottom temperature was held constant at approximately 1.5°C for the duration of the test, while the top temperature was varied from -4°C to -1°C (Figure 3.41(a,b), Table 3.3). Like test JSA04, the water supply valve was opened and closed throughout the test. The first 180 hours of the test elapsed with the supply valve in the open position. After approximately 180 hours, the valve was opened during

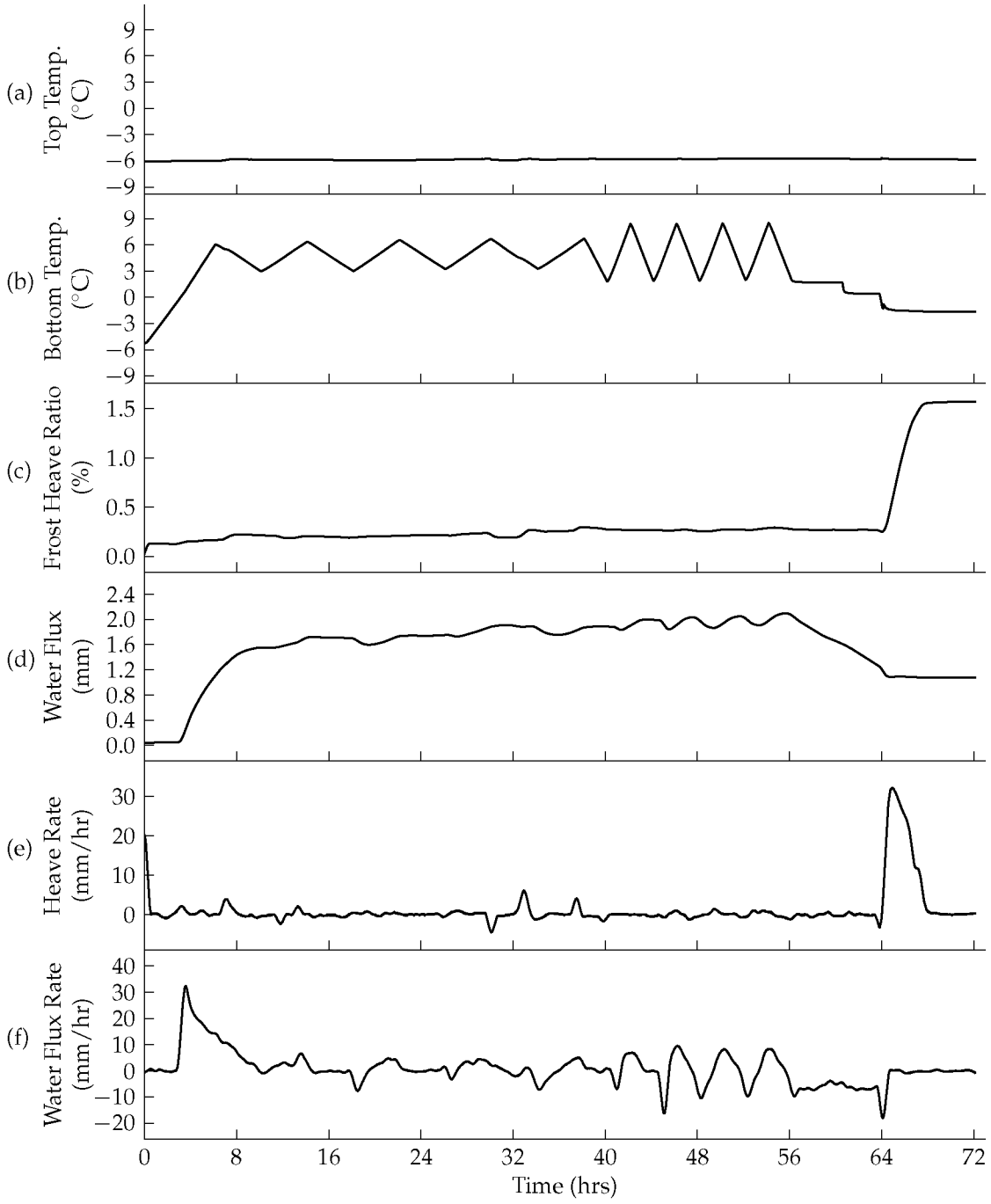

Figure 3.40. JSA04 soil temperatures (a,b), frost heave ratio (c), water flux (d), heave rate (e), and water flux rate (f). The water inflow valve was opened and closed manually during the testing program to create artificial closed-system cooling. The valve status during the test: 0.0 to 2.8 hrs – closed, 2.8 to 13.9 hrs – open, 13.9 to 18.0 hrs – closed, 18.0 to 21.9 hrs – open, 21.9 to 26.1 hrs – closed, 26.1 to 37.9 hrs – open, 37.9 to 41.0 hrs – closed, 41.0 to 43.1 hrs – open, 43.1 to 45.1 hrs – closed, 45.1 to 72.1 hrs – open.

warming cycles, and closed during cooling cycles.

Figure A.12 (Appendix A) is a condensed time-lapse video of the total test progression for sample JGR01. Select stills from the video are in Appendix B, Figure B.12. Movement of the freezing front during the first 140 hours cycled between the bottom half of the thick ice layer and the bottom layer of coarse-grained sand. No vertical displacement or accumulation of ice occurred during this period. Several gas bubbles were visible during the first half of the test, mostly between the ice layer and the cell wall. After 140 hours the warming cycle was held at the warmest temperature for a longer time than previous cycles, allowing additional upward movement of the frozen-thawed interface. The prolonged warming cycle completely thawed the initial artificial ice layer, but did not extend up into the upper half of the soil sample. During the next cooling stage, the downward movement of the ice lens was visible, particularly on the left side of the sample in the video, where gas bubbles migrated downward with the movement of the freezing front. The gas bubbles were oriented vertically as long, thin streaks, that started as round bubbles, and tapered as they were forced downwards. The next warming stage moved the freezing front through the entire ice layer and into the upper half of sand. Reorientation of sand grains near the upper soil-ice interface was observed during this cycle. After approximately 180 hours into the test the water supply valve was closed for cooling cycles. The next cooling stage after the valve was reopened froze the entire ice layer and increased its thickness (Figure 3.41(c,e)), because additional water was allowed in during the previous warming cycle, and was prevented from exiting the sample during the cooling stage.

The following warming and cooling cycles were varied similarly to JSA04 — the water valve was opened during warming (upward movement of the frozen-thawed interface). During cooling (downward movement of the freezing front), the additional water brought into the sample during warming was not permitted to exit because the water valve was closed (Figure 3.41(c,e,f)). The water flux rate increased during warming cycles, and then returned to zero during cooling, because movement of water into or out of the freezing soil was prohibited during cooling. In the first half of the test, the water flux rate was negative during cooling, because water was displaced out of the sample. Similarly, the heave rate remained zero throughout most of the test, except during cooling stages when the valve was closed and the rate would quickly rise above zero.

A moisture content profile for sample JGR01 was determined at the termination of the test (Figure 3.42). The sub-sample from 22 mm to 38 mm contained the ice lens. The

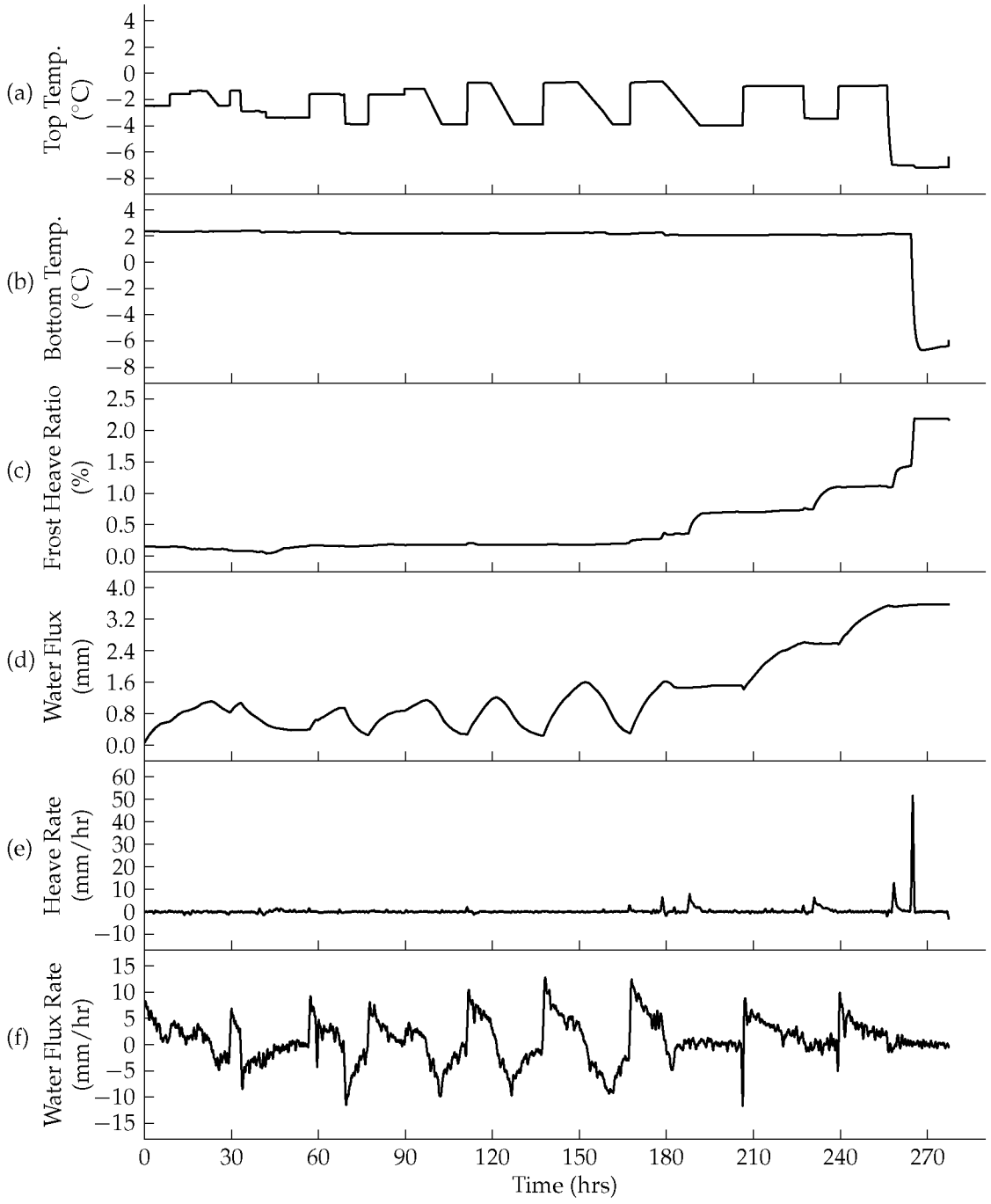

Figure 3.41. JGR01 soil temperatures (a,b), frost heave ratio (c), water flux (d), heave rate (e), and water flux rate (f). The water inflow valve was opened and closed manually during the testing program to create artificial closed-system cooling. The valve status during the test: 0 to 180 hrs – open, 180 to 210 hrs – closed, 210 to 225 hrs – open, 225 hrs to 240 hrs – closed, 240 hrs to 255 hrs – open, 255 hrs to test completion – closed.

moisture content immediately below the ice lens was slightly higher than that directly above, 33.8% versus 30.1%, respectively.

A μCT scan was performed (Figure 3.43, 3.44, D.7). The scan is a sub-sample of the test sample, imaged along the vertical axis of the core, centered across the ice layer in the sample. Individual soil grains are easily identified in Figures 3.43 and 3.44. Several grains near the top of the ice lens appear to be suspended immediately below the soil matrix, but not in grain-to-grain contact (Figure 3.44(a)). The movement of these particles was not observed during testing because they are near the center of the sample. It is likely that the downward displacement occurred immediately following the maximum extent of thawing, as the freezing front began to propagate downward in the sample. The initial refreezing during a cooling cycle was generally slower than the latter half of the cooling stages. Slow freezing conditions typically promote larger ice crystal formation and growth.

The μCT-derived relative density of the sample was plotted as a function of height (Figure 3.45). Figure 3.45(a) indicates three distinct regions: below the ice layer (higher density), the ice layer (lower density), followed by higher density above the ice layer. Figure 3.45(b) shows that the majority of the scanned region of the sample was composed of low density material – mostly ice.

3.3.4 Summary of experiments with coarse-grained soils

Coarse-grained soils tested under open-system cooling and warming conditions did not develop significant ice layers. During closed-system cooling tests the samples developed appreciable layers of ice with FHR values of approximately 10% to 15%. The thickness of the ice developed in the sample was directly proportional to the number of total temperature cycles, as well as the amplitude of the temperature fluctuations.

3.4 General summary of results

Fourteen warming and cooling tests were conducted on several soil types. Testing was divided into three major groups: experiments with fine-grained homogeneous soils, experiments with fine-grained soils with coarse-grained base layer, and experiments with coarse-grained soils (Table 3.4). The magnitude of the thickness of soil subjected to freeze-thaw cycles was varied between tests, and was controlled by the magnitude and duration of applied soil temperatures. In general, when the frozen-unfrozen boundary was shifted downward while under closed-system conditions, the ratio of ice to the final sample length

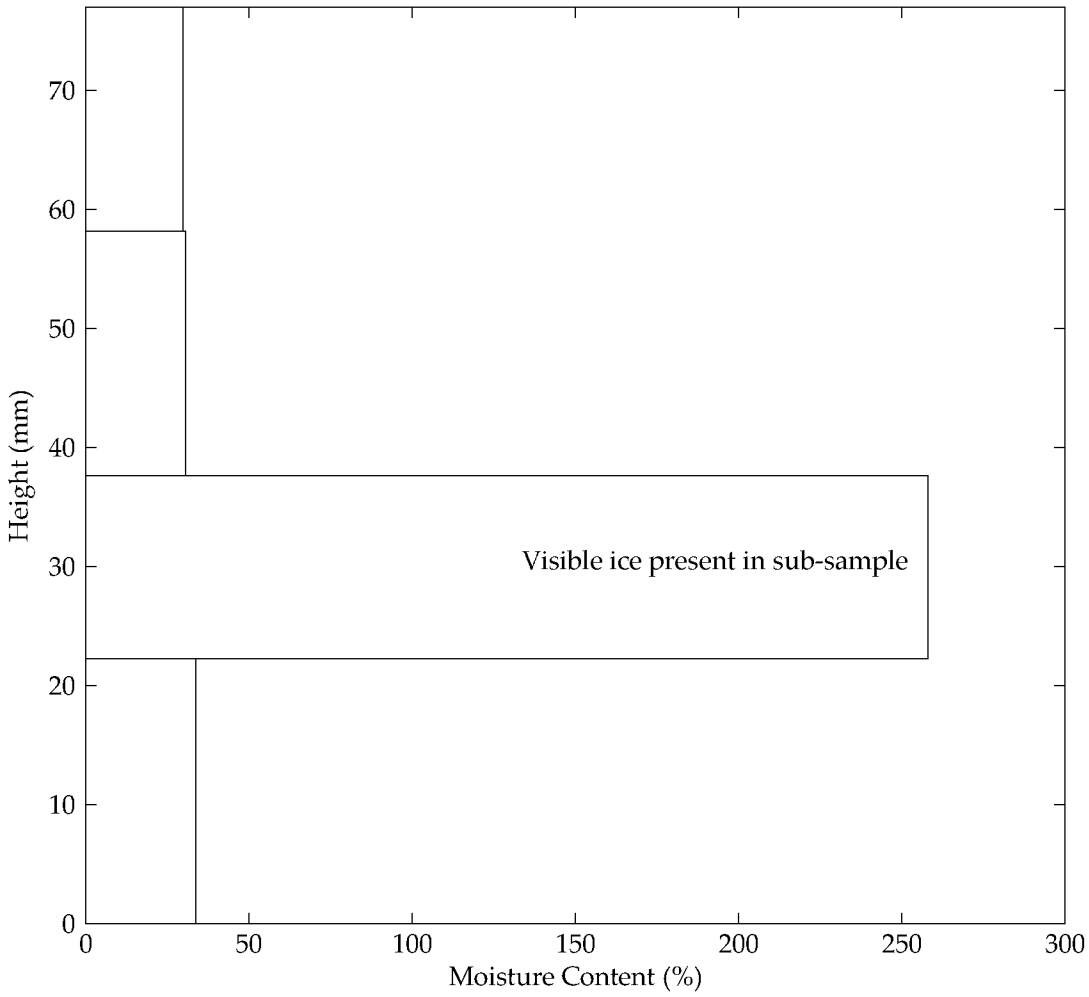

Figure 3.42. JGR01 moisture content variation with height.

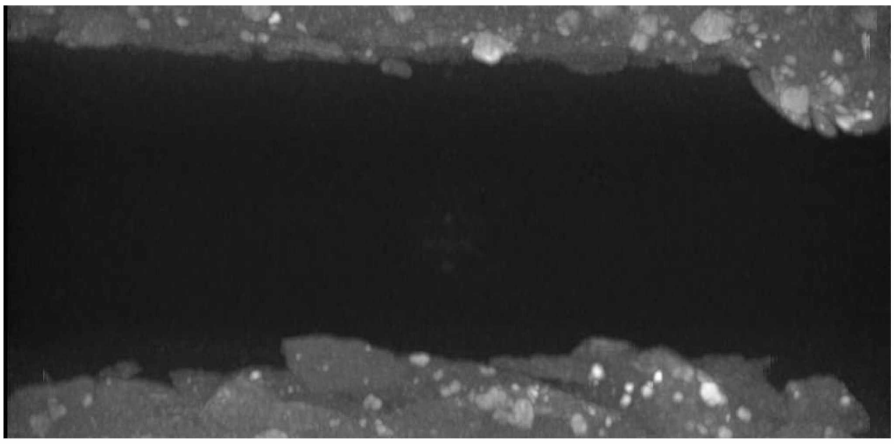

(a) Maximum density projection, vertical profile, height = 16.82 mm, diameter = 34.46 mm. Coarse-grained sand at top and bottom, center black layer is ice.

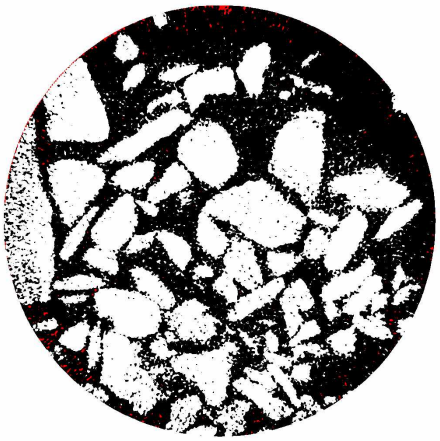

(b) Horizontal plane at height of 0.55 mm

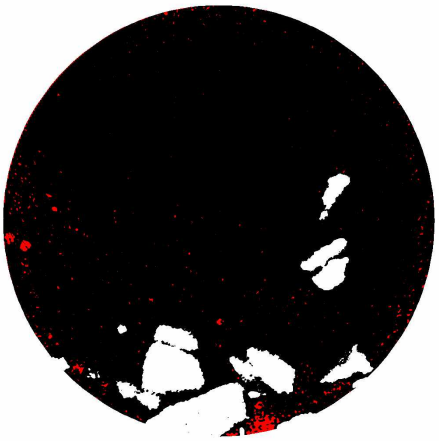

(c) Horizontal plane at height of 3.17 mm

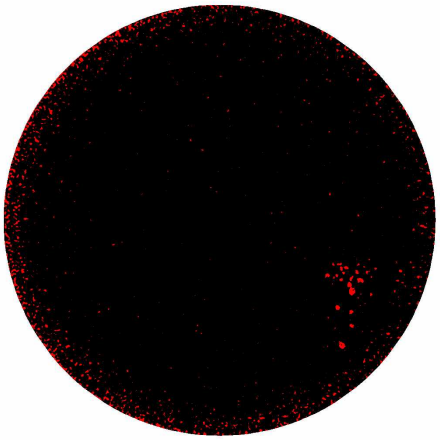

(d) Horizontal plane at height of 7.68 mm

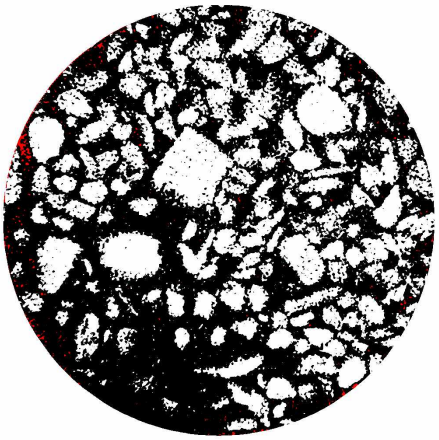

(e) Horizontal plane at height of 16.40 mm

Figure 3.43. JGR01 X-ray μCT cross-sections. See Figure 3.45 for threshold value. Threshold methods discussed in Section 2.3

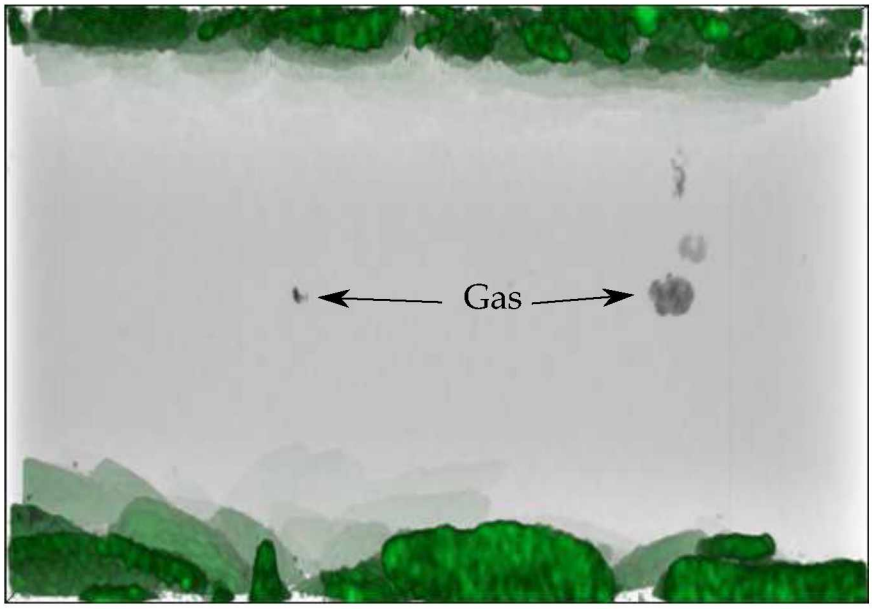

(a) Rendering view 1

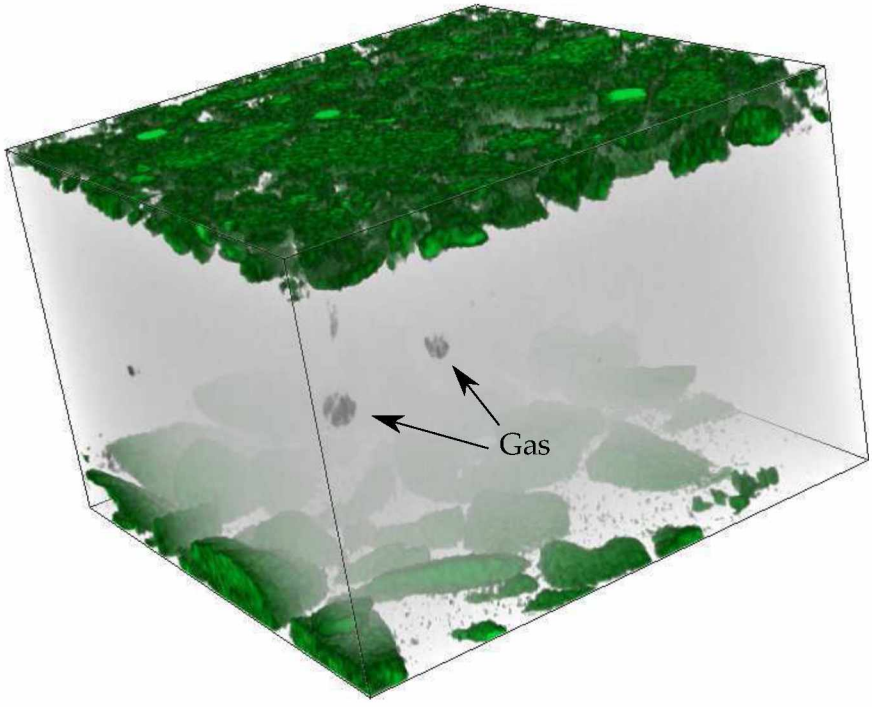

(b) Rendering view 2

Figure 3.44. JGR01 μCT soil renderings. Sub-sample is 16.82 mm tall, 24.26 mm wide and deep. See Figure 2.7 for color transfer function.

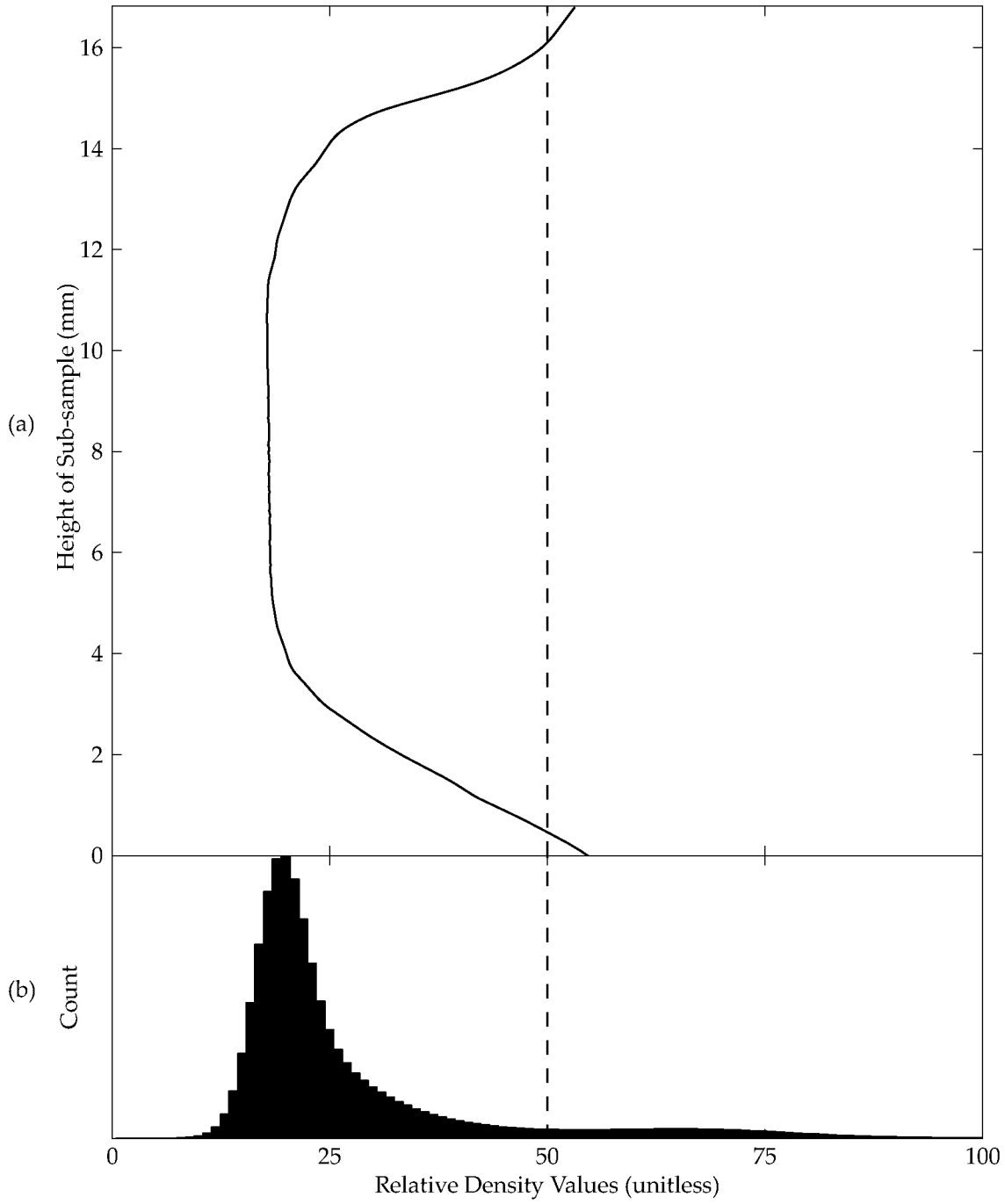

Figure 3.45. JGR01 μCT-derived relative density profile (a) and density histogram (b). Threshold value of 50 selected for scan data. See Section 2.3 and Figure 2.7 for information regarding density values.

Table 3.4. Summary of cyclic freezing tests

Sample	Cooling Open?	Original Length (mm)	Frost Heave Ratio (%)	Water Flux (mm)	Ice Thickness (mm)	Ratio of Ice to Final Length (%)
Experiments with fine-grained homogeneous soils						
JSI08	yes	55	2.4	0.7	1.9	3.4
JSI01	no	69	23.5	24.0	10.5 (multiple)	12.3
CSI01	no	169	25.7	45.3	34.0 (multiple)	16.0
JCL02	yes	129	0.3	8.5	2.9	2.2
Experiments with fine-grained soils with coarse-grained base layer						
JCL01	yes	82	15.1	19.4	9.1	9.6
JSI02	yes	53	0.1	2.7	2.9	5.5
JSI03	yes	65	0.6	1.3	1.1	1.7
JSI04	yes	63	0.1	0.9	1.2	1.9
JSI05	yes	63	0.9	19.6	0.8	1.3
Experiments with coarse-grained soils						
JSA02	yes	100	0.0	4.3	0.0	0.0
JSA01	no	66	18.1	10.1	11.4	14.6
CSA01	no	195	11.3	19.7	23.8	11.0
JSA04	no	96	1.6	1.1	1.4	1.4
JGR01	no	77	2.1	3.4	12.7*/13.8	1.4

*Initial artificial ice layer

was markedly higher. This was observed for both fine- and coarse-grained soils tested. In samples that developed ice, most were formed in single, discrete masses. Samples JSI01 and CSI01 were subjected to extreme temperature swings, and as a result, formed several discrete layers in the initial phases of testing.

Ice thickness ranged from 0 mm (JSA04) to 34 mm (CSI01). The average ice thickness for the experiments with fine-grained homogeneous soils under open-system cooling was 3.4 mm, compared to 27.5 mm for closed-system cooling. The average ice thickness for the experiments with fine-grained soils with coarse-grained base layer was 3 mm (all tested under open-system cooling conditions). The average ice thickness for the experiments with coarse-grained soils under open-system cooling was 0 mm, compared to 7.5 mm for closed-system (or partial closed-system) cooling.

The ratio of ice thickness to the final sample length for the experiments with fine-grained soils with coarse-grained base layer (which were all tested under open-system cooling) were generally greater than the frost heave ratio, indicating that excess ice formed in the sample with minimal surface displacement. Samples JSI02, JSI03, JSI04, and JSI05 all had minimal ratios of frost heave, effectively zero, but had between 1.3% and 5.5% of the final length of the sample made up of a discrete ice layer.

Measured water flux into the samples at the end of testing was generally greater than that of the final ice thickness. This discrepancy becomes more pronounced when the water flux is converted to "ice flux," by multiplying the water flux in mm by 1.09.

Seven samples were scanned with the μCT scanner at the completion of the warming and cooling tests. The sub-samples scanned were analyzed in 2D cross-sections, and visualized as 3D reconstructions. The scans revealed the presence of discrete, and in the case of CSA01 and JCL01, oriented gas bubbles. The gas bubbles in JCL01 were stretched vertically, while those in CSA01 were clustered in layers between each the ice layers developed between during each temperature cycle. The scan for JSA01 revealed the presence of trapped grains of sand between ice layers, suspended in the center of the ice layer. Sand grains were identified in the scan for sample JGR01 that were not experiencing grain-to-grain contact.

Eight samples were sub-sampled and tested for gravimetric moisture content after warming and cooling tests, and if applicable, after μCT scanning. Moisture content for the sub-samples containing the accumulated ice layers was higher than the moisture content for the remainder of the sample. All of the samples tested, aside from JSI02 and CSA01,

were found to generally have higher moisture content below the ice layer than above.

Samples JSI01 and CSI01 were both tested for organic content after the moisture content was determined. The sub-samples were found to have higher concentrations of organic material, which is consistent with the time-lapse observations of organic material migration during testing of JSI01.

Chapter 4
Discussion and Conclusions

4.1 General discussion

Fine-grained soils (Fox silt) that did not develop segregated ice due to traditional frost heave mechanisms during slow, uniform freezing conditions (that is, during the initial freezing of the samples prior to testing) were found to be susceptible to the development of ice due to vacuum-filtration (Fel'dman, 1988a). No segregated ice was formed during the initial freezing of the samples, however ice accumulation occurred with cyclic warming and cooling, particularly when the outflow of water during cooling was limited or prevented. By breaking the connection to the water supply during refreezing, closed-system conditions were initiated, which was found to promote the development of ice at the location where the frozen-unfrozen boundary was at its highest point in the sample. By simulating these conditions on a sample composed of coarse-grained soil, similar results were observed.

The internal structure of several samples were analyzed using μCT methods. In general, ice formed due to the vacuum-filtration mechanism was found to be relatively free of entrapped gas, and was typically clear. Ice formed under segregation conditions is typically cloudy and opaque, with significant entrapped gas. In cryofacial classification, the distinction between the two types of ice can provide evidence supporting the method of ice genesis (ice segregation or vacuum-filtration).

4.1.1 Pingos and ice-cored mounds

Open- and closed-system pingo formation has been described by Leffingwell (1919), Holmes et al. (1968), Washburn (1980), Péwé (1982), Brown and Kreig (1983), and Mackay (1977, 1979, 1998). French (2007) describes two forms of pingos - those developed due to open-system conditions, and those from closed-system conditions. Open-system pingos develop in permafrost when groundwater, typically under artesian pressure, migrates towards the ground surface and becomes ice through injection mechanisms just below the ground surface. Closed-system pingos typically develop in drained lakebeds, when the permafrost table aggrades following the drainage of the lake. The pore water is expelled ahead of the aggrading permafrost, and as the water approaches the ground surface it freezes and forms a conical hill.

Pingo formation can be described with the observations made from this study. During summer, water is brought from the ground surface to the base of the active layer through precipitation events, or perhaps from nearby water sources. The increase in moisture content of the soil at the top of the permafrost table is caused by perched water in this zone, due to the impermeable nature of permafrost. At the onset of winter, as the surface begins to freeze, the water in the active layer is under pressure due to the closed-system. This water is injected into the weak area where pingo ice has already begun to form, or where it will form. During the following spring thaw, the water supply is replenished. During the following summer, some or all of the pingo ice may thaw, depending on the amount of ice accumulated, the surface conditions, and climatic conditions.

Mackay (1977) described observations of "pulsating pingo," that is, pingos that were found to rise and fall in response to the groundwater pressure below them. Artesian water was found in several borings at Mackay's research site, indicating that significant uplift pressures were acting on the pingo. Similar rising and falling of the surface was observed in the temperature cycles presented in the current study, particularly in samples JSA01, CSA01, JSI08, JCL01, and JCL02.

Yuri Shur (personal communication) provided a similar example to Mackay's pulsating pingo. A pingo, approximately 4 to 5 meters high was observed in northern Alaska, near Galbraith Lake (Figure 4.1(a)) during the spring of 1994. Upon return to the site approximately one year later, the entire formation had subsided (Figure 4.1(b)). This is likely due to significant water movement both in and out of the pingo, possibly at a hydraulic head, coupled with highly permeable coarse-grained soils.

Another periglacial formation similar to the pingo is the smaller-scale ice-cored mound Brown and Kreig (1983). Brown and Kreig hypothesized that ice-cored mounds formed at the base of Sukakpak Mountain, near Coldfoot, Alaska due to "frost damming" at the road prism. They proposed that water was transported downslope to the base of the mountain, and blocked from draining due to the road (however, they noted that the mounds were present at this site prior to the construction of the road). Additionally, water in the active layer could feed the formation of the frost mounds through cryosuction. The formation of ice-cored mounds may also be described as being induced by the closed-system cooling and open-system warming mechanism described for pingo formation.

(a) Galbraith Lake pingo, Spring 1994

(b) Galbraith Lake pingo, Spring 1995

Figure 4.1. Galbraith Lake pingo, Spring 1994 and 1995. Photos courtesy of Yuri Shur.

4.1.2 Discussion of Benkleman team results

Figure 4.2 is an illustration of a hypothetical freezing scenario submitted by Watkins, as discussed in Section 1.2.1.3.2. Watkins noted thin, evenly-spaced ice layers in previous experiments, and attempted to describe them using the theory proposed by the Benkleman team. He produced the proposed freezing conditions to create cryogenic structure based on his interpretation of the Michigan researchers' hypothesis. The furthest left element of the figure represents the soil profile, curves X and Z represent two different frost penetration profiles required to produce the large ice layers on the left, and O represents the necessary freezing front conditions to produce the thin, evenly spaced ice layers near the top of the sample.

Watkins stated that curve O is improbable, and that the likely cause of the thinly spaced layers is capillary suction to the base of the frozen layer of soil and rapid expansion and settlement of the soil layer directly below the frozen soil. While Watkins believed these conditions to be unrealistic, it could be argued that curve O is entirely probable, especially when considering natural soils and temperature conditions. Diurnal and other temperature variations could produce a frost profile similar to this, especially at the beginning of winter, when the daily air temperature tends to decrease with time.

It appears that the accuracy of curves X and Z in Figure 4.2 are questionable, and that Watkins did not fully recognize what was being presented by the Michigan team. In general, curves X and Z show a frost line that is decreasing with time. There are several small peaks in the curves, where the direction of the frost line reverses, moving upwards slightly (presumably due to an increase in air temperature above the soil). In Figure 4.2, these peaks occur in the locations where Watkins illustrated a thick ice plate in the soil profile.

These small reversals are not what the Michigan team presented in their research. They initially froze their cores from the top down, moving the freezing front almost completely to the bottom of the sample. Then, the frost line was moved up in the core by changing the temperature of the circulation water at the bottom of the sample. In their figures, they indicated that it was necessary to move the frost line to the bottom of the sample for subsequent plates to form, which was also identified as a necessity for ice formation in the present study.

The small peaks (Figure 4.2) appear to correspond with an upward movement of the frost line by 1 to 3 cm. This upward motion of the frost line is not sufficient to generate

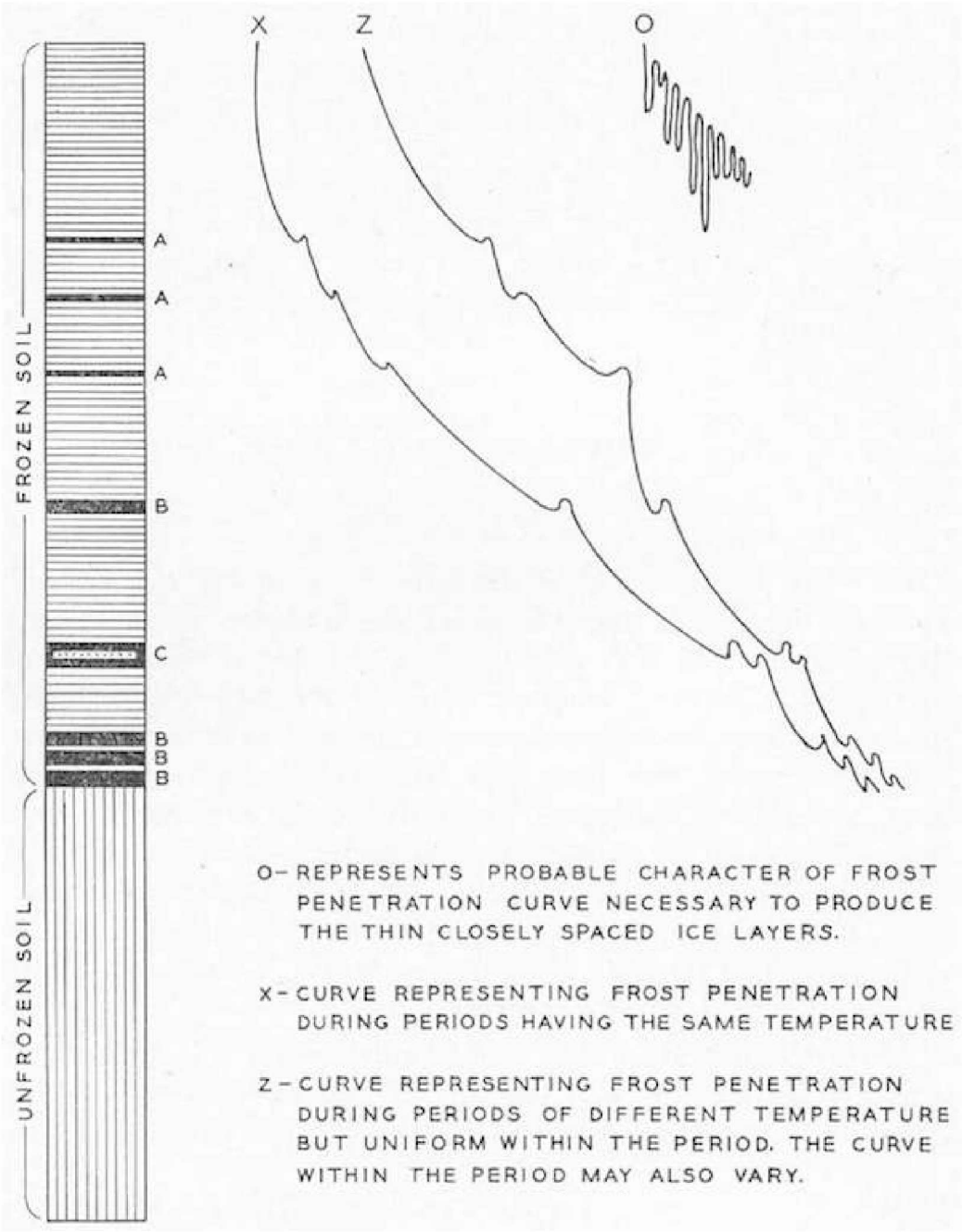

Figure 4.2. Proposed freezing conditions to create thin, evenly spaced ice layers in silt and fine-grained sand (reproduced from Watkins, 1931). Curves O, X, and Z represent the depth of the freezing front (y-axis) with time (x-axis) as relative, unitless processes. The curves are designed to be read in conjunction with the soil profile on the left side of the plot, and represent independent freezing scenarios proposed by Watkins.

those large ice plates, not in one cycle. With multiple cycles this may be possible; however, with only one cycle the thickness of the void that is filled with water is directly related to the initial volume expansion and the subsequent thawing of the soil on the upward movement of the frozen-unfrozen boundary. The Michigan crew emphasized that for significant ice accumulation, there needs to be multiple cycles. The formation of the small, evenly spaced ice layers is most likely due to cryosuction creating segregated ice lenses, i.e. primary frost heave. These mechanisms likely could occur concurrently.

Similarly, Casagrande stated that the samples in the Benkleman tests were adhering to the sides of the glass tubes. The current study identified and documented upward and downward displacement of the samples inside the cell, proving that in many cases the samples were not adhering to the sidewall of the cell. However, it could be argued that freezing to the sidewall is a phenomenon that has possible analogues in natural scenarios. For example, in a road's subgrade, traditional frost heave and/or pore ice formation could cause upward soil expansion that would displace the surface asphalt layer as well as the leveling course. If the prevailing ambient air temperature were to increase, thus causing the frost line to move upward, towards the asphalt, a portion of the subgrade could thaw beneath the asphalt. Because the asphalt was still exposed to freezing temperatures, it is likely that it would maintain the deformed shape of the displaced road as seen prior to the warming temperatures. This would create a void, beneath the asphalt/frozen layer of subgrade, and the subsided subgrade that had thawed during warming. If there was free water, this void could become filled with water, and upon subsequent cooling of the air temperature (thus moving the frost line down), the water void would become ice, and experience a volume expansion, possibly further deforming the roadway surface. The bridging effect of the asphalt is arguably equivalent to the sample adhering to the sides of the test apparatus.

Johnson (1952) included the work of the Michigan team in his state-of-the-field literature review for the Highway Research Board. He noted the dissatisfaction of Casagrande and Taber with the theory of ice growth under cyclic temperatures. Johnson included a quote from a geotechnical engineer of the day who sided with the Michigan researchers conclusions:

> [They] have answered the obvious discrepancy between Taber's theory and the field experience in Michigan soils and provided a more adequate basis for identifying frost heave soils and locations. The theory of the fluctuating frost line

> does not necessarily supplant Taber's theory, however, as it is entirely possible that frost heaves may be produced under the conditions of a constant frost line and soils of high capillarity. Both theories have practical value and, within their specific limits of application should be useful in identifying objectionable field conditions (Housel, 1938).

Otis described his observations of the impact of mild winters on road damage via frost heave:

> It has been observed that there is no direct correlation between the amount of heaving and the number of degree days, since some cold winters have caused less heaving than other milder winters. We may assume that ground-water conditions at the time of freeze-up and the occurrence of midwinter thaws have a major bearing on the total build-up of ice lenses (Otis, 1952).

Otis' mention of midwinter thaws is an occurrence noted by many others. A survey questionnaire was sent out in 1951 in preparation of the Highway Research Board special report on frost action. The survey focused on frost action specific to roadways. The following question was posed to States that experienced roadway damage due to frost action: "Is there correlation between [the] degree of distress attributable to frost action and climatic conditions?" The answers were submitted as "yes" or "no", with remarks from the respondent. Following is a summary of relevant comments (Shelburne, 1952):

L. F. Erickson (Idaho): "Yes. Varies with [the amount] of moisture available and cycles of freezing and thawing. Exceed[ingly] wet fall or spring gives trouble for breakup. Use total thickness of 6-15 inches. Frost penet[ration] range to depths of 4 feet in some areas."

J. E. Wood (Maryland): "Yes. Repeated freezing and thawing cycles causes severe damage."

W. C. Davis (Missouri): "Yes. Worst frost trouble have (sic) occurred at time of spring thaw after a winter of cycle freezing and thawing."

R. H. Gagle (Montana): "Yes. A dry season before winter freeze minimizes frost action. Slow and intermittent freezing and thawing increases frost damage."

P. S. Otis (New Hampshire): "Yes. A dry season before winter minimizes frost action. Midwinter thaws apt to increase frost action. Rapid spring thawing increases spring breakup."

A. W. Potter (South Dakota): "Yes. Degree of damage due to frost action dependent largely on the [amount] of moisture present in the soil at the time of freezing. A wet fall, followed by a severe winter and a quick spring thaw causes most damage. A great number of freeze thaw cycles also play an important part in causing frost damage."

4.1.3 Additional research

Bystrov (1984) reported that numerous Russian researchers, in the field, had found excessive frost heave after a brief period of thaw during winter. This heave was generally much greater than that due to monotonic freezing. He described a process of freezing front fluctuations, up and down in the soil, and the influx of moisture into the newly created void. Bystrov proposed the following equation for the evaluation of this type of frost heave:

$$\Delta h_n = \xi_f \gamma_{dr} (w_o - w_{un}) x 10^{-3} (1.09^{n-1} - 1) \tag{4.1}$$

where:

Δh_n = frost heave after n fluctuations of freezing front (cm)

ξ_f = amplitude of fluctuations (cm)

γ_{dr} = dry unit weight of soil (kg/m^3)

w_o = moisture content of soil (kg/kg)

w_{un} = unfrozen water content of soil (kg/kg)

In Bystrov's laboratory experiments, a soil sample was initially frozen at a constant rate of V=0.14x10^{-6} m/sec, with a thermal gradient in the unfrozen part of 15 °C/m. Once the sample reached the thermal steady-state, the thermal regime was modified so that the freezing front oscillated up and down in the sample, traversing a 1 cm length of soil over the course of 24 hours. The initial soil freezing formed lenticular ice lenses, while the fluctuations of the freezing front formed a layer of ice. At the end of the test, the ice was 2.4 cm thick.

Researchers have known about the impact cyclic temperatures have on soils, but most have not explored beyond the theoretical. Jumikis (1962) states "...ice segregation in soil also takes place under cyclic freezing and thawing conditions when the thawed ice waters

freeze again," referring to the thawing and refreezing of the isolated ice body that develops when the freezing front moves towards the soil surface.

Gravis (1974) noted that development of cracks in freezing fine-grained soil initiates injection of water if soil freezing is open-system. Gravis stated that the formation of ice lenses in coarse-grained soils can possibly be explained through a similar mechanism.

Preferantceva (1946) studied frost heave at several monitoring sites in the Moscow region. She noted that massive accumulation of ice in freezing soils occurred in winters with frequent thaws, as was also hypothesized by the Michigan researchers.

Tsytovich (1975) presented results from his studies of moisture migration in saturated coarse-grained soils:

> It was established that in water-saturated sands with free drainage of water in at least one direction, water does not migrate toward the freezing front, but is squeezed out, with the result that the porosity of frozen water-saturated sands remains practically the same (variations less than 0.2 percent). But when no drainage is provided, as when the material is frozen from all sides, an increase in the porosity of the frozen water-saturated sand was observed, ranging up to 4 percent at certain levels.
> (Tsytovich, 1975, p. 59)

Laboratory tests exploring the mechanics of injection ice involving temperatures oscillations on one side of a uniform gravel were performed by Gorelik (2009). The laboratory results showed the formation of isolated, thick bands of ice in the soil sample.

4.1.4 Up-freezing and Fel'dman's vacuum-filtration mechanism

Washburn (1980, p. 86) discussed the concept of "upfreezing" of objects, such as stones in fine-grained soils. The mechanism of upfreezing has been used to describe the formation of stone circles. One hypothesis for upfreezing is that during freezing, the fine-grained soil surrounding the stone forms an adfreeze bond to the sides of the stone, and moves the stone upwards through tangential frost heave forces (Figure 4.3(a)). The void that develops below the stone fills with water, and subsequently becomes ice when the freezing front passes through the water-filled void. The water migration into the void can be explained by Feld'man's theory of vacuum-filtration. The stone is like a plunger, and as it moves upward, the negative pressure that develops below the stone in the void sucks water into

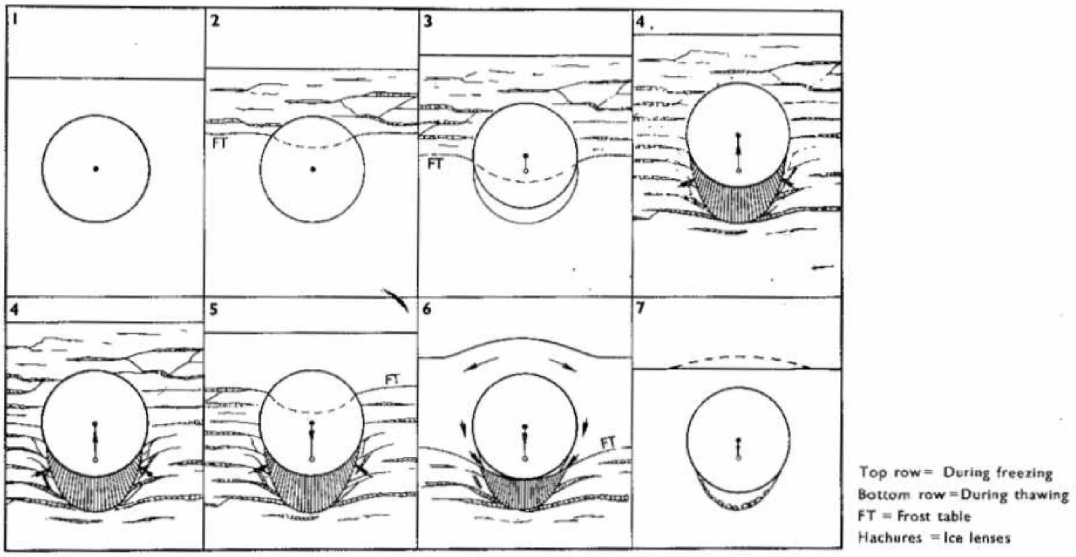

(a) Upfreezing of stones according to the frost-pull hypothesis (Washburn, 1980)

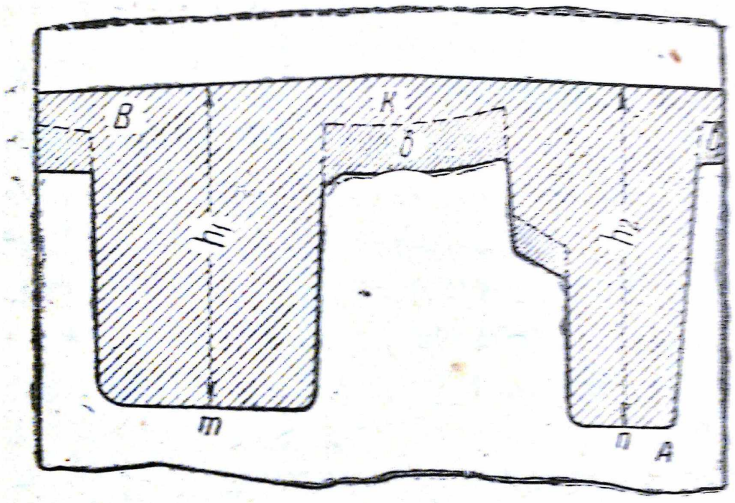

(b) Upfreezing of soil (Bykov and Kapterev, 1940)

Figure 4.3. Depictions of upfreezing mechanisms.

the void through the surrounding soil matrix. A similar mechanism is described by Bykov and Kapterev (1940) where two dissimilar soils are adjacent to each other (Figure 4.3(b)), and experience freezing from the surface. During freezing, the shaded soil on the left and right of the schematic freeze before the soil in the middle. While freezing, the shaded soil is upwardly displaced, leaving a void at the interface of the two soils in the middle. This void becomes filled with water, and subsequently becomes ice as the freezing front passes through the void. This scenario describes a two-dimensional freezing scenario, where soils vary laterally, as well as with depth. The tests conducted for the current study considered one-dimensional conditions, however, the observations from the tests conducted during the current study can be extrapolated to apply in the case presented by Bykov and Kapterev. The void that forms in between the two soil blocks can fill with water through the vacuum filtration mechanism, which then is converted into ice upon freezing.

4.1.4.1 Frost jacking

The formation of ice due to the vacuum-filtration mechanism has significant impact of the process of frost-jacking of deep foundation systems. Frost jacking is the upward movement of a pile, or slender body, due to the tangential frost heave forces that are applied to the circumference of the pile during freezing of the soil. Typically the basal forces are not considered in the analysis and prediction of frost jacking. Figure 4.4 (Kudriavtsev, 1978) presents a scenario of frost jacking on a pile. During the initial freezing (I and II), the tangential forces acting along the circumference of the pile slightly jack the pile out of the ground, producing a small void at the base of the pile. The upward movement of the pile can act like a plunger, creating a vacuum below the pile, which has the tendency to draw water into the void, as described in the experiments performed in the current study. As the freezing front passes the water-filled void, the water is converted into ice, which in turn experiences an increase in total volume, applying additional forces (basally) on the pile (III). Upon thawing during the following summer (IV and V), the pile will tend to settle again, however a small void will be left behind due to the increase in volume of the void below the base of the pile. The cumulative effect of this process (VI) can lead to failure of the pile due to lack of embedment.

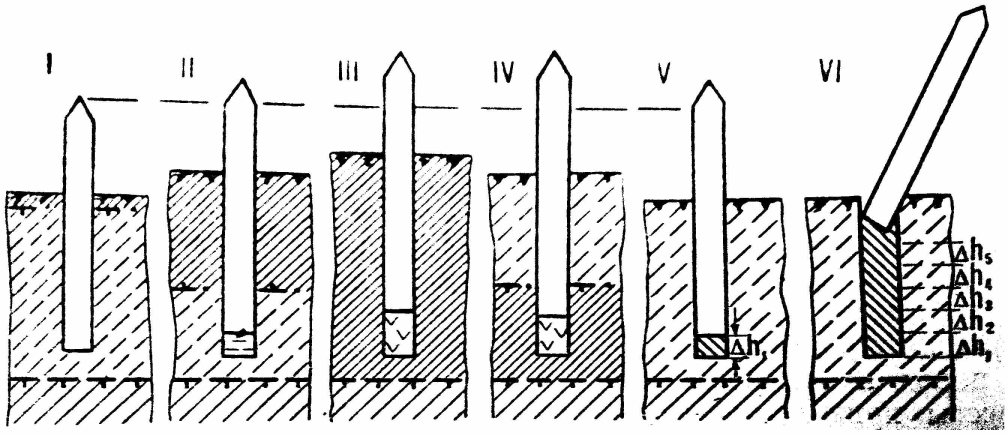

Figure 4.4. Impact of the vacuum-filtration mechanism on frost jacking (Kudriavtsev, 1978)

4.1.5 The Miller experiment

Williams and Smith (1991) presented a brief discussion on frost heave, and the impact of frost action on engineered structures. To illustrate their point, two photos (Figures 4.5(a) and 4.5(b)) were presented that demonstrate the ability of a freezing soil to displace a significant mass. The photos are credited to R. D. Miller, however no additional details are provided. Williams and Smith were contacted for additional details regarding the Miller experiment during the current study, however no response was received.

The post-freezing photo (Figure 4.5(c)) indicates the presence of ice lenses in the sample. The ice lenses that have formed in the Miller test have a strong similarity to the formation of uniform lenses in sample JSI01 (Figure 4.5(d)). Ice lenses that form due to segregation (such as the ice in the samples tested by Taber and Beskow) tend to increase in thickness as the freezing front propagates through the sample. The ice lenses presented in the Miller experiment are uniform in thickness and regularly spaced, like those in sample JSI01.

4.2 Conclusions

Our studies have proved findings by Benkleman, Burton, and Olmstead (as well as by Fel'dman). While their theory was considered controversial when first presented almost 100 years ago, modern technology has helped to facilitate an in-depth look at this process of ice formation. The formation of thick layers of ice via a mechanism other than traditional frost heave associated with the traditional ice segregation mechanism has been

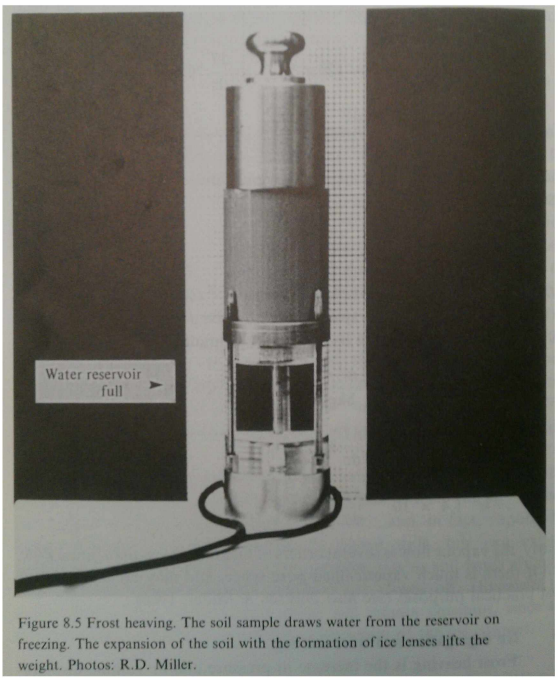

(a) Miller experiment, before freezing

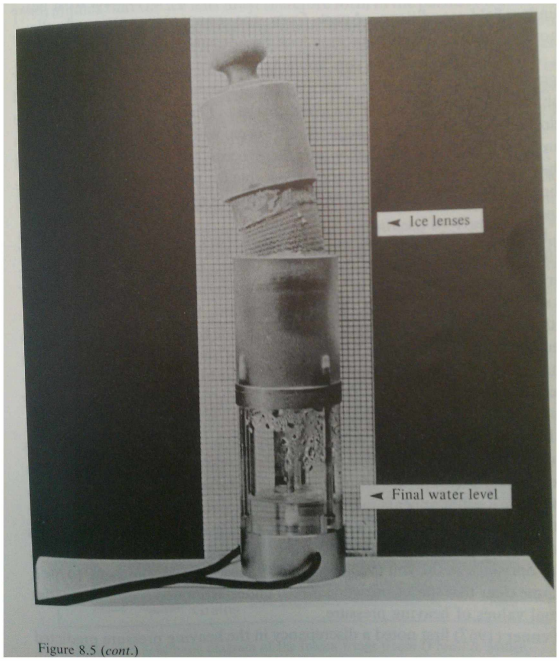

(b) Miller experiment, after freezing

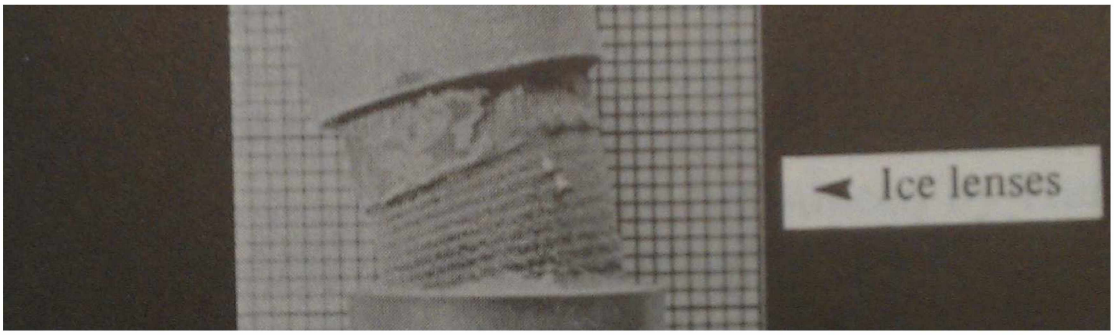

(c) Miller experiment, ice close-up

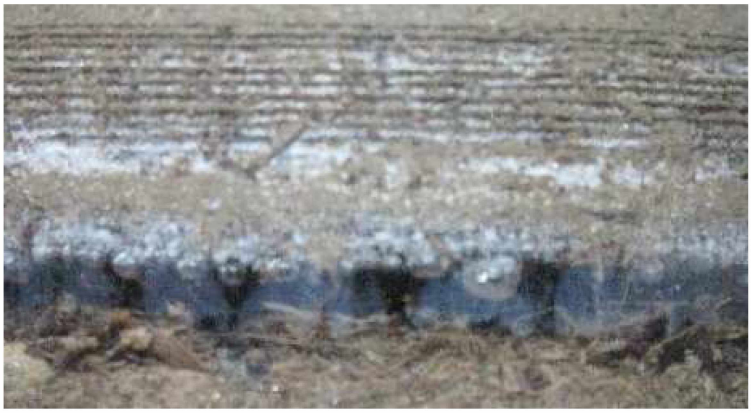

(d) JSI01, ice close-up

Figure 4.5. Miller experiment (Williams and Smith, 1991)

demonstrated in both non-cohesive fine-grained soils and coarse-grained soils. Our study has clarified that the formation of a discrete layer of ice will occur during the thermal process that involves fluctuations of the frozen-unfrozen boundary soil, particularly when freezing (downward movement of the freezing front) occurs under closed system conditions, and soil thawing occurs under open system conditions (upward movement of the frozen-unfrozen boundary). In fine-grained soils, such as Fox silt (which did not produce segregated ice during continuous freezing stages during our tests), cooling and warming cycles under open system conditions promoted the development of appreciable layers of ice. When the freezing was accomplished under closed system, the development of ice increased significantly.

The movement of water out of coarse-grained soil during freezing has been demonstrated by Tsytovitch (1975) when saturated coarse-grained soils were frozen under open-system conditions. Our study has demonstrated that the migration of water out of fine-grained non-cohesive soil freezing under open system conditions also takes place.

Under certain conditions, the sorting and segregation of organics in organic-rich soils was noted, creating a layer of concentrated organics, due to the buoyancy of organic material when compared to mineral soil.

Micro-computed tomography was utilized in this study to aid in visual characterization of frozen soil and ice. This technology helped to identify features in the samples that otherwise would have been undetectable to the naked eye, such as entrained air, suspended sediment, and re-orientation of sediment.

Our study explains findings reported by highway engineers who have noticed that maximum frost heave in areas that are not underlain with permafrost tends to occur during winters that experience thaw events. Our findings can contribute to the understanding of the role of basal frost heave forces in frost jacking, as well. The study also explains the formation of frost mounds with ice cores in coarse soil, and introduces additional factors for consideration when describing cryostructure formation.

While detailed in nature, this investigation was in no way exhaustive. Future work to elaborate on this study could entail:

1. Cyclic warming and cooling tests on fine-grained cohesive soils.

2. The investigation of pore water pressure during the freezing/cooling segment of the temperature cycles in coarse-grained and fine-grained soils.

3. Sorting and movement of coarse-grained soil embedded in a fine-grained soil matrix during temperature cycling.

References

Andersland, O., Ladanyi, B., 2004. Frozen ground engineering, 2nd Edition. John Wiley and Sons.

ASTM, 2007a. Standard D2974-07a. 10.1520/D2974-07a.

ASTM, 2007b. Standard D4959-07. 10.1520/D4959-07.

Benkelman, A., Olmstead, F., 1931. A new theory of frost heaving. In: Proceedings of the Highway Research Board. Vol. 11. Highway Research Board, pp. 152–165.

Beskow, G., 1935. Soil freezing and frost heaving with special applications to roads and railroads. Vol. Year Book no. 3. Swedish Geological Society.

Black, P., Hardenberg, M., 1991. Historical perspectives in frost heave research: the early works of S. Taber and G. Beskow. No. SR91-23. CRREL.

Bray, M., French, H., Shur, Y., 2006. Further cryostratigraphic observations in the CRREL Permafrost Tunnel, Fox, Alaska. Permafrost and Periglacial Processes 17 (3), 233–243.

Brown, J., Kreig, R. A., 1983. Guidebook to permafrost and related features along the Elliott and Dalton Highways, Fox to Prudhoe Bay, Alaska. Guidebook 4, University of Alaska.

Burton, V., Benkelman, A., February 1931a. Frost action in silt soils defined by field and cold-room studies. Engineering News-Record 106 (7).

Burton, V., Benkelman, A., 1931b. The relation of certain frost phenomena to the subgrade. In: Highway Research Board Proceedings. Vol. 10. Highway Research Board, pp. 259–279.

Bykov, N., Kapterev, P., 1940. Permafrost and construction (Vechnaia merzlota i stroitel'stvo na ney). Transzheldorizdat.

Bystrov, N., 1984. Design of flexible pavement with layers of thermal insulation taking into account freezing front fluctuations. Ph.D. thesis, Moscow Institute on Automotive Roads.

Casagrande, A., 1931. Discussion of "A new theory of frost heaving". In: Proceedings of the Highway Research Board. Vol. 10. pp. 152–165.

Darrow, M., 2007. Experimental study of adsorbed cation effects on the frost susceptibility of natural soils. Ph.D. thesis, University of Alaska Fairbanks.

Dillon, M., Fortier, D., Kanevskiy, M., Shur, Y., 2008. Tomodensitometric analysis of basal ice. In: D.L. Kane, K. H. (Ed.), Proceedings of the Ninth International Conference on Permafrost. Vol. 1. Institute of Northern Engineering, pp. 361–366.

Fel'dman, G., 1988a. Formation problem of thick ice streaks, ice saturated horizons in permafrost. In: Senneset, K. (Ed.), Proceedings of the Fifth International Conference on Permafrost. Vol. I. pp. 339–343.

Fel'dman, G., 1988b. Migration of moisture in freezing, frozen, and thawing soils. In: Water movement in unfrozen and freezing soils. Nauka, Novosibirsk, pp. 206–234.

French, H. M., 2007. The periglacial environment, 3rd Edition. John Wiley and Sons Ltd.

Gorelik, J., 2009. Modeling of ice accumulation in freezing ground at injection moisture entry (in Russian). Earth Cryosphere 13 (3), 45–53.

Gravis, G., 1974. Ground ice, cryogenic structure and cryofacies analysis of frozen ground. In: Mel'nikov, P., Tolstikhin, N. (Eds.), General Permafrost. Nauka, Novosibirsk, pp. 135–160 (in Russian).

Henry, K., 2000. A review of the thermodynamics of frost heave. TR 00-16, U.S. Army Corps of Engineers Cold Regions Research and Engineering Laboratory.

Holmes, G., Hopkins, D., Foster, H., 1968. Pingos in central Alaska. Tech. Rep. 1241-H, Geological Survey Bulletin.

Housel, W., 1938. Applied soil mechanics, part 1: Soil as an engineering material. Tech. rep., Civil Engineering Department, University of Michigan.

Johnson, A., 1952. Frost action in roads and airfields. Special Report 1, Highway Research Board.

Jumikis, A., 1962. Frost action in soils. In: Soil mechanics. D. Van Nostrand Company, p. 246.

Krzewinski, T., Washholz, W., Miller, D., Lotakis, G., 2006. ARRC rail alignment improvements Birchwood, Alaska railroad design - construction in marginally frozen relic ice and soil. In: Proceedings of the 13th International Conference: Cold regions engineering 2006, Current practices in cold regions engineering. Orono, Maine.

Kudriavtsev, V. (Ed.), 1978. General Permafrost (Geocryology). Moscow University Press.

Leffingwell, E., 1919. The Canning River region, northern Alaska. No. nos. 109-110. Government printing office.

Mackay, J., 1977. Pulsating pingos, Tuktoyaktuk Peninsula, N.W.T. Canadian Journal of Earth Sciences 14, 209–222.

Mackay, J., 1979. Pingos of the Tuktoyaktuk peninsula area, Northwest territories. Géographie physique et Quaternaire 33 (1).

Mackay, J., 1998. Pingo growth and collapse, Tuktoyaktuk Peninsula area, western arctic coast, Canada: A long-term field study. Géographie physique et Quaternaire 52 (3).

Otis, P., 1952. Frost action and spring break-up. Special Report 2, Highway Research Board.

Péwé, T. L., 1982. Geologic hazards of the Fairbanks area, Alaska. Special Report 15, Department of Natural Resources Division of Geological and Geophysical Surveys.

Preferantceva, L., 1946. Moisture regime of roadbed. Moscow, pp. 6–36 (in Russian).

Rice, E., 1975. Building in the north. The Geophysical Institute, University of Alaska Fairbanks, AK.

Shelburne, T., 1952. Results of a questionnaire on remedies and treatments. In: Frost action in soils: A symposium. No. 2. pp. 357–372.

Taber, S., 1929. Frost heaving. Journal of Geology 37, 428–461.

Taber, S., 1930. The mechanics of frost heaving. Journal of Geology 38, 303–317.

Taber, S., 1931. Discussion of "A new theory of frost heaving". In: Proceedings of the Highway Research Board. Vol. 10. pp. 152–165.

Tsytovich, N., 1975. The mechanics of frozen ground, 2nd Edition. Scripta Book Company.

U.S. Army Corps of Engineers, 1984. Engineer manual. Pavement criteria for seasonal frost conditions. EM 1110-3-138. Washington, D.C.

Washburn, A., 1980. Geocryology, 2nd Edition. Halsted Press.

Watkins, W., 1931. Discussion of "A new theory of frost heaving". In: Proceedings of the Highway Research Board. Vol. 10. pp. 152–165.

Williams, P., Smith, M., 1991. The frozen earth: fundamentals of geocryology. Cambridge University Press.

Willis, E., 1931. Discussion on "The relation of certain frost phenomena to the subgrade". In: Highway Research Board Proceedings. Vol. 10. Highway Research Board, pp. 259–279.

Appendix A: Time-lapse Videos

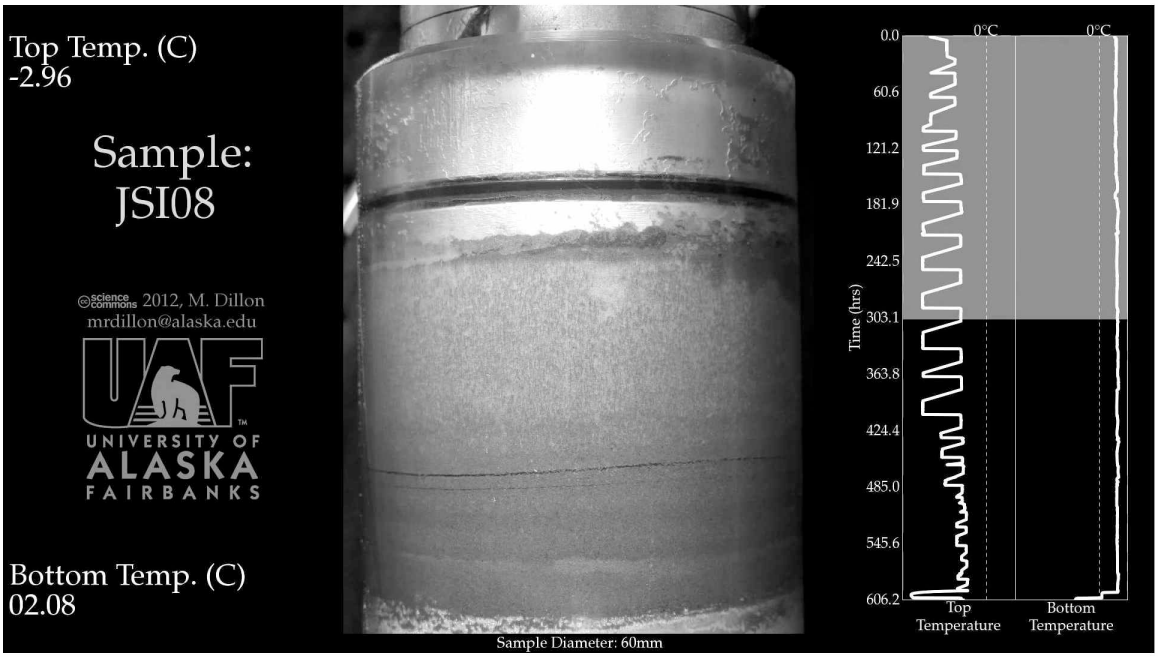

Figure A.1. JSI08 time-lapse video. Video file may be found on attached DVD.

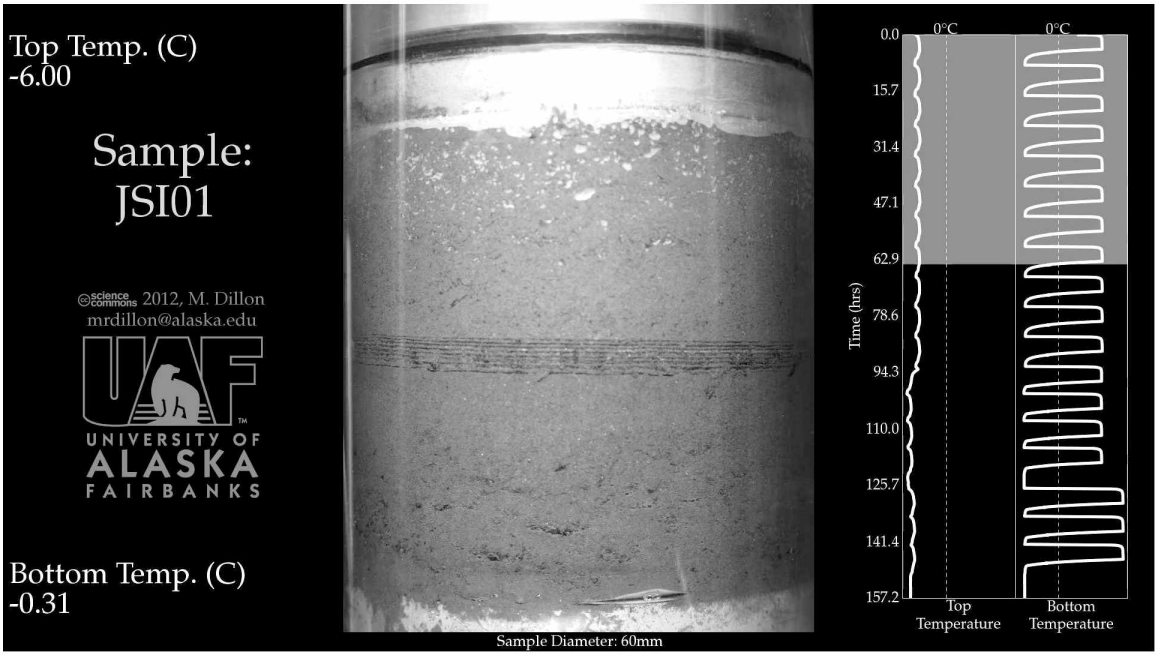

Figure A.2. JSI01 time-lapse video. Video file may be found on attached DVD.

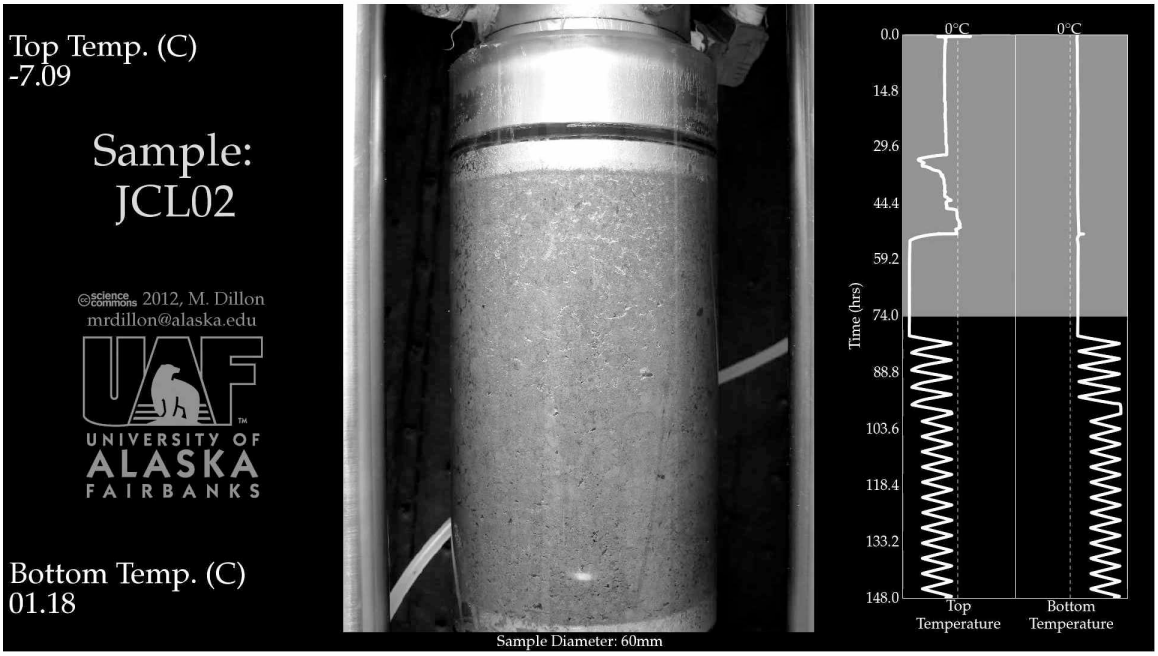

Figure A.3. JCL02 time-lapse video. Video file may be found on attached DVD.

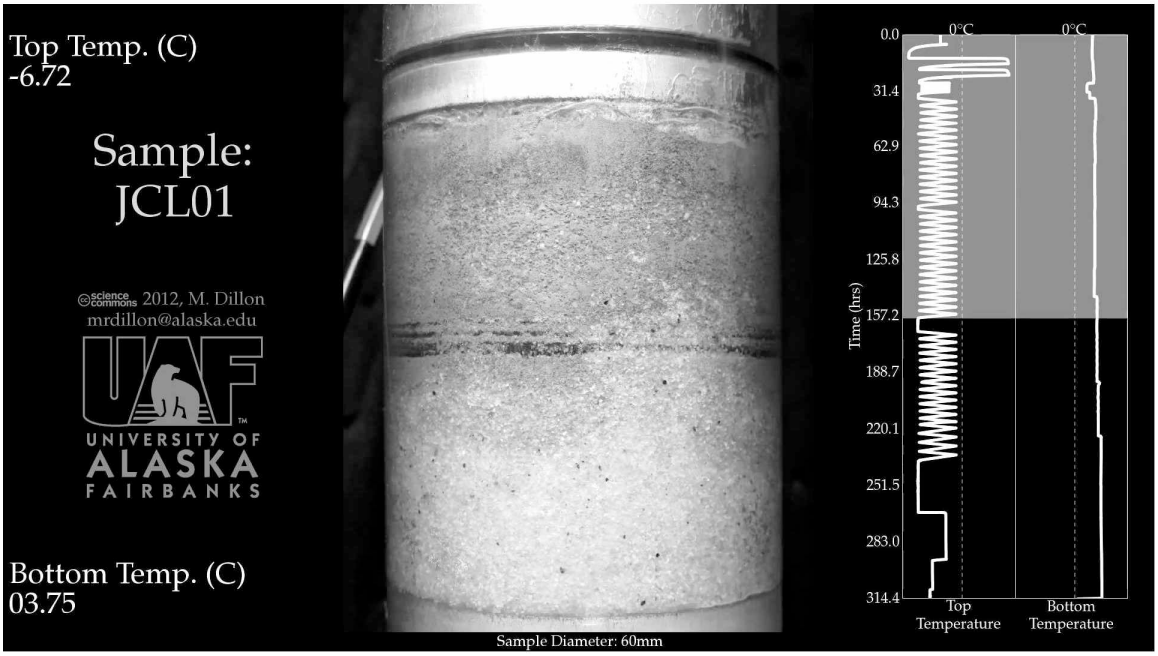

Figure A.4. JCL01 time-lapse video. Video file may be found on attached DVD.

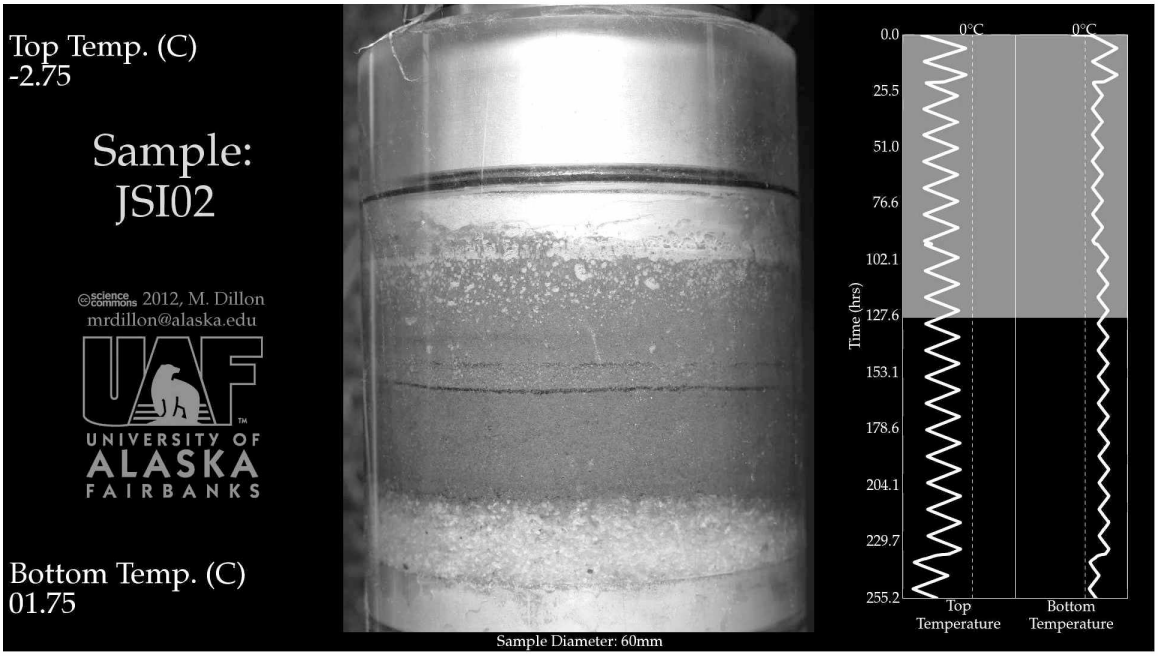

Figure A.5. JSI02 time-lapse video. Video file may be found on attached DVD.

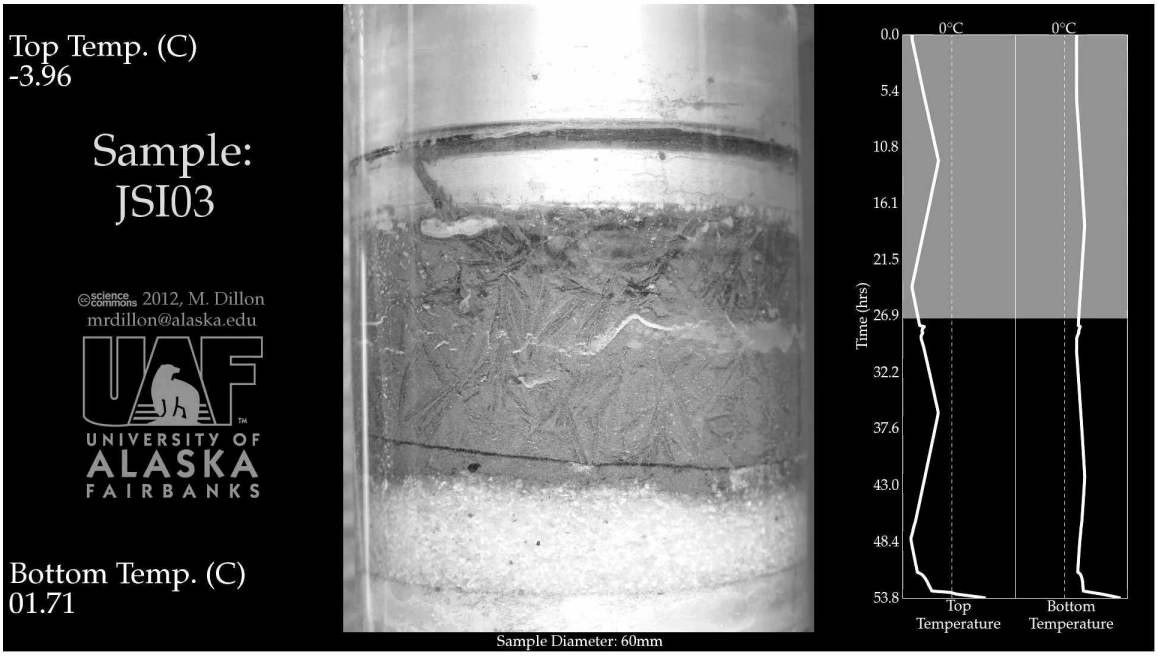

Figure A.6. JSI03 time-lapse video. Video file may be found on attached DVD.

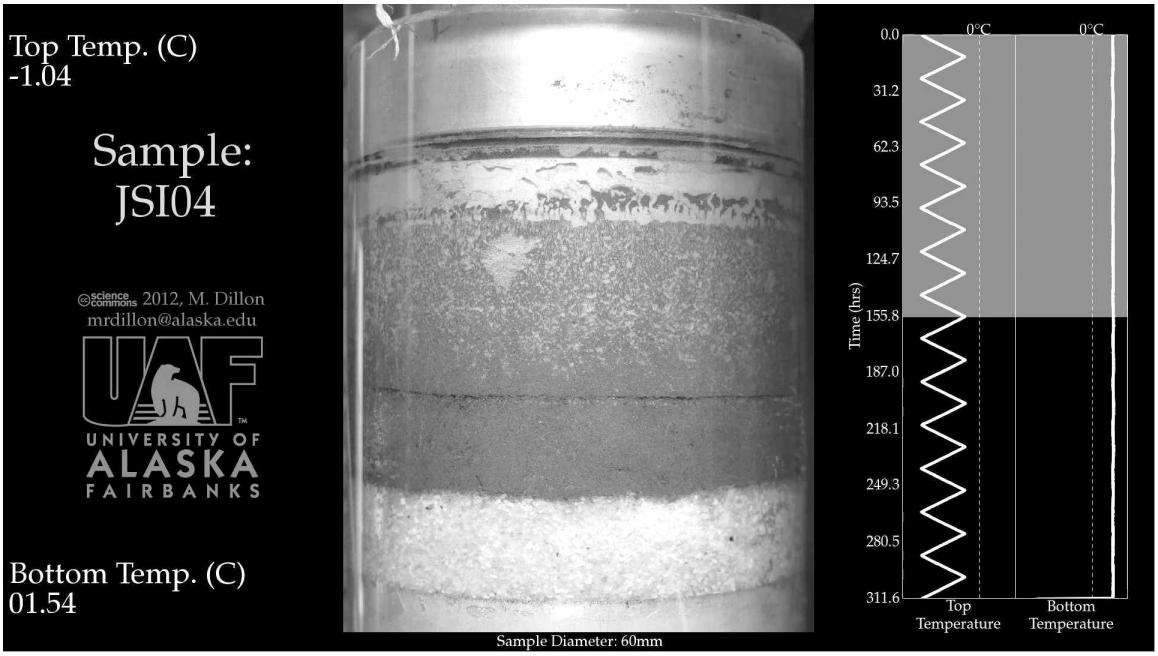

Figure A.7. JSI04 time-lapse video. Video file may be found on attached DVD.

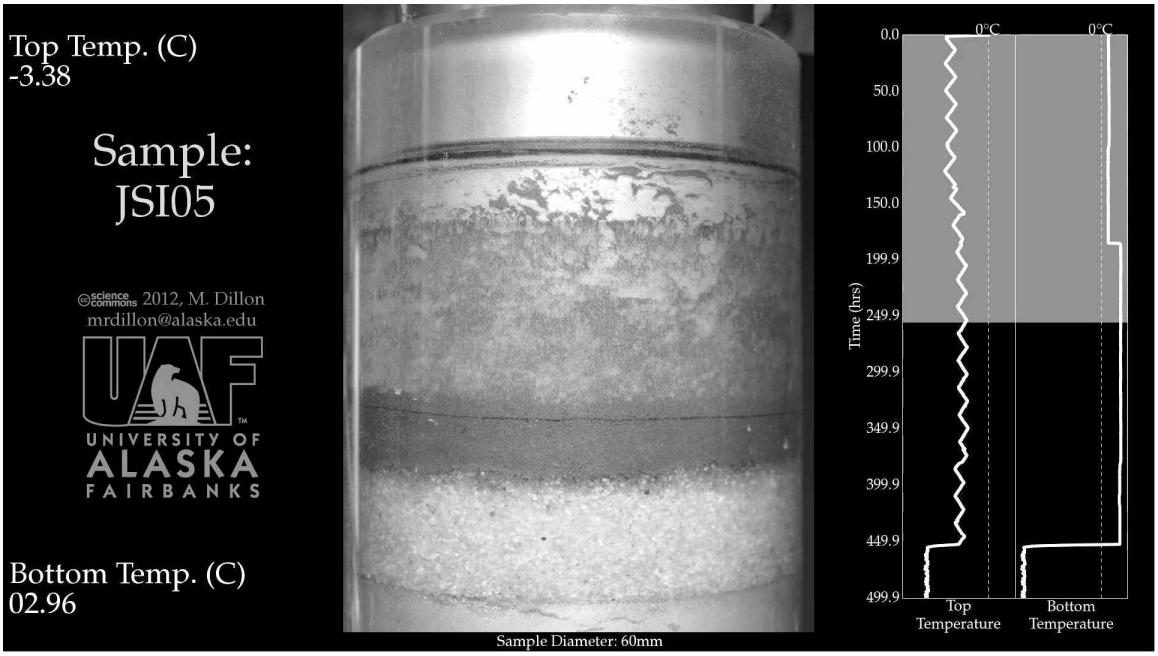

Figure A.8. JSI05 time-lapse video. Video file may be found on attached DVD.

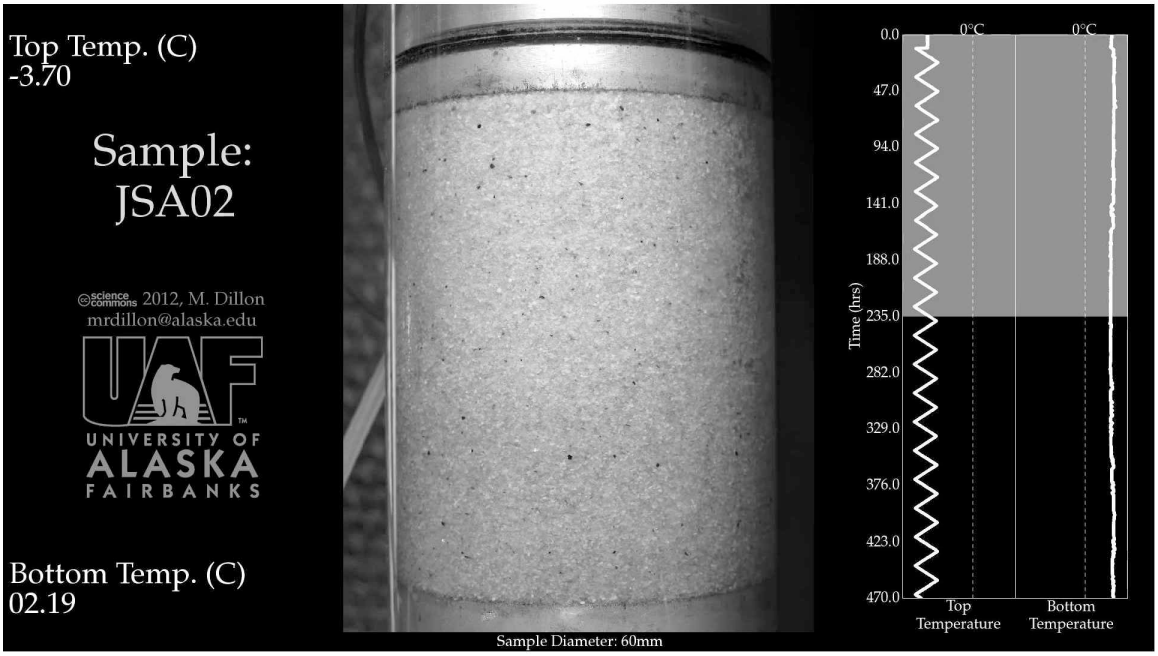

Figure A.9. JSA02 time-lapse video. Video file may be found on attached DVD.

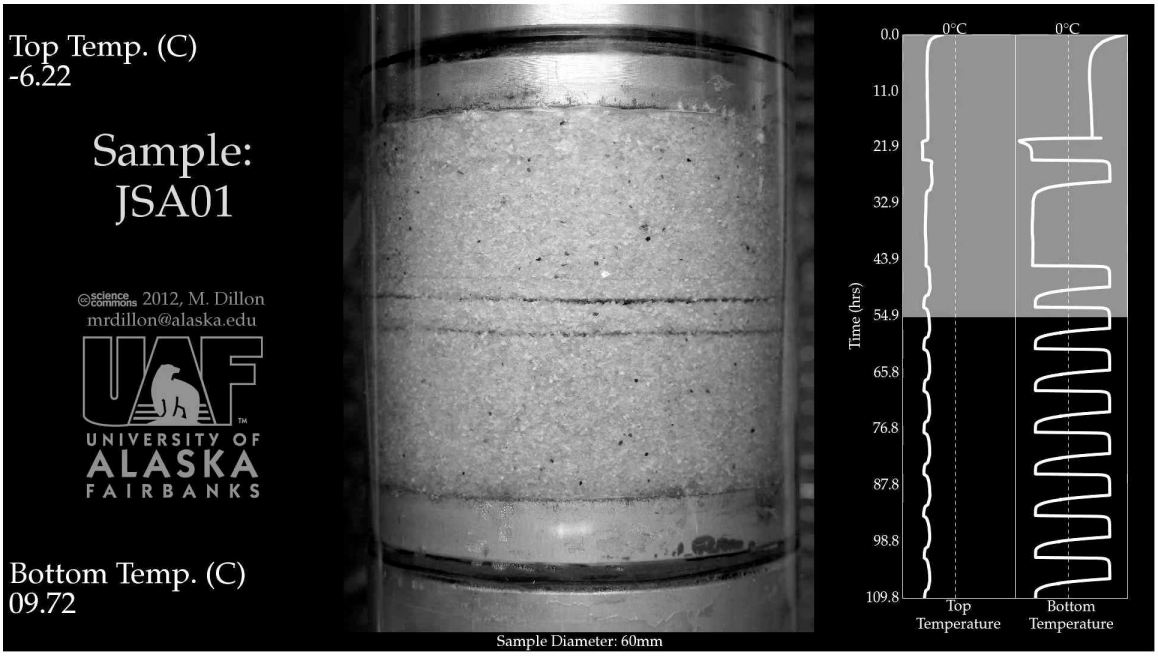

Figure A.10. JSA01 time-lapse video. Video file may be found on attached DVD.

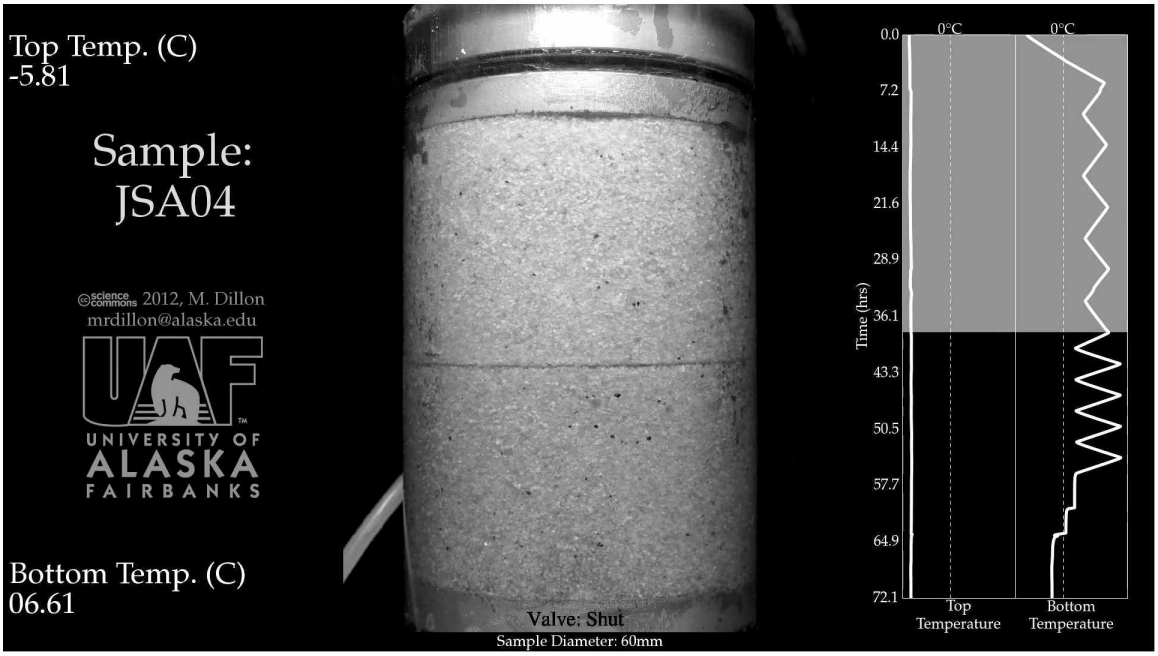

Figure A.11. JSA04 time-lapse video. Video file may be found on attached DVD.

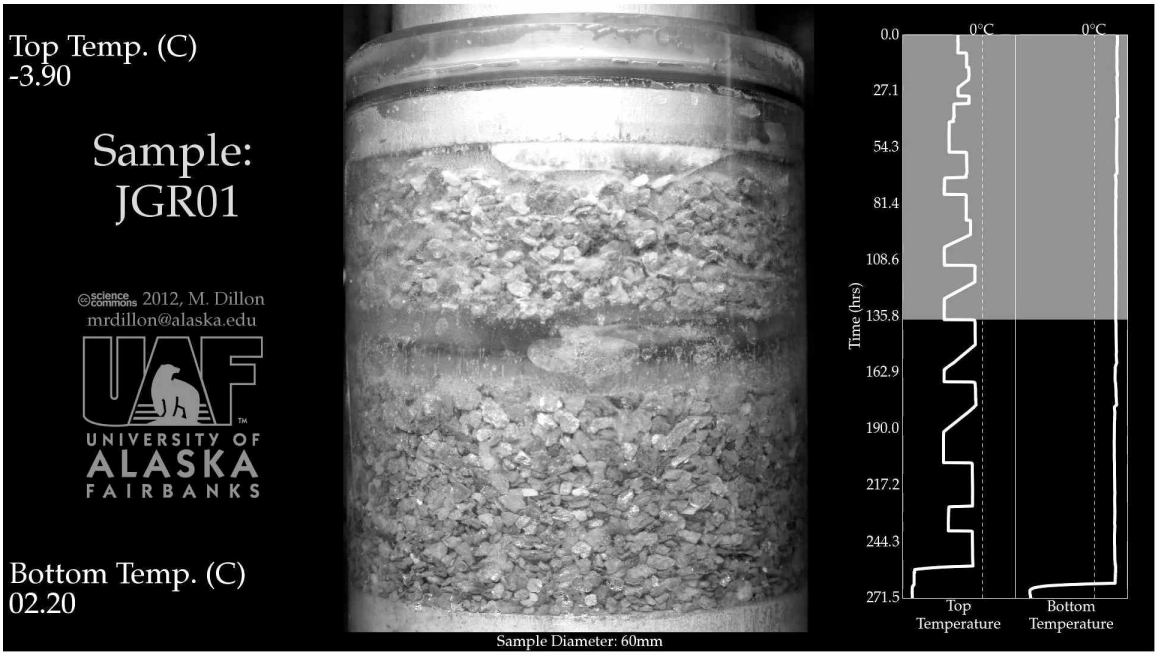

Figure A.12. JGR01 time-lapse video. Video file may be found on attached DVD.

Appendix B: Test Progression Image Sequences

(a) 0 hrs (b) 75.8 hrs (c) 151.6 hrs

(d) 227.4 hrs (e) 303.2 hrs (f) 379.0 hrs

(g) 454.8 hrs (h) 530.6 hrs (i) 606.2 hrs

Figure B.1. JSI08 test progression image sequence. Sample diameter is 60 mm. Initial sample height is 55 mm.

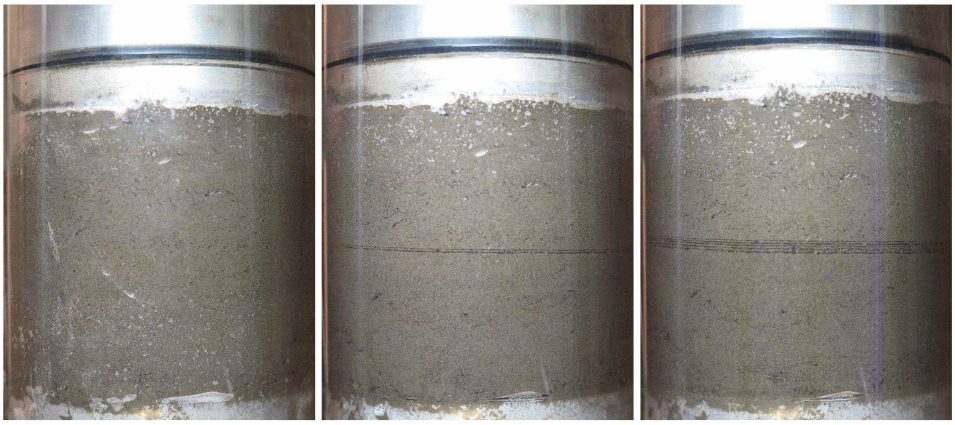

(a) 0 hrs (b) 19.7 hrs (c) 39.4 hrs

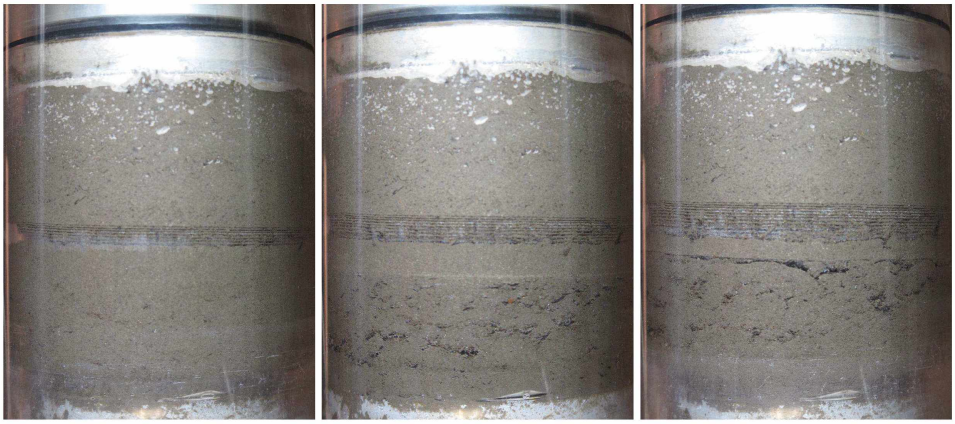

(d) 59.1 hrs (e) 78.8 hrs (f) 98.5 hrs

(g) 118.2 hrs (h) 137.9 hrs (i) 157.2 hrs

Figure B.2. JSI01 test progression image sequence. Sample diameter is 60 mm. Initial sample height is 69 mm.

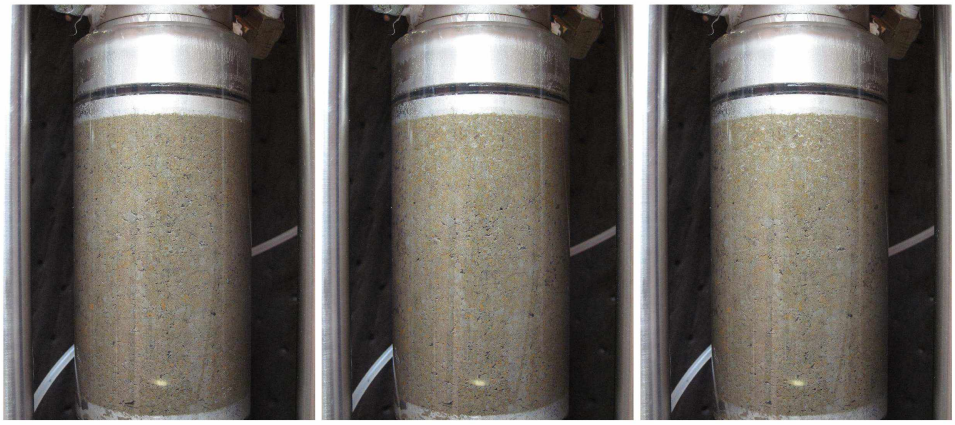

(a) 0 hrs (b) 18.5 hrs (c) 37.0 hrs

(d) 55.5 hrs (e) 74.0 hrs (f) 92.5 hrs

(g) 111.0 hrs (h) 129.5 hrs (i) 148.0 hrs

Figure B.3. JCL02 test progression image sequence. Sample diameter is 60 mm. Initial sample height is 129 mm.

(a) 0 hrs (b) 39.3 hrs (c) 78.6 hrs

(d) 117.9 hrs (e) 157.2 hrs (f) 196.5 hrs

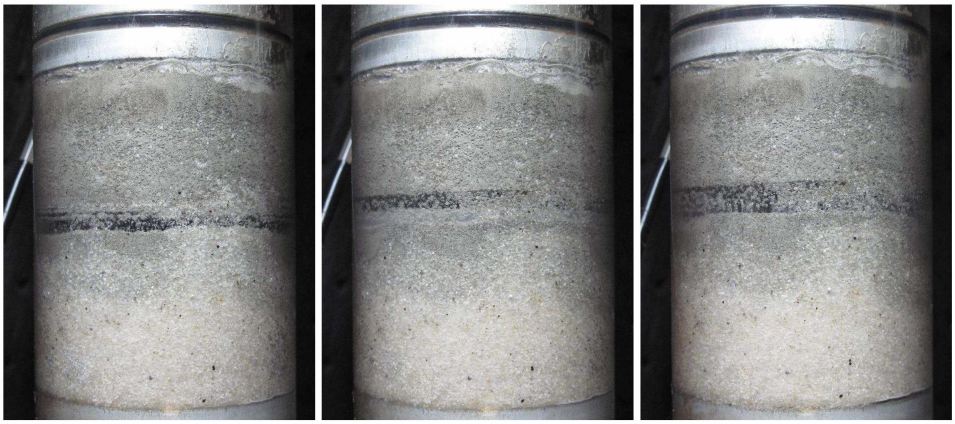

(g) 235.8 hrs (h) 275.1 hrs (i) 314.4 hrs

Figure B.4. JCL01 test progression image sequence. Sample diameter is 60 mm. Initial sample height is 82 mm.

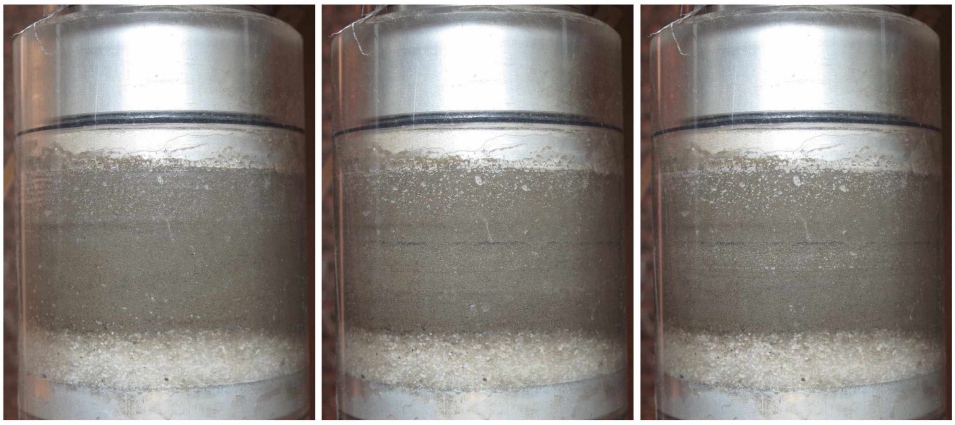

(a) 0 hrs (b) 31.9 hrs (c) 63.8 hrs

(d) 95.7 hrs (e) 127.6 hrs (f) 159.5 hrs

(g) 191.4 hrs (h) 223.3 hrs (i) 255.2 hrs

Figure B.5. JSI02 test progression image sequence. Sample diameter is 60 mm. Initial sample height is 53 mm.

(a) 0 hrs (b) 6.7 hrs (c) 13.4 hrs

(d) 20.1 hrs (e) 26.8 hrs (f) 33.5 hrs

(g) 40.2 hrs (h) 46.9 hrs (i) 53.8 hrs

Figure B.6. JSI03 test progression image sequence. Sample diameter is 60 mm. Initial sample height is 65 mm.

(a) 0 hrs (b) 39.0 hrs (c) 78.0 hrs

(d) 117.0 hrs (e) 156.0 hrs (f) 195.0 hrs

(g) 234.0 hrs (h) 273.0 hrs (i) 311.6 hrs

Figure B.7. JSI04 test progression image sequence. Sample diameter is 60 mm. Initial sample height is 63 mm.

(a) 0 hrs (b) 62.5 hrs (c) 125.0 hrs

(d) 187.5 hrs (e) 250.0 hrs (f) 312.5 hrs

(g) 375.0 hrs (h) 437.5 hrs (i) 499.9 hrs

Figure B.8. JSI05 test progression image sequence. Sample diameter is 60 mm. Initial sample height is 63 mm.

(a) 0 hrs (b) 58.8 hrs (c) 117.6 hrs

(d) 176.4 hrs (e) 235.2 hrs (f) 294.0 hrs

(g) 352.8 hrs (h) 411.6 hrs (i) 470.0 hrs

Figure B.9. JSA02 test progression image sequence. Sample diameter is 60 mm. Initial sample height is 100 mm.

(a) 0 hrs (b) 13.7 hrs (c) 27.4 hrs

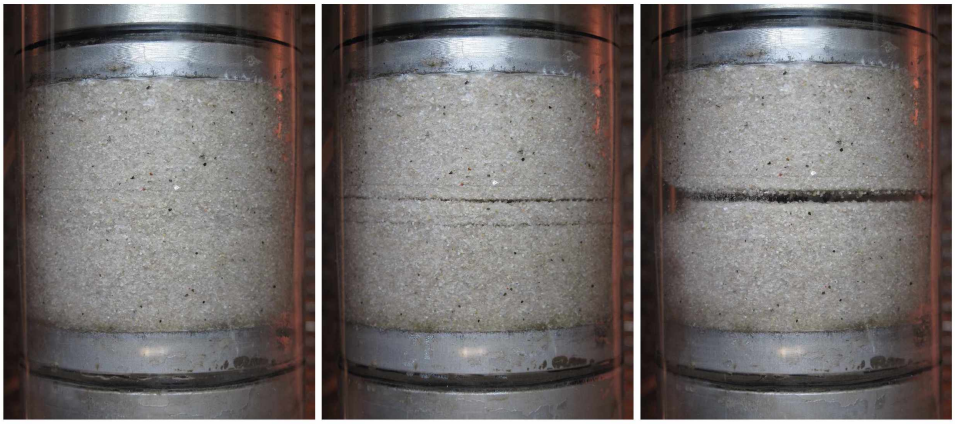

(d) 41.1 hrs (e) 54.8 hrs (f) 68.5 hrs

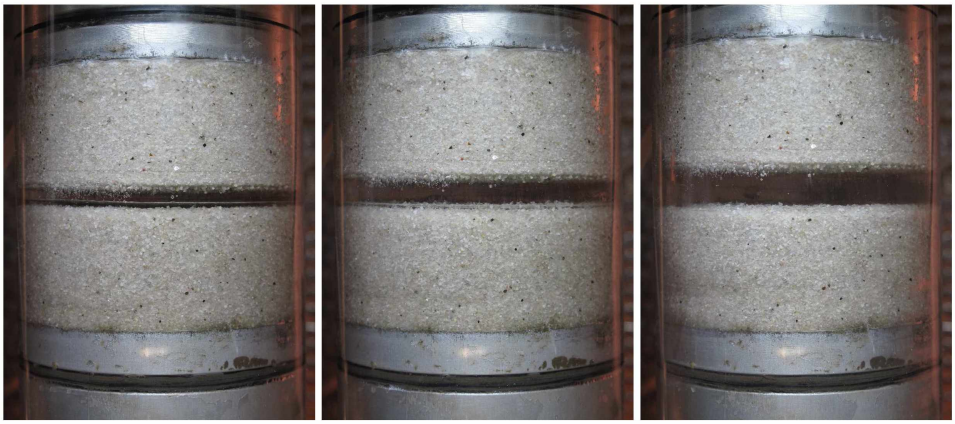

(g) 82.2 hrs (h) 95.9 hrs (i) 109.8 hrs

Figure B.10. JSA01 test progression image sequence. Sample diameter is 60 mm. Initial sample height is 66 mm.

(a) 0 hrs (b) 9.0 hrs (c) 18.0 hrs

(d) 27.0 hrs (e) 36.0 hrs (f) 45.0 hrs

(g) 54.0 hrs (h) 63.0 hrs (i) 72.1 hrs

Figure B.11. JSA04 test progression image sequence. Sample diameter is 60 mm. Initial sample height is 96 mm.

(a) 0 hrs (b) 33.9 hrs (c) 67.8 hrs

(d) 101.7 hrs (e) 135.6 hrs (f) 169.5 hrs

(g) 203.4 hrs (h) 237.3 hrs (i) 271.5 hrs

Figure B.12. JGR01 test progression image sequence. Sample diameter is 60 mm. Initial sample height is 77 mm.

Appendix C: Supplementary Tests

Sample JCL02

Sample JCL02 was composed of screened Fox silt, initially consolidated and saturated in the Hokkaido Cell prior to testing as described in Section 2.4. The first 80 hours of the test were spent pre-freezing the sample. The cooling equipment malfunctioned halfway through pre-freezing (around 32 hours), and was resumed after troubleshooting the issue. The test was split into two distinct phases of testing (Table 3.1). The top temperature was varied linearly from approximately -7.0°C and -1.0°C for the duration of the test, while the bottom temperature was varied linearly from 1.0°C to 7.5°C over a 4 hour period (Figure C.1(a,b), Table 3.1). The thermal conditions ensured that the sample was under open system conditions while warming and cooling.

Figure A.3 (Appendix A) is a condensed time-lapse video of the total test progression for sample JCL02. Select stills from the video are in Appendix B, Figure B.3. The initial freezing of the sample did not produce any segregated ice. Similar to JSI08, the test conditions produced a thin zone of excess ice in the soil sample. The total FHR at the conclusion of the test, prior to refreezing the bottom of the sample, was approximately 0.3%. There was a large spike in water flux (Figure C.1(d)), heave rate (Figure C.1(e)), and water flux rate (Figure C.1(f)), beginning at 48 hours, which corresponded to a drop in the top temperature. After 80 hours, water was taken in during the upward movement of the frozen-thawed interface, and then expelled during the downward movement of the freezing front (Figure C.1(d)). The FHR shows a similar trend, wherein the sample length decreases slightly during thawing (Figure C.1(c)). The results are similar to JSI08, in that the sample was free to move up and down and was not adhering to the sidewalls of the cell.

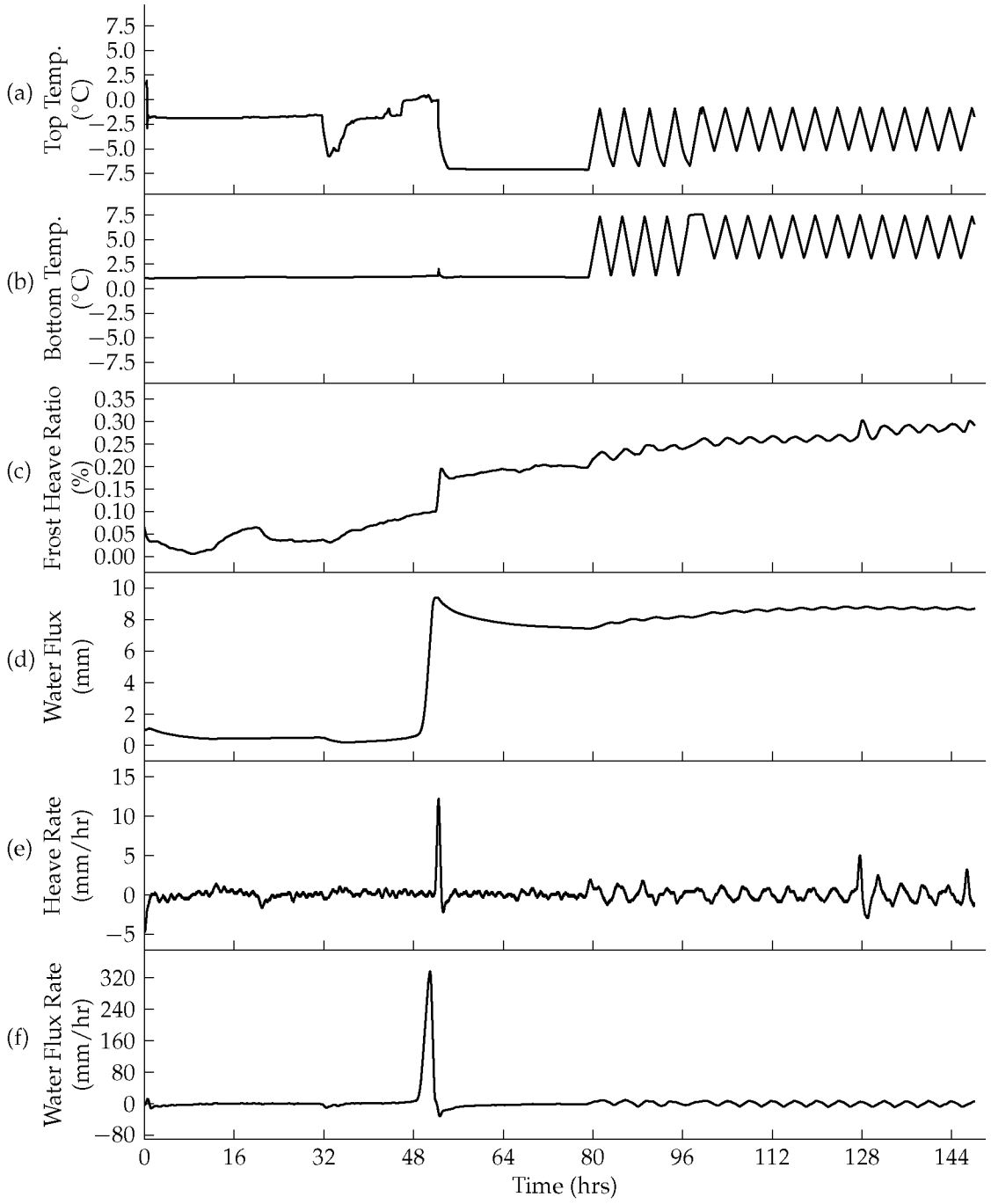

Figure C.1. JCL02 soil temperatures (a,b), frost heave ratio (c), water flux (d), heave rate (e), and water flux rate (f).

Sample JSI03

Sample JSI03 was composed of unscreened Fox silt, over a layer of clean uniform sand, initially consolidated, saturated, and frozen in the Hokkaido Cell prior to testing as described in Section 2.4. The top temperature was varied linearly from approximately -5°C to -1.5°C for the duration of the test, while the bottom temperature was varied linearly from approximately 1.5°C to 2.5°C (12 hours warming, 12 hours cooling, top and bottom cycles offset by 6 hours, Figure C.2(a,b), Table 3.2). These thermal conditions ensured that the sample was under open system conditions while cooling and warming.

Figure A.6 (Appendix A) is a condensed time-lapse video of the total test progression for sample JSI03. Select stills from the video are in Appendix B, Figure B.6. The initial freezing of the sample prior to testing did not form any segregated ice. A water-filled void was visible during testing after approximately 11 hours, when the frozen-unfrozen interface exited the sand layer and entered the silt. The void developed at different heights across the sample, due to uneven refrigerator temperatures (several light bulbs for heat control burned out simultaneously). The burnt-out bulbs also caused the ambient air temperature to fall below freezing, which promoted ice development along the circumference of the sample that was not related to the cyclic temperature test. As the cooling cycle began, the water-filled void was converted to ice, and the interface moved downward. The frost heave ratio (Figure C.2(c)) and the water flux (Figure C.2(d)) remained effectively zero throughout the duration of the test. At the conclusion of the second and final cycle, several millimeters of ice had accumulated just above the sand layer.

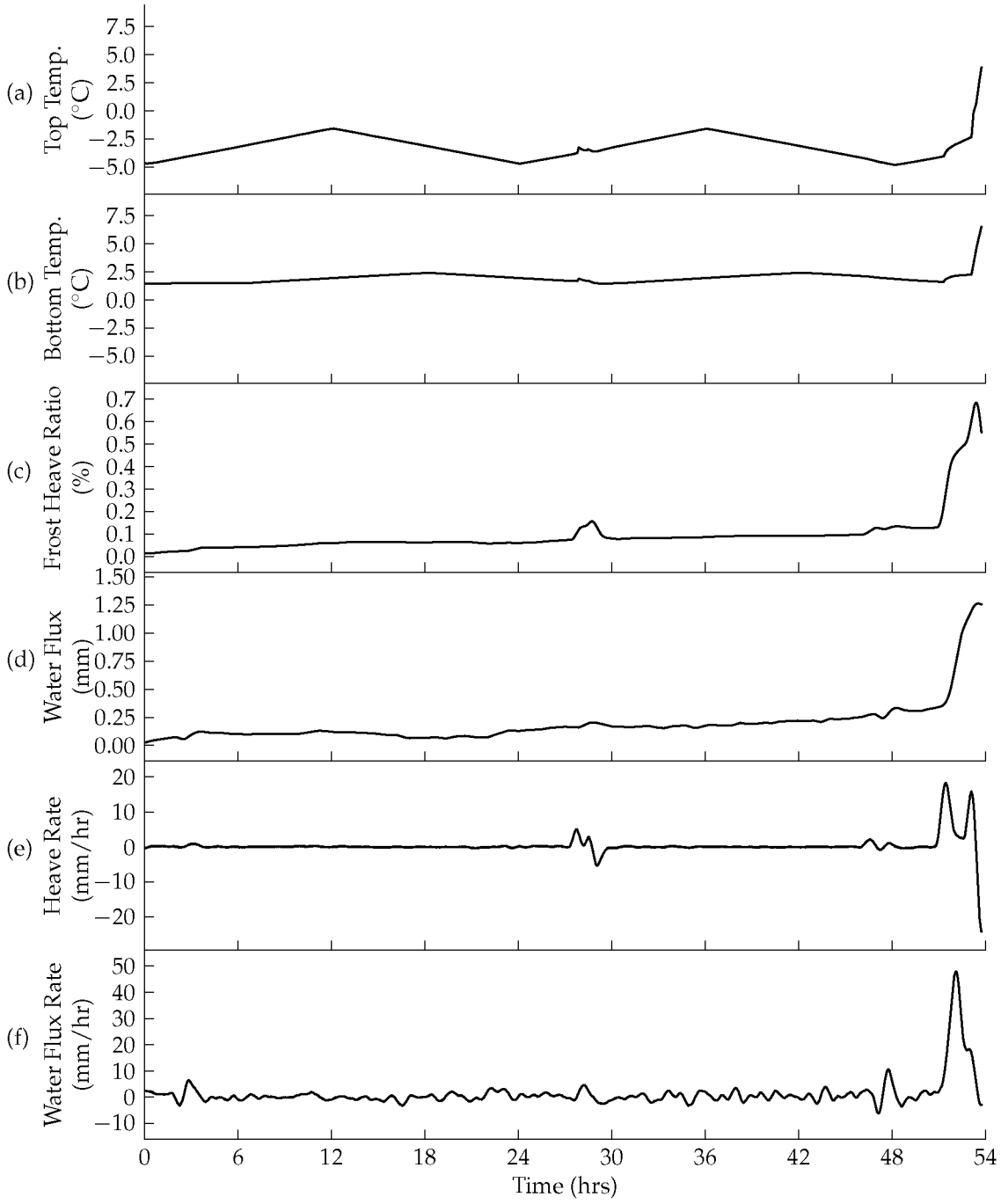

Figure C.2. JSI03 soil temperatures (a,b), frost heave ratio (c), water flux (d), heave rate (e), and water flux rate (f).

Sample JSI04

Sample JSI04 was composed of screened Fox silt, over a layer of clean uniform sand, initially consolidated, saturated, and frozen in the Hokkaido Cell prior to testing as described in Section 2.4. The top temperature was linearly varied from approximately -4°C to -1°C for the duration of the test, while the bottom temperature was held constant at approximately 1.5°C (12 hours warming, 12 hours cooling, Figure C.3(a,b), Table 3.2). These thermal conditions ensured that the sample was under open system conditions while cooling and warming.

Figure A.7 (Appendix A) is a condensed time-lapse video of the total test progression for sample JSI04. Select stills from the video are in Appendix B, Figure B.7. The initial freezing of the sample did not produce any segregated ice. A water-filled void was visible during testing after the first cooling cycle began. The freezing front moved down to just above the sand layer by the end of the first cooling cycle. As the cycle was repeated, the ice layer thawed and the silt below the void expanded upward into the void area, filling the void with soil. Upon refreezing, the freezing pore water pushed the soil downward, compressing the upper portion of the layer.

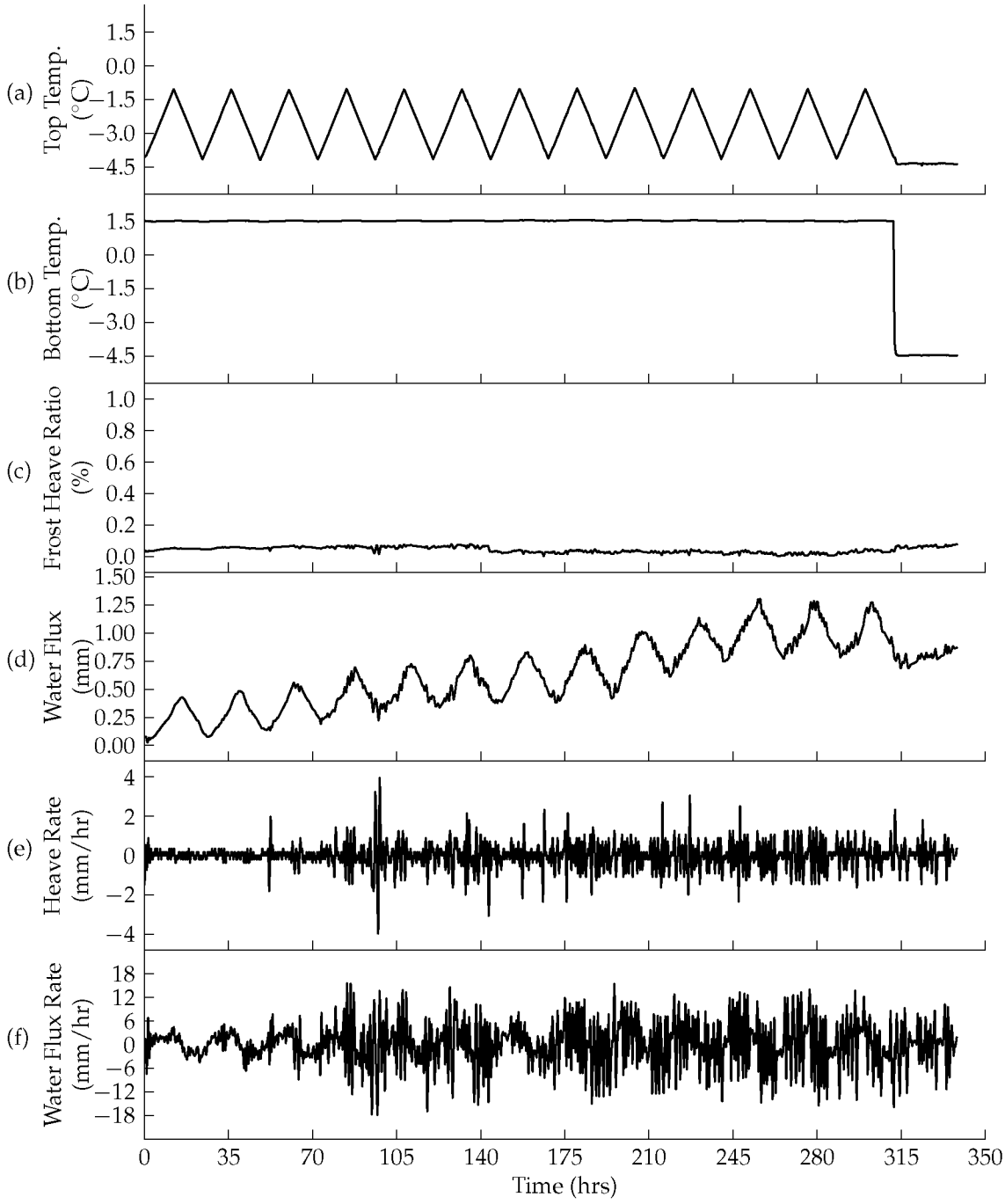

Figure C.3. JSI04 soil temperatures (a,b), frost heave ratio (c), water flux (d), heave rate (e), and water flux rate (f).

Sample JSI05

Sample JSI05 was composed of screened Fox silt, over a layer of clean uniform sand, initially consolidated and saturated in the Hokkaido Cell prior to testing as described in Section 2.4. The top temperature was varied linearly from approximately -6.5°C to -3°C for the duration of the test, while the bottom temperature was held constant at approximately 1°C initially, then warmed to 3°C (12 hours warming, 12 hours cooling, Figure C.4(a,b), Table 3.2). These thermal conditions ensured that the sample was under open system conditions while cooling and warming.

Figure A.8 (Appendix A) is a condensed time-lapse video of the total test progression for sample JSI05. Select stills from the video are in Appendix B, Figure B.8. The initial freezing of the sample did not produce any segregated ice. The first 180 hours of the test were designed to form ice in the lower sand layer by moving the freezing front up and down in the sand. No displacement occurred or ice formed, so the lower pedestal temperature was increased to 3°C (Figure C.4(c)). A water-filled void was visible during testing after the first cooling cycle began during the second half of the test. The surface displacement at the conclusion of the cyclic cooling testing program was effectively zero. Sample extraction from the cell post-testing requires freezing the entire sample. The final FHR of 1% can be attributed to the extraction freezing, and not the cyclic cooling test.

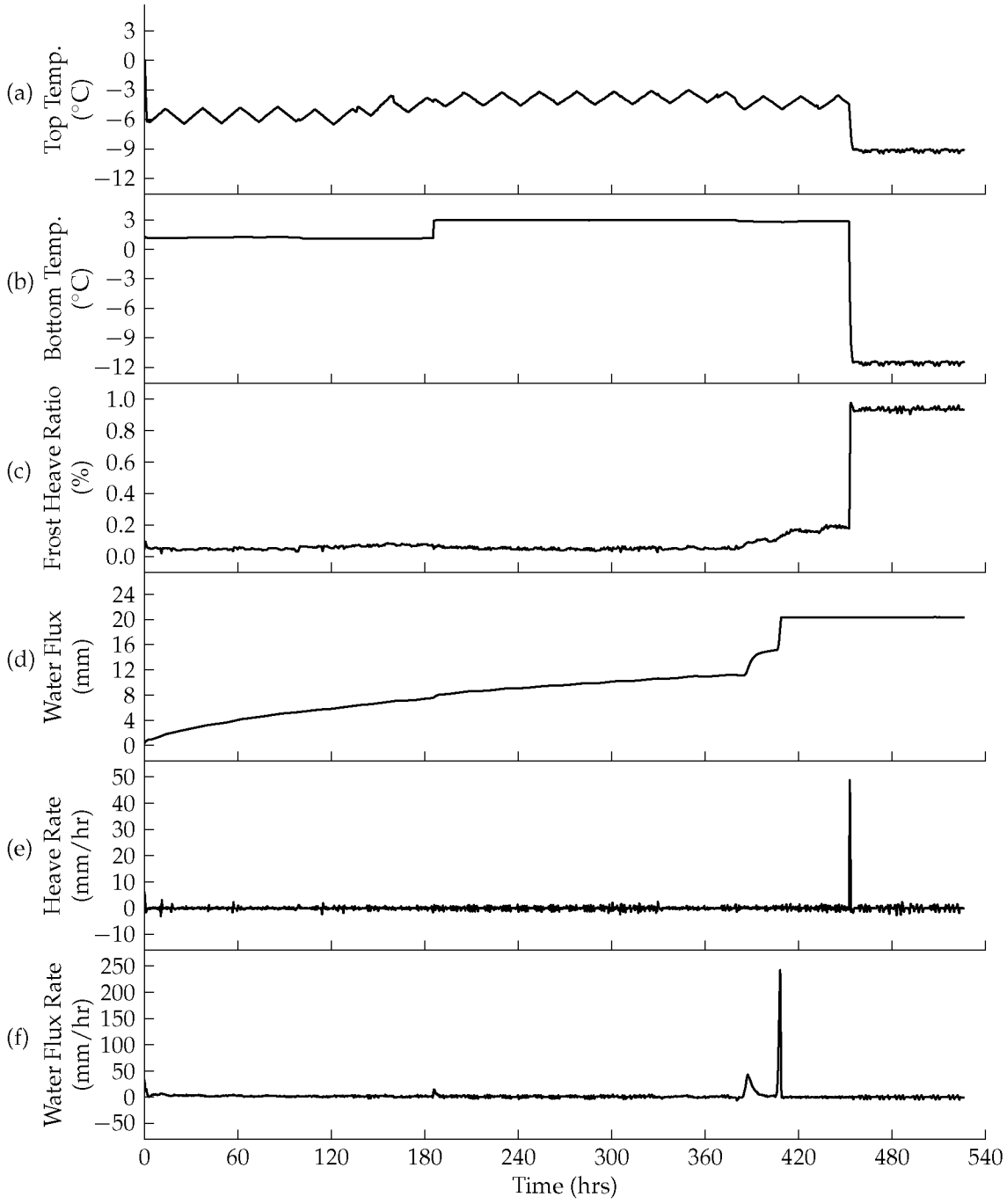

Figure C.4. JSI05 soil temperatures (a,b), frost heave ratio (c), water flux (d), heave rate (e), and water flux rate (f).

Appendix D: μCT Rendering Videos

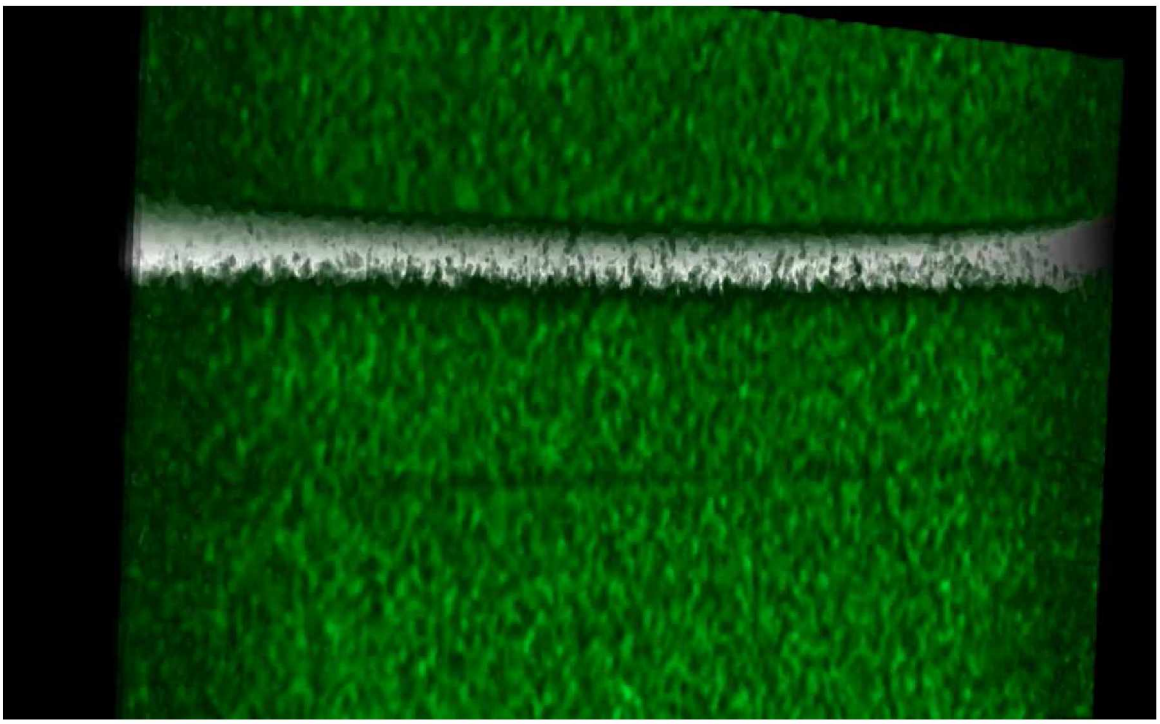

Figure D.1. JSI08 μCT rendering video. Video file may be found on attached DVD. Sample is 16.82 mm tall, 24.26 mm wide and deep.

Figure D.2. JSI01 μCT rendering video. Video file may be found on attached DVD. Sample is 16.82 mm tall, 24.26 mm wide and deep.

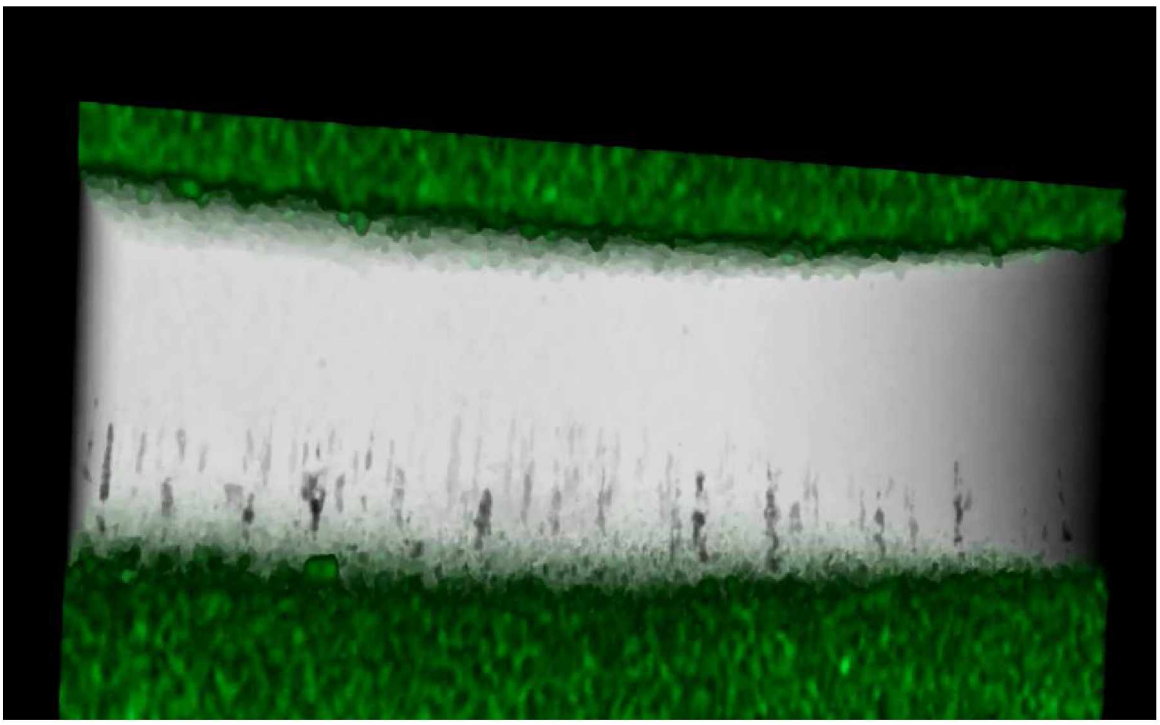

Figure D.3. JCL01 μCT rendering video. Video file may be found on attached DVD. Sample is 16.82 mm tall, 24.26 mm wide and deep.

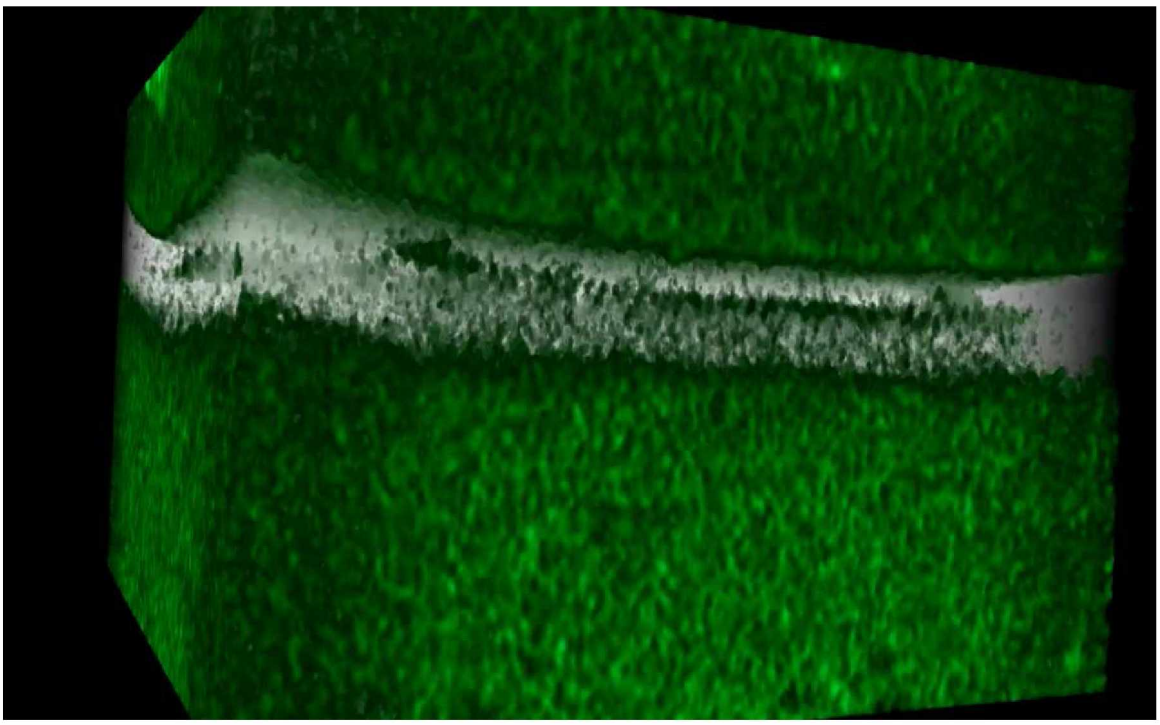

Figure D.4. JSI02 μCT rendering video. Video file may be found on attached DVD. Sample is 16.82 mm tall, 24.26 mm wide and deep.

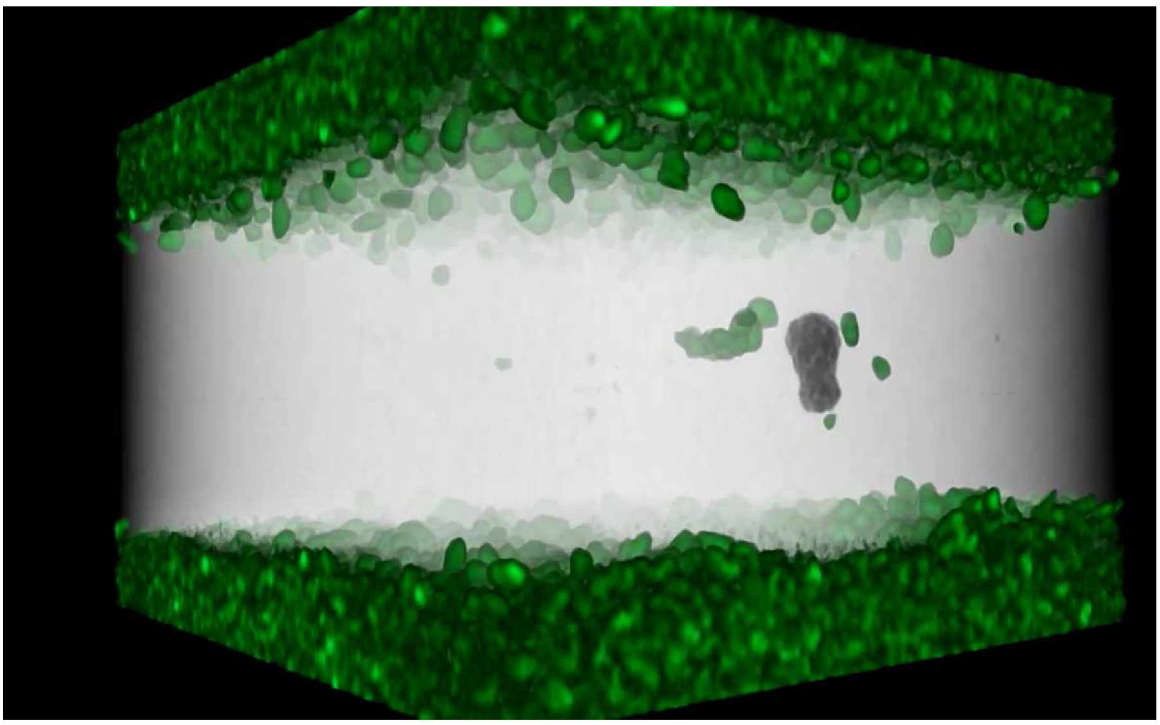

Figure D.5. JSA01 μCT rendering video. Video file may be found on attached DVD. Sample is 16.82 mm tall, 24.26 mm wide and deep.

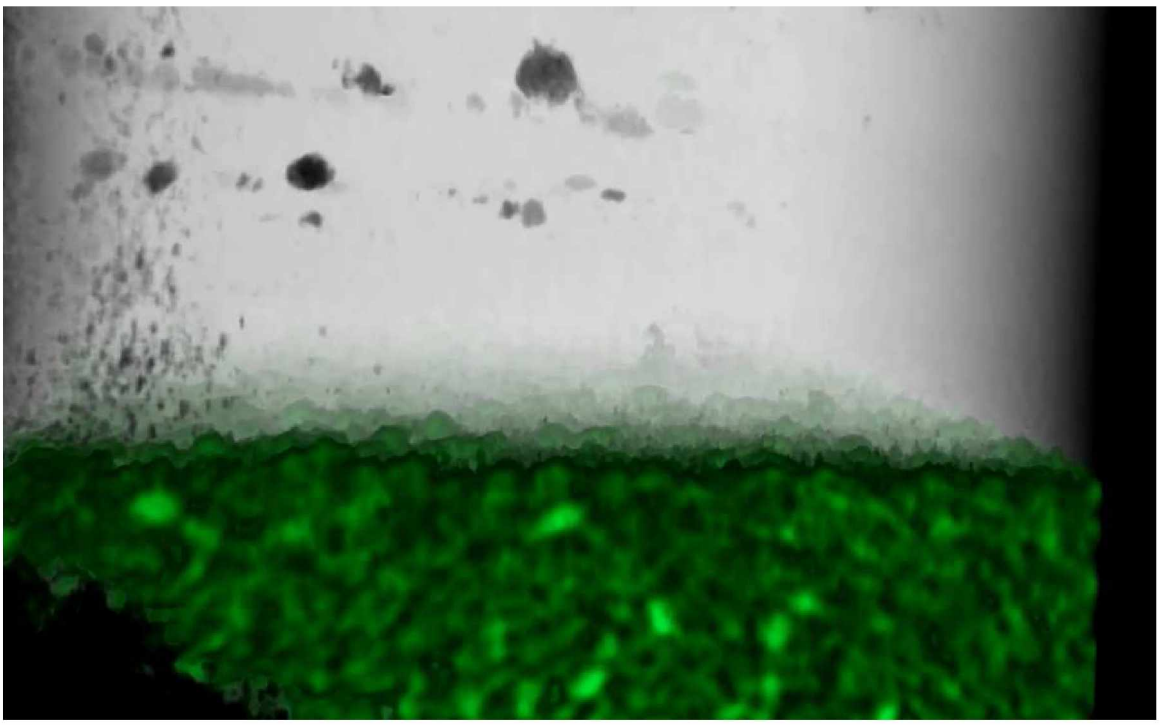

Figure D.6. CSA01 μCT rendering video. Video file may be found on attached DVD. Sample is 29.88 mm tall, 24.26 mm wide and deep.

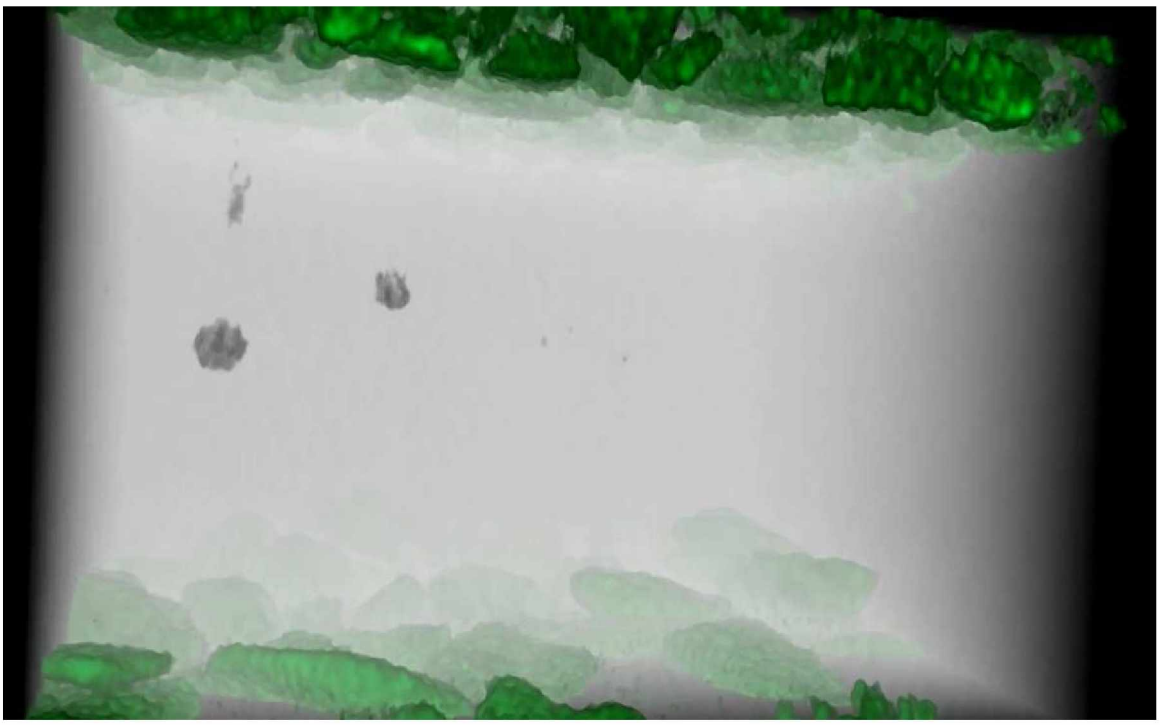

Figure D.7. JGR01 μCT rendering video. Video file may be found on attached DVD. Sample is 16.82 mm tall, 24.26 mm wide and deep.